U.S.NRC

United States Nuclear Regulatory Commission

Protecting People and the Environment

NUREG/CR-7105

Radionuclide Release from Slag and Concrete Waste Materials

Part 2: Relationship Between Laboratory Tests and Field Leaching

Office of Nuclear Regulatory Research

AVAILABILITY OF REFERENCE MATERIALS IN NRC PUBLICATIONS

NRC Reference Material

As of November 1999, you may electronically access NUREG-series publications and other NRC records at NRC's Public Electronic Reading Room at http://www.nrc.gov/reading-rm.html. Publicly released records include, to name a few, NUREG-series publications; *Federal Register* notices; applicant, licensee, and vendor documents and correspondence; NRC correspondence and internal memoranda; bulletins and information notices; inspection and investigative reports; licensee event reports; and Commission papers and their attachments.

NRC publications in the NUREG series, NRC regulations, and *Title 10, Energy*, in the Code of *Federal Regulations* may also be purchased from one of these two sources.

1. The Superintendent of Documents
   U.S. Government Printing Office
   Mail Stop SSOP
   Washington, DC 20402–0001
   Internet: bookstore.gpo.gov
   Telephone: 202-512-1800
   Fax: 202-512-2250
2. The National Technical Information Service
   Springfield, VA 22161–0002
   www.ntis.gov
   1–800–553–6847 or, locally, 703–605–6000

A single copy of each NRC draft report for comment is available free, to the extent of supply, upon written request as follows:

Address: U.S. Nuclear Regulatory Commission
Office of Administration
Publications Branch
Washington, DC 20555-0001
E-mail: DISTRIBUTION.RESOURCE@NRC.GOV
Facsimile: 301–415–2289

Some publications in the NUREG series that are posted at NRC's Web site address http://www.nrc.gov/reading-rm/doc-collections/nuregs are updated periodically and may differ from the last printed version. Although references to material found on a Web site bear the date the material was accessed, the material available on the date cited may subsequently be removed from the site.

Non-NRC Reference Material

Documents available from public and special technical libraries include all open literature items, such as books, journal articles, and transactions, *Federal Register* notices, Federal and State legislation, and congressional reports. Such documents as theses, dissertations, foreign reports and translations, and non-NRC conference proceedings may be purchased from their sponsoring organization.

Copies of industry codes and standards used in a substantive manner in the NRC regulatory process are maintained at—

The NRC Technical Library
Two White Flint North
11545 Rockville Pike
Rockville, MD 20852–2738

These standards are available in the library for reference use by the public. Codes and standards are usually copyrighted and may be purchased from the originating organization or, if they are American National Standards, from—

American National Standards Institute
11 West 42nd Street
New York, NY 10036–8002
www.ansi.org
212–642–4900

Legally binding regulatory requirements are stated only in laws; NRC regulations; licenses, including technical specifications; or orders, not in NUREG-series publications. The views expressed in contractor-prepared publications in this series are not necessarily those of the NRC.

The NUREG series comprises (1) technical and administrative reports and books prepared by the staff (NUREG–XXXX) or agency contractors (NUREG/CR–XXXX), (2) proceedings of conferences (NUREG/CP–XXXX), (3) reports resulting from international agreements (NUREG/IA–XXXX), (4) brochures (NUREG/BR–XXXX), and (5) compilations of legal decisions and orders of the Commission and Atomic and Safety Licensing Boards and of Directors' decisions under Section 2.206 of NRC's regulations (NUREG–0750).

U.S.NRC
United States Nuclear Regulatory Commission
Protecting People and the Environment

NUREG/CR-7105

Radionuclide Release from Slag and Concrete Waste Materials

Part 2: Relationship Between Laboratory Tests and Field Leaching

Manuscript Completed: September 2011
Date Published: October 2011

Prepared by
W. L. Ebert

Argonne National Laboratory
9700 South Cass Avenue
Argonne, IL 60439

M. Fuhrmann, NRC Project Manager

NRC Job Code N6669

Office of Nuclear Material Safety and Safeguards

ABSTRACT

Technical literature has been evaluated to assess the several-orders-of-magnitude discrepancy that is commonly reported between the mineral dissolution rates that are inferred from mass-balance calculations for natural systems and those measured in laboratory experiments. This was done to gain insights that may be useful for modeling the weathering behaviors and contaminant releases from waste materials in surface disposal sites. Predicting the concentrations and movement of contaminants in groundwater requires an understanding of (1) groundwater flow, (2) processes affecting contaminant dispersal and groundwater mixing, and (3) physical and chemical reaction processes that affect the concentration of a contaminant in groundwater. Inverse modeling of field measurements to extract mineral dissolution rates is affected by uncertainties in all three of these factors, whereas most laboratory measurements used in direct modeling address only the dissolution of an isolated material in a well-constrained system. Both approaches and the origins of uncertainties in each that are likely to contribute to the differences between the dissolution rates that are determined are evaluated. Information and insights pertinent to assessing the long-term weathering of waste materials under subaerial conditions are provided by each approach, and several aspects are evaluated in detail to support the use of inverse and direct modeling in future applications.

Table of Contents

List of Figures

List of Tables

Executive Summary

A large discrepancy exists between the mineral dissolution rates that are inferred from mass-balance calculations performed for natural systems based on the analyzed stream water and ground water compositions from large watersheds, catchments, and aquifers and the dissolution rates that are measured directly in laboratory experiments conducted with single, pure minerals in a dilute solution at an imposed pH value. Differences of up to five orders of magnitude between the field rates and laboratory rates have been reported for compositionally simple minerals. Although the numerical values of the rates are small and the differences may be between 1×10^{-12} and 1×10^{-17}, mol m^{-2} s^{-1}, the impact on the calculated release in a system with thousands of hectares of surface area is very significant. Several factors have been suggested to contribute to this discrepancy, including factors due to uncertainties in modeling the field conditions, uncertainties in the laboratory experimental measurements, and uncertainties in matching the field conditions with the laboratory tests. The sources of these uncertainties have been examined in this study. Particular attention is paid to laboratory measurements, because small errors in the direct laboratory measurements can lead to large errors when they are propagated in performance calculations with respect to both area and time. In contrast, errors in field measurements become less significant as the system is homogenized as it is down-scaled for comparison to laboratory values. In addition, and perhaps more importantly, the laboratory-measured rates used for comparisons with inferred field rates represent an isolated, single dissolution process, whereas the field rates represent highly coupled and complex systems. The question of whether agreement between laboratory and field rates should even be expected is discussed. Whether or not agreement should be expected, the comparison provides valuable insights into the uncertainties in both and the effects of other processes that must be taken into account in modeling a disposal system and contaminant transport.

Although many studies have pointed to the discrepancy between laboratory and field rates and proposed contributing factors, little has been written regarding the methods by which the data used to determine the rates are measured in the field and in the laboratory. That is the primary focus of this study, wherein the modeling methods used to determine the field rate and the experimental methods used to measure the dissolution rates are evaluated and critiqued. With regard to the field rates, this report focuses primarily on evaluation of the mass-balance and inverse modeling approaches developed during the past several decades. More recent forward modeling studies using coupled chemical reaction-mass transport models are also being used to address the discrepancy in rates, but have not yet resolved the differences. Many of the same issues regarding the field rates and mass-balance calculations pertain to reaction-transport modeling. With regard to laboratory tests, many of the important aspects of measuring dissolution rates with laboratory methods were addressed in a previous evaluation of conceptual dissolution models developed for silicate minerals and laboratory test methods (Ebert 2010). Insights from that analysis have been brought to bear in this evaluation of dissolution rate measurements, but the primary focus in this report is consideration of those artifacts associated with those test methods and aspects of the dissolution mechanism and atomistic model used to extract the dissolution rate from the test results that could affect its value.

The principle processes involved in mineral weathering include (1) factors that are related to the field environment and physical parameters such as climate, hydraulic conductivity, mineral grain size and exposed surface area, and (2) factors that are related to the mineral, such as kinetics of dissolution and precipitation reactions, solute catalytic and inhibiting effects, and solubility. Many of these factors are important in both field studies and laboratory tests. The range of values

affecting the dissolution rate is significantly different in the field, where minerals experience a full range of environmental variables, and in laboratory tests, where a single environmental value may be represented (e.g., one temperature and pH) or the effect of the variable may be neglected (e.g., the presence of other phases). Although the full ranges of variables may be experienced by the mineral in the field, an average or representative value must be selected for mass-balance modeling due to the spatial and temporal limits of the available data. Most laboratory tests are conducted under constant conditions, usually intended to represent the annual average values of the field conditions. For most variables that affect the dissolution rate, the rate based on the average value of the variable range may be significantly different than the average of the rates over the range of variable values if the effect of the variable is not linear. This is important regarding the temperature, the relationship between mineral grain size and surface area, and the ground water flow rate. The effect of the solution composition is also important due to feedback effects that may catalyze or inhibit the dissolution of a mineral and have a nonlinear effect on the approach to saturation. In addition, the precipitation of secondary (product) phases as the primary phase dissolves will affect the mineral dissolution rate. The impact of this effect may be very different in the field, where a mature assemblage of secondary phases is available, and in laboratory tests, where the secondary phases will in most cases be immature or absent altogether.

Differences between the dissolution rates inferred from field studies and those measured in laboratory experiments can be attributed to contributions from many factors related to differences in the field and laboratory systems and uncertainties and artifacts that primarily affect one or the other system. System differences include the complexities of the groundwater compositions, water hydraulics, and flow paths and differences in the assemblage of primary and secondary mineral phases and their surface textures. Uncertainties specific to field studies include the distributions of grain sizes and mineral surface areas, the wetted mineral surface areas in near-surface environments, and temperature fluctuations. Key uncertainties specific to laboratory experiments include the effects of comminution (crushing and sizing test materials), how to best normalize the rate to surface area and take into account the change in surface area that occurs during tests, account for the effects of fluid flow rate, measure dissolution under near-equilibrium conditions, and accountfor multi-phase interactions. These factors are identified and some of their effects on the dissolution rate are evaluated in detail based on results available in the open literature.

Both field studies and laboratory studies are necessary to understand the weathering of geologically important minerals in near-surface watersheds and deep aquifers and to predict the weathering of subaerial and deep geological waste disposal sites. Laboratory experiments are needed to understand individual and simply-coupled processes that contribute to the natural system. Field studies, including inverse modeling, are needed to provide insight into the behavior of the over-all system and calibrate or confirm the complex models that are constructed from many individual process models (including forward models). The discrepancy between the inferred field dissolution rates and the dissolution rates directly measured in laboratory experiments indicates the importance of processes other than primary phase dissolution in the over-all system behavior. These almost certainly include hydraulic factors related to the effects of pore (and fracture) structure of the natural system, the effects of other minerals (and amorphous phases) that dissolve and precipitate to affect the ground water chemistry and, in turn, the dissolution behavior of the mineral of interest, and local variations in temperature, ground water composition, and mineral distribution that might not be adequately represented by a single laboratory test. Field studies and laboratory studies should proceed iteratively to determine important aspects of the field environment that should be represented in laboratory experiments and identify those conditions that affect the reaction and reactivity in laboratory experiments that should be more thoroughly characterized in the field (including disposal systems).

Although the primary issue addressed in the study is the discrepancy between laboratory and field rates of mineral dissolution, the interest stems from the need to characterize surface disposal sites. The insights that are gained from comparing laboratory and field measurements will be applied directly to utilizing laboratory test results and field characterization to predicting the long-term performance of radioactively contaminated slags and concretes that have accumulated in surface disposal systems as acre-sized heaps of waste materials that are being naturally weathered. Many aspects of laboratory testing, field measurements, inverse and forward modeling are relevant to modeling the weathering behaviors of these systems and the release and transport of radioactive contaminants. The evaluations performed in this study are intended to inform future developments in modeling such systems. Although some methods by which laboratory tests, inverse modeling methods, and reactive transport modeling can be applied to these systems are discussed briefly in this report, they will be addressed in more detail in a later report.

The factors proposed previously to be contributors to the observed discrepancies are supported by the data considered in this study. These include uncertainty in the accessible and wetted surface area in the natural system; the importance of transport limits in the field; the presence of surface coatings and aged surfaces in the field compared with fresh and clean surfaces in laboratory experiments, plus comminution; and the different degrees of solution saturation in the field and laboratory systems. Additional factors identified herein include taking the effect of the flow rate on the laboratory rate into proper account, the mere presence of alteration phases, in addition to the effect of the precipitation rate and surface area of secondary phases, properly representing the surface area and condition of crushed material in the laboratory test. Based on these analyses, one should not expect agreements between laboratory and field rates due to (1) the uncertainties inherent in the laboratory measurements and the dependencies of the measured rates on test conditions, (2) the homogenization of key properties of natural systems necessary to infer a mineral dissolution rate with inverse modeling, such as mineral distributions and groundwater flow, and (3) the impossibility of identifying particular laboratory test conditions that match field conditions for direct modeling. These effects have been observed in large natural systems such as the catchment studies summarized and evaluated in this report and on much smaller scale lysimeter studies. An understanding of the observed discrepancies should be used instead to utilize aspects of inverse modeling to inform forward models with regard to the effects of mass transport and other processes on the dispersion of contaminants.

Acknowledgements

This report was prepared to document work performed by Argonne National Laboratory (contractor) for the Nuclear Regulatory Commission (NRC) under Contract No. 60-09-270 (job number N6669). The analyses reported here were performed on behalf of the NRC Office of Nuclear Regulatory Research, Division of Risk Analysis (Environmental Transport Branch). The NRC project manager is Mark Fuhrmann. This report is an independent product of Argonne National Laboratory and does not necessarily reflect the views or regulatory position of the NRC.

Quality of Data and Analyses

Only data from the literature sources cited in the report were used in these analyses. In many cases, the data presented in this report were generated by reading values from plotted data in the literature publications. These were used to analyze trends in the data to evaluate reaction behavior and analyze the effects of testing parameters, and not to extract results for other uses.

The spreadsheet program Microsoft EXCEL 2003 and the plotting program KaleidaGraph version 3.6 (Synergy software) were used to plot data, perform regression fits, and compute modeled values. These are commercial software packages.

This work was supported by the U.S. Department of Energy, Office of Nuclear Energy, under Contract DE-AC02-06CH11357 and the Nuclear Regulatory Commission work order 60-08-419.

ACRONYMS AND ABBREVIATIONS

ANL	Argonne National Laboratory
ASTM	ASTM-International
BET	Brunauer, Emmett, and Teller (model)
BLT	Breach, Leach, and Transport (computer code)
BNL	Brookhaven National Laboratory
DOE	U.S. Department of Energy
DUST	Disposal Unit Source Term (computer code)
EPICOR-II	Product name
ET	Evapotranspiration
IAEA	International Atomic Energy Agency
INEEL	Idaho National Engineering and Environmental Laboratory
NRC	U.S. Nuclear Regulatory Commission
ORNL	Oak Ridge National Laboratory
RESRAD	Residual Radioactivity (computer code)
REV	Representative element volume
SI	Saturation Index
VES	Vinyl ester styrene
WIPP	Waste Isolation Pilot Plant

1 Introduction

The U.S. Nuclear Regulatory Commission (NRC) issues licenses to possess nuclear materials and regulates the disposition of radioactive wastes in the United States. License termination requires a determination of whether a waste material is likely to remain sufficiently durable to retain radionuclides over a typical 1000-year compliance period while being weathered or if the waste must be further stabilized. This decision is typically made by considering the predicted long-term impact of waste degradation and contaminant release on the groundwater composition based on short-term measures of the degradation behavior of the waste material and limited characterization of the site. The calculations currently used to assess long-term waste material behavior utilize fairly simple models for radionuclide source terms, which may or may not be consistent with the degradation mechanisms of the wastes being evaluated. The ability to identify mechanistic bases for the laboratory tests and source term models used in assessment calculations will add credence to site assessments and the evaluations of site remediation plans.

Argonne National Laboratory (ANL) has initiated an NRC-sponsored activity to identify the laboratory and field tests used to characterize waste form degradation and measure the release of radionuclides and how they interface with the models used to predict radiation doses in risk assessment calculations. The terms "waste material" and "waste form" are used in this report to represent the source material from which the radionuclide is being released and the stabilized material, respectively. The current use of test methods to parameterize degradation and transport models is being evaluated to better represent the mechanisms of radionuclide release in site assessments. The expected output from this activity is a protocol that can be used by the NRC to integrate the results of short-term laboratory tests and field measurements that address waste material (or waste form) degradation and leaching into the model calculations that are used to assess the stability of wastes at NRC-regulated sites prior to decommissioning. The approach will be to (1) develop a mechanistic understanding of the weathering processes of the particular waste material, (2) identify the appropriate degradation model(s) to describe the release of radionuclides, and (3) follow an appropriate testing protocol to measure values of the model parameters to be used in performance assessment calculations. Guidance will also be developed for utilizing leach test data in source term models.

Two groups of waste materials of current interest to NRC are (1) slags produced during ore processing and metal recycling, and (2) contaminated concrete and metal debris from decommissioning activities. Slags are typically heterogeneous mixtures of glassy and crystalline phases, and can be hard, dense, and glassy, soft and porous, or rock-like. Since slags are formed as molten material solidifies, hazardous elements can become incorporated into the structures of both the glassy and crystalline phases that comprise the slag by substituting into structural lattice sites, at interstitial defects, forming separate phases, etc. Degradation of the host phase during weathering is expected to occur by the dissolution of each component phase at a rate that depends both on the intrinsic properties of that phase and the environment (groundwater composition, temperature, neighboring phases, etc.). The distributions of hazardous components in contaminated concrete are usually restricted by the accessibility of groundwater to transport contaminants into pores where interactions with other phases present in the concrete structure and pore water can occur. The later degradation of contaminated concrete by weathering is expected to occur by advection or diffusion of water through the pore structure coupled with the dissolution of both the occluded and structural phases of the concrete. The presence of other materials, such as rebar, may affect the weathering behavior by sorption, generation of colloids,

changing the pore water chemistry, redox, the corrosion of rebar and associated spalling of concrete, etc. It is expected that different models and testing protocols will be required to determine source term values for the releases of hazardous components from slags and concretes due to differences in the release mechanisms.

1.1 Technical Approach

The work described in this report includes literature reviews to identify materials of interest and existing information regarding corrosion behavior and test results, descriptions of degradation mechanisms, key interactions, and approaches for developing long-term predictions. Based on these reviews, source term modeling approaches will be recommended for slag and concrete waste materials and suites of test methods to provide data for use in the models will be identified. These activities are being conducted as four mostly sequential activities that are summarized below. Separate reports will be produced that focus on each part of the evaluation, although all aspects will be discussed in each report to some extent. It is anticipated that the evaluation of any particular aspect of the project will continue to be developed and will evolve over the course of the project as additional insights are gained. For example, aspects of field testing, leaching data for mineral phases, and basic approaches in degradation models are discussed in this report from the perspective of conceptual models and laboratory test methods to better understand what information is needed and how that information will be used. Subsequent reports that are focused on specific data bases and modeling approaches will probably include discussions that further elaborate the roles of various laboratory test methods. The primary technical issues to be addressed in the four parts of this work are summarized below.

Part I: Conceptual Model of Leaching from Complex Materials and Laboratory Test Methods

This report (published as NUREG/CR-7025) provides a summary of the initial review and analysis of existing literature regarding the weathering of various slag and concrete waste materials and waste forms, including experimental results, field measurements, and modeling approaches. The mechanistic basis of existing conceptual models and the current use of laboratory and field data are evaluated. The inherent uncertainties associated with current modeling approaches (both in concept and quantitation) are discussed and the need to develop models that better represent the release mechanisms of matrix and hazardous components is assessed. Various test methods currently used to study waste form weathering are summarized and evaluated with regard to the information provided, limitations of the test method, and the role of the test data in assessing the degradation mechanism and the long-term release behavior. The applications of specific test methods to slag and concrete wastes are discussed and test protocols recommended for parameterizing the source term models deemed to be appropriate for various waste types, including slag and concrete wastes.

Part II: Relationship between Laboratory Tests and Field Leaching

The relationships between the behavior measured in laboratory tests and field measurements will be evaluated and the methods used to relate laboratory-measured values to field measurements will be discussed. Insights from previous analyses of minerals and natural materials used in laboratory and field tests will be brought to bear on the systems of interest in this project. Weathering rates determined from field measurements are typically and systematically several orders of magnitude lower than rates determined from laboratory tests, and several reasons for this have been postulated. By design, most laboratory tests maintain constant environmental conditions to accurately measure the effect of a specific variable on the degradation rate, such as the effect of temperature or pH, whereas weathering in the field is affected by continuous changes

in many conditions that are not fully known and not represented explicitly (or perhaps not accurately) in laboratory tests. In general, values measured in specific laboratory tests should not be directly compared with values measured in the field, such as groundwater flow rates. Instead, values measured in the laboratory should be adjusted to take into account the range and combination of effects experienced in the field. From this perspective, field measurements can help "calibrate" laboratory measurements to better represent the effective averages of environmental conditions or identify other processes that should be taken into account in testing and/or modeling activities. It is anticipated that field leaching results would be better compared with coupled reaction-transport model results rather than directly with the results of a specific laboratory test. Laboratory tests specifically designed to represent the ranges of environmental conditions and interactions that affect in-field behavior, including lysimeters, are useful for confirming model results but are too complex to provide the mechanism-specific data that are needed to select or parameterize the appropriate degradation model. What we provide in this Task is a technically-based recommendation for addressing this difference in decommissioning analyses.

Part III: Application of Models to Leaching Data from Slags and Concrete

Existing source term models that may be useful for calculating weathering behaviors of slags and concretes will be identified, summarized, and evaluated. The consistency of these models with data available for the release of components from slags and concretes will be evaluated with several examples. How well current models represent the measured release behavior will be assessed with regard to the uncertainty in long-term predictions due to uncertainties in the measured model parameters and uncertainty in how well the model represents the degradation behavior. Alternative models or modeling approaches will be recommended as appropriate.

Part IV: Application of Leaching Model to Dose Assessment Codes

The source term models for radioactive and hazardous contaminants must be interfaced with a dose assessment code to evaluate the performance of a waste site. In most cases, mechanistic models must be simplified (abstracted) for use in performance assessment codes to meet constraints in performing the calculations or due to the limitations of aleatory (random chance) or epistemic (absence of knowledge) uncertainties. The abstraction may include the combining of several model parameters into a single parameter that can be tracked in the performance assessment, replacing a variable with a bounding constant value, etc. Abstraction is usually a consequence of changing from the atomic scale of the mechanistic model (nm) to the intermediate scale of laboratory tests (cm) and then to the large scale of waste sites (km). Guidance will be developed regarding the appropriate use (or the need for integration) of laboratory data and field test information in dose assessment codes such as DUST and RESRAD. The approach will be to combine insights gained with experience and insights from other site assessments done for other disposal systems at the Waste Isolation Pilot Plant (WIPP), Hanford, and Yucca Mountain to describe the use of test data and source models in dose assessment calculations. This will include propagating uncertainties in the mechanistic and abstracted source term models and in the coefficient values to estimate confidence levels. It is important that the abstracted models capture the environmental and temporal effects on material degradation and the release of hazardous components that are important to performance assessment.

1.2 Introduction to Relationship between Laboratory Tests and Field Leaching

The environmental importance of the natural weathering of minerals cannot be overstated. Mineral dissolution provides nutrients such as K, Ca, Mg, and PO_4 in soils utilized by flora and fauna; affects the fertility of soils through clay content, water retention, and drainage; affects the compositions of ground waters, which in turn impact plant, insect, and animal life; neutralizes acid rain; influences (and is influenced by) climate and geothermal cycles on a global scale.

Of particular interest in this evaluation is the weathering of radionuclide-bearing materials in near-surface environments and insights available from field studies of mineral weathering and the relationship with laboratory studies. Weathering can occur due to mechanical, chemical, and biological interactions. Physical weathering can occur due to abrasion, freeze/thaw cycling, thermal expansion, exfoliation, etc., which results in generation of smaller particles and an increase in the reactive surface area. This may initially increase the porosity of the system through the formation of cracks and later decrease transport by sedimentation. Biological weathering results from the effects of lichen and moss, which acidify the groundwater and generate chelating ligands both when they grow and when they decay (humic acids), and from root growth, which generates pressure in crevices that can result in spalling. Chemical weathering includes reactions with atmospheric reactants, primarily water and CO_2, to hydrate minerals, dissolve minerals in groundwater, and convert minerals to more stable secondary phases.

The issue addressed in this report is the discrepancy between the dissolution rates of minerals that have been measured in laboratory tests and the dissolution rates of those minerals that have been inferred from field studies. The discrepancy is often cited between the rates measured for particular minerals in laboratory tests and those inferred from field studies by Pačes (1983) and Velbel (1985), and both of those researchers have attributed the discrepancy to uncertainty in the reactive surface areas of minerals in the field system and differences in the reactivities of minerals in the field and laboratory samples:

"It is obvious that the accuracy and reliability of the absolute values of the field derived rate constants depend mainly on the uncertain estimate of the specific wetted surface of rock. The extremes of the estimate span a range of about three orders of magnitude" (Pačes 1983, p. 1861). And "the feldspar surfaces in an aquifer are old, compared to those of feldspars utilized in laboratory experiments. They have fewer defects and are smooth. The fresh surfaces of feldspars studied in the laboratory consist of many kinks and ledges and small-area terraces which dissolve faster" (Pačes 1983, p. 1855).

"The major source of uncertainty in any normalization of field rate data is the reactive surface area of the mineral in the weathering profile" (Velbel 1985, p.924).

The relationship between laboratory tests and field measurements presents an important example of scaling conservation of mass equations and kinetic rate constants over space with the objective of scaling the contaminant transport over time. Laboratory tests provide insights that are needed to understand and quantify the atomic-scale processes and material properties that are used in macroscale models developed, for example, to predict field behavior over times longer than can be monitored. Field measurements are important to laboratory testing because they help to identify the processes, environmental conditions, and materials interactions that must be quantified with laboratory tests, for example, the ambient temperature, ground water composition,

Eh, pH, hydraulics, and mineralogical composition. Field measurements are also important after laboratory testing and model development to confirm predictions of the system model, where the system model is the combination of several process models (or constitutive relationships) used to describe individual processes, such as material oxidation, dissolution, and solute transport.

The relationship between laboratory tests and field behavior that is of present interest is forward-looking in that dispersal of radioactive contaminants from a waste site will depend on future environmental factors, such as rainfall. However, the relationship will be evaluated by looking backwards in that the results of past field behavior, namely, mineral dissolution, are compared to laboratory results. The hypothesis being evaluated is that a dissolution rate measured in the laboratory (under particular conditions that may or may not represent the field conditions) can be used to calculate the extent of mineral dissolution in the field. In most cases, the extent of dissolution in the field is measured by mass-balance of the ground water composition and expressed as a dissolution rate. In some cases, the extent of dissolution is based on analysis of the residual solids. Also, the term "field leaching" is a misnomer for this evaluation, since almost all of the comparisons are made using solutes generated by material dissolution rather than leaching.

The "field" is considered to be a large mass of rock consisting of a vast collection of aggregated mineral grains, pores, and fractures that can be treated as a porous medium. On the large scales that are of interest, e.g., many hectares, it is not realistically possible to describe the pore structure of the rock in terms of individual pore volumes, fracture widths, and discontinuities in the mineral aggregates. Instead, the transport properties of ground water through the rock in the field, the interactions between the ground water and the minerals, and the transport of solutes are treated mathematically by assuming the properties of the field system are continuous. This is referred to as the continuum hypothesis (model). By treating the physical system properties as varying smoothly over space, differential calculus can be used to describe on a macroscale (hectares) all of the processes that vary on the microscale (molecular). Of course, all systems contain many discontinuities on the microscale. Discontinuities also occur on what may be considered the mesoscale (meters), such as the regions of soil, rubble, and bedrock. These and some of the microscale discontinuities can be taken into account based on the relationship between the physical property of the microsystem and the function used to model that property on the continuum scale. The continuum model uses the local average of the physical property for what is referred to as a representative elemental volume (REV), where the REV characterizes the local property of the system (Lichtner 1996). The dimensions of the REV are large on an atomistic scale but small relative to the scale over which the property changes. The properties of the REV include temperature, mineral content, ground water composition, porosity, pore saturation, ground water flow, etc. The microscale properties averaged over the REV define the macroscale properties used in continuum modeling. The appropriate size of the REV depends on the system to be modeled, and more than one REV is usually required. Different REV properties would be used to describe soil, bedrock, boulders, gravel, etc. Depending on the property, an average value may be determined from the REV itself, such as porosity and water flow, or small-scale variations may be measured and averaged, such as mineral abundance and compositions. In the present analysis of the literature, REV data include solid samples analyzed to identify the mineral content and compositions within the field systems, ground waters sampled from wells in the field, hydraulic properties measured for the rock, and rainfall and other meteorological records.

Recently, reactive transport modeling has been used to quantify the effects of coupled interactions between minerals, organisms, and dissolved species, including processes having nonlinear kinetics. These models do not presume local equilibria and include complex behavior of contaminant migration in heterogeneous porous systems. This ability to couple equations describing ground water flow; the advective, dispersive, and diffusive transport of solutes; and

large numbers of chemical reactions within reactive transport models requires a quantitative understanding of the physical and chemical properties of the solids and fluid that are involved. Almost all of the properties that contribute to the field behavior are complex and many remain the focus of research activities: thermodynamic equilibrium constants, dissolution and precipitation kinetics of rocks and minerals; aqueous diffusion coefficients and dispersivity of solutes; and porosity, tortuosity, and permeability of the host geology. The main focus of this report is the dissolution kinetics of minerals measured in laboratory tests and during natural weathering within catchments and aquifers.

The dissolution rates of minerals calculated based on field measurements and the rates measured in laboratory tests have been typically compared by one of two approaches: forward modeling and inverse modeling. Geochemical models based on weathering reactions for individual minerals and measured laboratory rates formulated in terms of mass transport are referred to as forward modeling. Rates derived from geochemical mass balances with fluxes measured for natural watersheds or aquifers based on the flow paths and fluid compositions are referred to as inverse modeling. Existing solution concentration (flux) data are used in inverse models to calculate the amount of each component that is input or removed by the set of reactions suspected to have caused the change in water composition between the initial and final samplings. Forward modeling predicts the final water composition from a known initial state and presumed set of reactions. Inverse modeling provides an explanation for the available data whereas forward modeling predicts the future evolution. Forward modeling is used to assess long-term performance, the reliability of the reactions (and transport processes) used in forward models can be assessed with inverse models. That is, inverse models provide the best means to assess the accurate use of laboratory measurements in forward models and that comparison is the primary focus of this report.

Weathering rates have been inferred from field measurements, measured by conducting laboratory tests with field samples, measured in laboratory tests with pure minerals, and measured in field tests with laboratory samples. Reported discrepancies between the weathering rates of particular minerals inferred from field studies (e.g., by mass balance approaches in soil profiles and watersheds) and those measured in laboratory tests typically range from about two to five orders of magnitude. It is not clear if the discrepancy arises from errors in kinetic theory applied to the laboratory rates, failure to adequately account for inhibiting factors in the field systems, artifacts in laboratory test methods, or poorly quantified uncertainties in the field conditions. Several factors that have been implicated as contributing to these discrepancies are listed below. These include various uncertainties in the physical and environmental characteristics that affect the field rate; factors related to the mineralogy, such as dissolution kinetics and solution saturation effects that affect both laboratory and field rates; and artifacts of the sample preparation and test methods that affect the laboratory rates. Most of these factors are evaluated in this report based on the key references listed and general information that is available.

Difficulty in quantifying the surface area and wetted surface in natural systems
Pačes 1983; White and Blum 1995; Brantley and Stillings 1996; Clow and Drever 1996; White et al. 1996; Brantley et al. 1999

Limitations on flow and transport into low permeability zones in heterogeneous materials in natural systems
White and Peterson 1990; Drever and Clow 1995; White 1995; Malmstrom et al. 2000

Transport control rather than reaction control in natural systems
Drever and Clow 1995; White 1995; Kump et al. 2000

Differences in degree of saturation and reaction affinity in laboratory experiments and in natural systems
Nagy et al. 1992 ; Burch et al. 1993; Velbel 1993; Clow and Drever 1996; Mogollon et al 1996; Kump et al. 2000; White 1995; Taylor et al. 2000a; Taylor et al. 2000b; Cama et al. 2000; Hellmann and Tisserand 2006

Slow precipitation of secondary minerals
Alekseyev et al. 1997; Steefel and Lichtner 1998; Baxter and DePaolo 2000; White and Brantley 2003

Inhibition by surface coatings in natural systems
Chou and Wollast 1984; Mast and Drever 1987; Oelkers et al. 1994 ; Nugent et al. 1998; Stillings and Brantley 1995; Carrol and Knauss 2005

Greater soil age in natural systems
Pačes 1983; Taylor and Blum 1995; White and Brantley 2003; Maher et al. 2004

Brief duration of laboratory experiments relative to natural systems
Swoboda-Coberg and Drever 1993

Temperature differences between in laboratory experiments and in natural systems
Velbel 1990; White and Blum 19995; White et al. 1999b

Lower pH values in laboratory experiments than in natural systems
Knauss and Wolery 1986; Casey et al. 1993; Chen and Bradley 1997.

Grain size effects in laboratory experiments
Anrhein and Suarez 1992; Anbeek 1992a; Anbeek 1992b; Anbeek 1993; Eggleston et al. 1989; Hodson et al. 1997; Hodson 1999; Holdren and Speyer 1985; Holdren and Speyer 1987;

Disturbed near-surface regions due to comminution (crushing for size reduction) in laboratory experiments
Petrovich 1981a; Petrovich 1981b; Eggleston et al. 1989;

The approach taken in the evaluations summarized in this report was to (1) consider the proposed contributions to the discrepancy that are listed above both as separate and accumulated effects, and (2) consider the methods used to determine the rates that lead to the proposed discrepancy. Silicate minerals are the primary focus of the evaluation because it is the dissolution rates of silicate minerals that are at the heart of the discrepancy. While the focus of the overall project is the spread of radioactive contaminants, the release of radionuclides is only discussed peripherally in this report in some examples due to limited information regarding field measurements. Most of the evaluations described in this report address mineral dissolution and the methods used to measure dissolution rates. The aspects of relating laboratory measurements to field behavior discussed in this report are generic and apply to radionuclides the same as to stable nuclides. The added effects of radioactivity (radiolysis and decay) will be considered in later analyses.

Section 2 provides a brief summary of the geological aspects pertinent to the issue, including the minerals used in literature examples as part of the evaluation, mineral conversions, and a discussion of the theoretical rate law for mineral dissolution. The latter is important because

chemical affinity effects have been cited often as the primary source of the discrepancy by some researchers and rejected by others. Section 3 presents a fairly detailed discussion of particle surface area, including methods for measuring it, how it affects the measured dissolution rate, and how it is integrated in the dissolution rate law. This is important because laboratory rates measured on a per-area basis are scaled (along with any errors and uncertainties) by many orders of magnitude to model field systems. Section 4 discusses the flow-through column test method, since that method is most-often used to measure dissolution rates in the laboratory. This section expands on the detailed evaluation of laboratory test methods presented elsewhere (Ebert 2010). Static tests to study the effects of secondary phase formation are included in Section 4. Section 5 provides a fairly detailed mathematical evaluation of the mass-balance method used by Pačes (1983) and Velbel (1985) (and others) to determine dissolution rates from field data. This is done to identify the various sources of uncertainty in the inferred mineral dissolution rates. Two other studies comparing field rates and laboratory rates for systems that are somewhat more controlled are included in Section 5 as examples of the effects of other factors. Studies conducted by Drever and students on small catchment areas represent better-controlled environments and provide insights into the effects of environmental variables. Studies by Zhu and co-workers were conducted using well waters rather than surface water and show another application of the mass balance modeling and comparison with dissolution rates measured in the laboratory. Also included are methods for modeling the wetted surface area and an analysis of how temperature is treated in these models. Section 6 provides a brief summary of field tests in which the surface alteration of the solid is examined to assess the corrosion process, including naturally-occurring glasses and waste forms, and the use of field lysimeters to better evaluate processes occurring under the field conditions. Section 7 provides discussion of the discrepancy of the laboratory and field rates based on these analyses, a summary of reactive transport forward modeling, which includes coupling chemical reactions with mass transport and utilizes both the laboratory and field methods, and a discussion of the relevance of the discrepancy and modeling approaches to surface disposal systems. Finally, Section 8 provides a summary of the report and list of conclusions and comments based on this evaluation. Comments are distinguished from conclusions because both the laboratory and field systems are complex and some aspects require further and more quantitative considerations beyond the scope of this analysis. Final comments are provided regarding the relevance of this review and analysis on future evaluations that will address modeling surface disposal systems with contaminated slags and concrete.

2 Geochemistry and Weathering Reactions

This section provides a brief introduction and background information for the approaches used by geochemists and geologists to study and model the natural weathering of minerals that are pertinent to both comparisons of mineral dissolution rates in the field and laboratory tests and the development of approaches for modeling the degradation of materials in surface waste disposal systems. The relative stabilities of minerals provide insights to both modeling and laboratory experiments, particularly under highly concentrated solution conditions where the precipitation of secondary phases is possible. Minerals that are formed at high temperatures and pressures deep in the earth's interior are unstable when contacted by meteoric or ground waters and dissolve or transform into secondary minerals that are more stable under near-surface conditions. The decomposition of rocks and minerals due to interactions with the earth's atmosphere, including water from rain and snow, dissolved gasses, and biological materials is referred to as weathering. Weathering is distinguished from erosion and scouring, which occur when a solid is disaggregated into finer particles by moving water or wind. Weathering is also distinguished from diagenesis and metamorphism, which address changes in existing rocks and minerals in the absence of atmospheric interactions, such as through heat and pressure.

Chemical weathering is the primary focus of this report because it leads to the production of transportable solutes. The effects of physical and biological weathering are taken into account implicitly through the size distribution of particles in the physical system being considered and the groundwater chemistry. Rain is naturally weakly acidic due to dissolved CO_2 forming carbonic acid (about pH 5.6). Carbonic acid is consumed by the hydrolysis of silicate minerals, such as the hydrolysis of orthoclase to form kaolinite

$$\underset{\text{orthoclase}}{2KAlSi_3O_8} + 2H_2CO_3 + 9H_2O \rightleftharpoons \underset{\text{kaolinite}}{Al_2Si_2O_5(OH)_4} + 4H_4SiO_4 + 2K^+ + 2HCO_3^-. \qquad (2.1)$$

Groundwater can be further acidified (to about pH 3) by NO_2 that is dissolved as nitric acid and SO_2 from volcanic eruptions or combusted fossil fuels that is dissolved as sulfuric acid. The dry deposition of these gasses is also important.

2.1 Mineralogy

There are three abundant rock-forming aluminosilicate minerals common in the earth's crust: potassium feldspar (K-spar) $KAlSi_3O_8$; albite $NaAlSi_3O_8$; and anorthite $CaAl_2Si_3O_8$. Solid solutions of K-spar and albite are common and called alkali feldspars, and solid solutions of albite and anorthite are called plagioclase feldspars (or simply plagioclase). Solid solutions of K-spar and anorthite are compositionally limited. Orthoclase is monoclinic $KAlSi_3O_8$ and microcline is triclinic $KAlSi_3O_8$ and is the preferred low temperature phase. Anorthoclase is triclinic $(K,Na)AlSi_3O_8$ and sanadine $(K,Na)AlSi_3O_8$, which is the preferred high temperature phase, is monoclinic. The solid solutions of albite and anorthite are identified by the anorthite content:

albite $NaAlSi_3O_8$
oligoclase (10 -30% anorthite) $(Na,Ca)(Al,Si)AlSi_2O_8$
andesine (30 -50% anorthite) $NaAlSi_3O_8$ - $CaAl_2Si_3O_8$
labradorite (50 -70% anorthite) $(Ca,Na)(Al,Si)AlSi_2O_8$
bytownite (70 -90% anorthite) $(NaSi,CaAl)AlSi_2O_8$
anorthite $CaAl_2Si_3O_8$.

Perthite is formed by the ingrowth of a plagioclase and an alkali feldspar (orthoclase or microcline), which form a separate phases (phase-separates) upon cooling.

The genesis of alteration phases will depend on the reaction conditions, most importantly the water chemistry. For example, albite will degrade to form gibbsite in acidic solutions with little dissolved silica and then form kaolinite in solutions with moderate amounts of dissolved silica

$$\underset{\text{albite}}{NaAlSi_3O_8} + H^+ + 7H_2O \rightleftharpoons Na^+ + \underset{\text{gibbsite}}{Al(OH)_3} + 3H_4SiO_4 \qquad (2.2)$$

and

$$\underset{\text{albite}}{2NaAlSi_3O_8} + 2H^+ + 9H_2O \rightleftharpoons 2Na^+ + \underset{\text{kaolinite}}{Al_2Si_2O_5(OH)_4} + 4H_4SiO_4. \qquad (2.3)$$

As the albite continues to dissolve, gibbsite reacts with the excess dissolved silica to form kaolinite

$$\underset{\text{gibbsite}}{2Al(OH)_3} + 2H_4SiO_4 \rightleftharpoons \underset{\text{kaolinite}}{Al_2Si_2O_5(OH)_4} + 5H_2O. \qquad (2.4)$$

After the gibbsite is consumed, kaolinite reacts with sodium and silica (which continues to be released as albite continues to dissolve) to form smectite (written as the Na-beidellite end-member)

$$\underset{\text{kaolinite}}{1.15Al_2Si_2O_5(OH)_4} + 0.3H^+ + 0.3Na^+ + 14H_4SiO_4 \rightleftharpoons \underset{\text{smectite}}{Na_{0.3}Al_{2.3}Si_{3.7}O_{10}(OH)_2} + 3.95H_2O. \qquad (2.5)$$

The regions of thermodynamic stability for minerals in contact with ground water solutions are often displayed as activity-activity diagrams, such as that for the Na_2O-Al_2O_3-SiO_2-H_2O system given in Figure 2.1. Such diagrams can be used to represent the evolution of the solution chemistry during weathering reactions. The phase boundaries are defined by the free energy of reaction between the two phases and the equilibrium conditions. The solubilities of quartz and amorphous silica are shown by the dashed lines.

The red arrows show the evolution of the solution chemistry as albite begins to dissolve into an initially dilute acidic water containing a small amounts of Na^+ and H_4SiO_4, the composition of which is identified for this example by the black dot.

- Step 1: Albite reacts with H^+ to form gibbsite and release Na^+ and H_4SiO_4 into solution until the solution composition reaches the phase boundary between gibbsite and kaolinite.
- Step 2: Albite reacts with H^+ to form kaolinite and release Na^+ and H_4SiO_4 into solution and gibbsite reacts with H_4SiO_4 in solution to form kaolinite. The H_4SiO_4 concentration remains constant until all of the gibbsite formed in Step 1 is consumed.
- Step 3: Albite reacts with H^+ to form kaolinite and release Na^+ and H_4SiO_4 into solution until the phase boundary between kaolinite and smectite is reached.
- Step 4: Albite dissolves to form smectite and release Na^+ and H_4SiO_4 into solution and kaolinite reacts with Na^+ and H_4SiO_4 in solution to form smectite. This continues until all of the kaolinite formed in Steps 2 and 3 is consumed.
- Step 5: Albite dissolves to form smectite and release Na^+ and H_4SiO_4 into solution until equilibrium is reached at the phase boundary between smectite and albite.

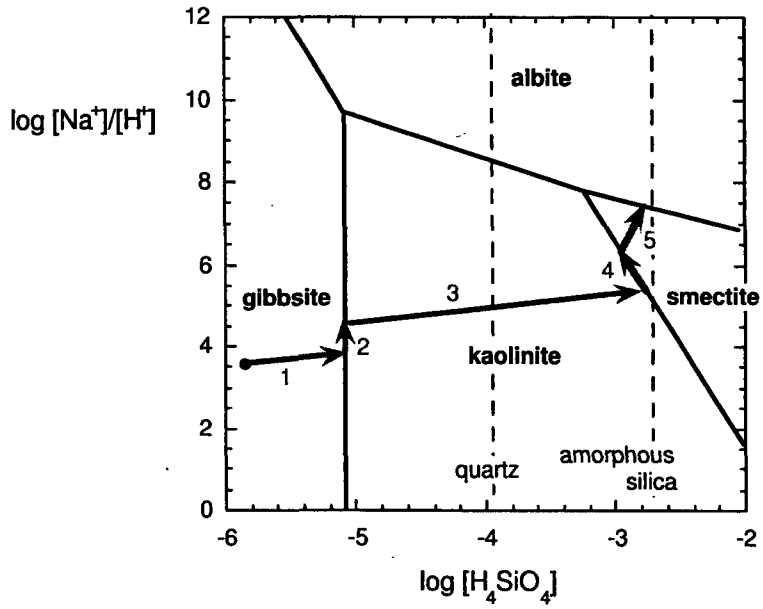

Figure 2.1. Schematic activity-activity diagram for dissolution of albite.

The activity diagrams provide useful descriptions of the solution chemistries, but do not account for the mineral dissolution kinetics and the often sluggish precipitation rates of product phases that will be important in real systems. For example, the actual path of step 2 in Figure 2.1 where gibbsite converts to kaolinite would probably lie within the kaolinite region due to the dissolution and precipitation kinetics. That is, gibbsite would be present even when the solution composition lies within the kaolinite field. The importance of this is that (1) the mineral composition will lag behind the solution composition and (2) the precipitation and dissolution kinetics of secondary minerals (e.g., gibbsite, kaolinite, and smectite) must be considered in addition to the dissolution kinetics of the primary minerals (e.g., albite) because the dissolution and precipitation kinetics are coupled. It may be misleading to compare the relatively short-term rates based on solution input-output relationships to the compositions of the solid phases in the system. The solids may provide a more reliable basis for estimating long-term weathering rates through the accumulation of weathering products (Velbel 1993). Laboratory tests with several minerals will be discussed in this report, and the chemical compositions of these and other minerals that are discussed are listed in Table 2.1 for convenience.

The relative durabilities of several common minerals that had been measured by various researchers were compared by Lasaga et al. (1994) and ranked in order of durability based on the time required to completely dissolve 1-mm particles into a dilute solution representing a surface water (pH 5 and 25°C). The results are summarized in Table 2.2; see Lasaga et al. (1994) for references to the rates used to calculate the mineral lifetimes. The relative durabilities of various primary and secondary minerals must be considered when assessing optional reaction paths in field weathering models and mass-balance operations.

Table 2.1. List of minerals and compositions used in this report

Mineral	Composition	Comment
Albite	$NaAlSi_3O_8$	Alekseyev, Fu
Almandine	$Ca_{0.2}Mg_{0.5}Mn_{0.2}Fe_{2.1}Al_2Si_3O_{12}$	Velbel
Analcime	$NaAlSi_2O_6$	Alekseyev
Andesine	$NaAlSi_3O_8$ - $CaAl_2Si_3O_8$	(30 -50% anorthite)
Anorthite	$CaAl_2Si_3O_8$	(70 -90% anorthite)
Biotite	$(K_{0.98}Mg_{1.00}Fe_{1.33}Ti_{0.18}Al_{0.33})(Al_{1.35}Si_{2.65})O_{10}(OH)_2$	Velbel
Biotite	$K_{3.85}Na_{0.02}(Mg_{1.2}Fe_{1.3}Al_{0.45})(Al_{1.2}Si_{2.8})O_{10}(OH)_2$	Velbel
Boehmite	AlO(OH)	Fu
Bytownite	$(NaSi,CaAl)AlSi_2O_8$	(70 -90% anorthite)
Calcite	$CaCO_3$	
Chabazite	$(Ca,Na_2,K_2,Mg)Al_2Si_4O_{12}\cdot 6H_2O$	
Chlorite	$(Mg_{1.81}Fe_{2.27}Al_{1.39})(Al_{1.23}Si_{2.77})O_{10}(OH)_8$.	Clow
Diaspore	AlO(OH)	
Diopside	$MgCaSi_2O_6$	
Dolomite	$CaMg(CO_3)_2$	
Enstatite	$MgSiO_3$	
Epidote	$Ca_2(Fe,Al)Al_2(SiO4)(Si_2O_7)O(OH)$	Velbel
Forsterite	Mg_2SiO_4	
Garronite	$Na_2Ca_5Al_{12}Si_{20}O_{64}\cdot 27H_2O$	
Gibbsite	$Al(OH)_3$	
Gypsum	$CaSO_4\cdot 2H_2O$	
Gyrolite	$Ca_4Si_6O_{15}(OH)_2\cdot 3H_2O$	
Halite	NaCl	
Halloysite	$Al_2Si_2O_5(OH)_4$	
Hydrotalcite	$Mg_6Al_2(CO_3)(OH)_{16}\cdot 4H_2O$	
Kaolinite	$Al_2Si_2O_5(OH)_4$	Fu
Labradorite	$(Ca,Na)(Al,Si)AlSi_2O_8$	(50 -70% anorthite)
Lizardite	$(Mg,Fe)_3Si_2O_5(OH)_4$	
Microcline	$KAlSi_3O_8$	triclinic
Microcline	$KAlSi_3O_8$	Clow
Muscovite	$KAl_3Si_3O_{10}(F,OH)_2$	

Table 2.1. (cont.)

Nepheline	$Na_3KAl_4Si_4O_{16}$	
Oligoclase	$(Na_{0.73}Ca_{0.27})Al_2Si_3O_8$	Clow
Orthoclase	$KAlSi_3O_8$	monoclinic
Phillipsite	$(Ca,K_2,Na_2)_3Al_6Si_{10}O_{32}\cdot 12H_2O$	
Plagioclase	$Ca_{0.38}Na_{0.62}Al_{1.38}Si_{2.62}O_8$	Zhu
Potassium feldspar	$KAlSi_3O_8$	K-spar
Pyrophylite	$Al_2Si_4O_{10}(OH)_2$	
Quartz	SiO_2	
Sanadine	$(K,Na)(Si,Al)_4O_8$	Alekseyev
Silica	SiO_2	
Smectite	$Na_{0.3}Al_{2.3}Si_{3.7}O_{10}(OH)_2$	
Smectite	$(K_{0.32}Fe_{0.25}Ca_{0.10}Mg_{0.39}Al_{1.93}Si_{3.54})O_{10}(OH)_2 \cdot nH_2O$	Clow
Smectite	$K_{0.27}Ca_{0.15}(Mg_{1.005}Al_{1.26})((Al_{0.36}Si_{3.64})O_{10}(OH)_2$	Zhu
sodic plagioclase	$Ca_{0.25}Na_{0.75}Al_{1.25}Si_{2.75}O_8$	Velbel
Staurolite	$Fe_2Al_9Si_4O_{22}(OH)_2$	Velbel
Thompsonite	$NaCa_2Al_5Si_5O_{20}\cdot 6H_2O$	
Tobermorite	$Ca_5Si_6O_{16}(OH)_2 \cdot 4H_2O$	
Wollastonite	$CaCO_3$	

Table 2.2. Estimated time to completely dissolve a 1-mm spherical particle at pH 5 and 25°C

Mineral	Time, years	Mineral	Time, years
Quartz	34,000,000	Enstatite	10,100
Kaolinite	6,000,000	Diopside	6,800
Muscovite	2,600,000	Forsterite	2,300
Epidote	923,000	Nepheline	211
Microcline	921,000	Anorthite	112
Albite	575,000	Wollastonite	79
Sanadine	291,000	Dolomite	1.6
Gibbsite	276,000	Calcite	0.1

2.2 Rate Law for Mineral Dissolution

The general formulation of the rate equation for silicate mineral dissolution includes a series of terms that quantify the kinetics due to catalytic and inhibiting processes and an affinity term, which quantifies the difference in free energy for the existing system and the system at equilibrium (Lasaga 1981; Aagaard and Helgeson 1982; Lasaga 1995). The general form of the rate equation used for transition state formulations is

$$rate_{net} = k_0 \bullet 10^{\eta * pH} \bullet \exp\left(-E_a/RT\right) \bullet \prod_j a_j^{\nu} \bullet fn(\Delta G_r) \ . \tag{2.6}$$

where k_0 is the intrinsic rate constant of the material, η is the pH dependence, and E_a is the activation energy for the Arrhenius form of the temperature dependence. These terms are often grouped and expressed as the forward rate, k_f. The pH and temperature are system variables with model coefficients η and E_a, respectively. The term k_0 is an empirical constant that depends on the mineral composition, although an analytical expression to calculate that dependence has so far eluded researchers. Additional terms may be needed to quantify the effects of variables such as the oxygen fugacity, chloride concentration, etc., based on a mechanistic or empirical understanding of the material dissolution behavior. These terms are expressed with a power law dependence a_j^{ν} , where v quantifies the effect of the activity of component j on the rate. The H^+ concentration affects the rate of most dissolution reactions and is shown explicitly in this representation. The form of the pH dependence is empirical. Although the concentration of active surface sites could be included as one of the a_j^{ν} terms in the rate equation, neither the concentration of active surface sites not the functional dependence is currently known for most minerals. The rate is instead expressed on a per unit total surface area basis. The last term, $fn(\Delta G_r)$, represents the deviation of the system from thermodynamic equilibrium with respect to the rate-limiting reaction, and is expressed as an empirical function of the Gibbs free energy of the reaction. That term can be thought of as the effect of the saturation state of the system on the dissolution rate. The functional form of the free energy dependence depends on the reaction mechanism (see Lasaga 1995). For example, the functional relationship commonly used in transition state theory models is

$$fn(\Delta G_r) = 1 - \exp\left(\frac{\Delta G_r}{RT}\right). \tag{2.7}$$

The change in free energy with reaction progress is defined as the thermodynamic chemical affinity, $-A$, which can be expressed in terms of the saturation of the solution as

$$fn(\Delta G_r) = 1 - \exp\left(\frac{\Delta G_r}{RT}\right) = 1 - \exp(-A) = 1 - \frac{Q}{K_{sp}}, \tag{2.8}$$

where Q is the ion activity product of the solution and K_{sp} is the solubility product of the dissolving solid. The components included in Q are the same as those included in K_{sp}. The ratio Q/K_{sp} quantifies the deviation of the system from equilibrium (and from saturation). The general rate law with this free energy dependence is written as

$$rate_{net} = k_0 \bullet 10^{\eta \bullet pH} \bullet \prod_j a_j^{\nu} \exp\left(-E_a/RT\right)\left(1 - Q/K_{sp}\right). \quad (2.9)$$

The term $(1\text{-}Q/K_{sp})$ is referred to as the affinity term. When the system is far from equilibrium, the value of the affinity term is very near one. When the system is at equilibrium, the value of the affinity term is zero. The rate equation is comprised of two parts: the leading terms describe the dissolution kinetics under far-from-equilibrium conditions and the affinity term moderates the rate as the system approaches equilibrium. As a point of caution, the mechanism may change as the system approaches equilibrium such that both the kinetic and affinity term expressions need to be modified. This could occur because a process that has negligible impact on the rate under far-from-equilibrium conditions may limit the rate near equilibrium. The forms of the affinity term and the preceding terms are all empirical. Although the simple linear form given in Equation 2.9 is found to represent many systems, the affinity term is sometimes expressed as an exponential function such as $(1 - Q/K_{sp})^{\sigma}$ or $[1 - (Q/K_{sp})^{p}]^{q}$ or as a sum of two terms to better represent more complicated mechanisms. Although work is in progress to determine parameter values from first principles, the form of the affinity term and the parameter values used in the rate law are currently determined from laboratory experiments, including which species to include in the $\prod_j a_j^{\nu}$ term.

Another important role of the affinity term is that it quantifies the effects of other materials on the dissolution behavior of the material of interest through the common solution composition. Rate expressions such as Equation 2.9 can be written for all materials that dissolve by affinity-controlled reactions, each with the appropriate values for k_0, η, E_a, and K_{sp}. The reaction affinities of two or more minerals contacted by the same solution will differ according to their equilibrium constants (K_{sp}) and deviation from equilibrium (Q/K_{sp}). The solution could be undersaturated, saturated, or oversaturated with respect to a particular mineral, which would then dissolve, be at equilibrium, or precipitate according to the controlling kinetics. The dissolution or precipitation of one of the minerals would affect the solution chemistry and behaviors of the other minerals. The complex mineral and solution systems in field systems are expected to affect the kinetics and the dissolution rates determined from field data. Geochemical computer codes such as Geochemist's Workbench, PHREEQ, and EQ3 can be used to calculate saturation indices for solutions in contact with a large number of solid phases and simulating dissolution by stepwise changes to the solution chemistry. The saturation index (SI) is defined as

$$SI = \log\left(\frac{Q}{K_{eq}}\right) \quad (2.10)$$

Gross kinetic effects have been approximated by constraining the precipitation or dissolution of particular phases (for example, preventing the precipitation of quartz).

2.3 Congruent and Incongruent Dissolution

If a mineral simply dissolves to generate aqueous species, the dissolution mechanism is referred to as congruent dissolution. If a secondary solid phase forms and consumes one or more of the released species, the dissolution mechanism is referred to as incongruent dissolution. Almost all of the mineral phases considered in this report dissolve incongruently. The dissolution rate of the primary mineral and the precipitation rate of the secondary mineral are coupled through the solution chemistry. However, as discussed briefly in Section 2.1 and in more detail in Section 4,

the precipitation of the secondary phase follows separate kinetics and often lags behind dissolution of the primary mineral. The precipitation of secondary phases can accelerate the dissolution of the primary mineral and slow the approach of the system to equilibrium. This effect is important in the evolution of alteration phase assemblages during the corrosion of mineral phases (e.g., Wronkiewicz et al. 1992) and the dissolution of waste glass (Ebert et al. 1991). The effects of precipitated phases on mineral dissolution rates are very likely important contributing factors to the difference between the field and laboratory dissolution rates of the primary phases of interest. The dissolution rates measured in laboratory tests in the absence of alteration phases can be very different than that dissolution rates in field systems in the presence of alteration phases. This is because the overall reaction changes from the simple dissolution of the primary phase to the coupled dissolution of the primary phase and precipitation of the secondary phase. The thermodynamic driving force changes and the kinetic dependencies change. This is discussed in Section 4.2.

3 Particle Surface Area

Dissolution and precipitation reactions occur on specific surface sites having the necessary geometry and energetics to support the reaction; these are often referred to as active sites. The reactivity of a site may depend on its shape and structure, and defect sites in the surface structure, such as corner, edge, or kink sites, are usually the most reactive. The surface area of interest for kinetic formulations of reaction rates is the reactive surface area representing the concentration of these reactive sites on the surface; atomistic models often include the mole fraction of active sites as an independent parameter in the formulated rate law (e.g., Aagaard and Helgeson 1982, Lasaga 1984; Lasaga 1995). Because the reactive surface sites cannot currently be quantified directly, the total surface area is used in rate calculations and assumed to be proportional to the reactive surface area through the surface roughness, fractal dimension of a grain, morphology of etch pits, etc. Clearly, these will change over time as the mineral dissolves (or precipitates). Most laboratory tests used to measure dissolution rates are conducted with crushed materials to provide enough surface area that that extent of dissolution can be determined by analyzing the test solution. The use of small particles adds uncertainty to the rate due to uncertainty in the surface area available for reaction (dissolution) uncertainty, the reactivity of the surface (i.e., the concentration and nature of active sites), and the change in both over time. The uncertainties in the laboratory rates measured with small particles are one reason for discrepancies with the field rates. The analyses conducted as part of this report are intended to evaluate the uncertainties and fully take them into account when comparing laboratory and field rates.

In this section, approaches that are used to quantify the surface area of a laboratory sample of crushed material are described and evaluated, including the impact of the assumed surface area on the rate that is determined using a laboratory test. The accuracy of the surface area that is used to calculate the dissolution rate of a laboratory test sample is of critical importance because it is used to up-scale the results of laboratory tests conducted with samples having surface areas on the order of cm^2 to macroscopic systems (field systems) having surface areas on the order of km^2 and also to down-scale those results for comparisons to molecular-scale models that consider total surface areas on the order of nm^2. Perhaps more important than the available surface area is the reactivity of the surface: differences between the roughness of freshly crushed material surfaces commonly used in laboratory tests and the aged materials present in the field will have a very significant effect on the dissolution rates. Test materials prepared by comminution (crushing for size reduction) have sharp edges that are more reactive than the smoothed surfaces of aged materials. Both the methods to estimate the surface area of particulate samples and the effects of roughness are considered in detail in this section, since both have a significant effect on the dissolution rates measured in laboratory tests and contribute to the differences between laboratory and field rates. The reactive surface areas in natural field systems must also take into account fracture and pore surfaces with restricted accessibilities and water contact depending on the degree of saturation and ground water flow, both of which vary with time.

3.1 BET Surface Area

Many researchers use the surface area measured with the method that was developed by Brunauer, Emmett, and Teller (Brunauer et al. 1938). The so-called BET method is based on the physical adsorption of a gas (typically N_2 or Kr) onto a surface at a temperature near the condensation temperature of the gas (e.g., liquid nitrogen temperature). The sorption isotherm, which is a plot of the volume of gas adsorbed vs. the relative partial pressure at a fixed temperature, is analyzed to determine the amount of gas that is sorbed at monolayer coverage.

The area occupied by each gas molecule or atom is then used to calculate the surface area of the specimen based on the amount of gas that forms the monlolayer. For example, a nitrogen molecule covers 0.162 nm^2 and Kr 0.152 nm^2 at liquid nitrogen temperature (78 K). It is commonly found that the surface area measured with Kr is less than that measured with N_2 (Brantley and Mellott 2000). The BET measurements usually require finely divided solids to provide sufficient surface area to sorb enough gas to cause a measurable pressure difference in the gas phase. The BET equation is

$$\frac{1}{\upsilon\left[(P_{sat}/P)-1\right]} = \frac{C-1}{\upsilon_m C}\left(\frac{P}{P_{sat}}\right) + \frac{1}{\upsilon_m C} \tag{3.1}$$

where υ is the quantity of gas that is sorbed and υ_m is the amount of gas in a monolayer (both normalized as g gas g^{-1} solid), P_{sat} is the saturation pressure of the gas at the temperature of adsorption, P is the equilibrium pressure, and C is the BET constant:

$$C = \exp\left(\frac{E_1 - E_L}{RT}\right) \tag{3.2}$$

where E_L is the heat of adsorption for the first layer (adsorbate-surface), E_1 is the heat of adsorption for second and higher layers (adsorbate-adsorbate), R is the ideal gas constant, and T is temperature. For most systems, $E_L > E_1$ and the first layer will be completed before multilayers form. The difference in the heats of adsorption for the first and subsequent layers varies significantly for different sorbents and sorbates. For most systems, a plot of the left-hand side of Equation 3.1 vs. (P/P_{sat}) is linear over the range $0.05 < (P/P_{sat}) < 0.35$ and the slope and y-intercept can be used to calculate υ_m and C as

$$\upsilon_m = \frac{1}{\text{slope} + (y - \text{intercept})} \tag{3.3}$$

and

$$C = 1 + \frac{\text{slope}}{(y - \text{intercept})}. \tag{3.4}$$

The low end of this range corresponds to the famous "point B" knee of the isotherm that is taken to indicate the completion of the first monolayer and initiation of multilayer adsorption. The surface area S is calculated from the number of moles of gas adsorbed in the monolayer n_m and the coverage of a gas molecule σ

$$S = N_A \sigma n_m \quad = \frac{N_A \sigma \upsilon_m}{V}, \tag{3.5}$$

where N_A is Avogadro's number and V is the molar volume of the gas (at 78 K). It is worth noting that isotherms can be generated by sorption of water at near-ambient temperatures and a water molecule covers about 0.114 nm^2 (1.14×10^{-19} m^2) of surface (Ebert et al. 1991). It is

possible that water can access small pores that are too small for N_2 or Kr, and water sorption may provide a more representative measure of the surface area available for reaction.

The assumption that all multilayers beyond the first have the same heat of adsorption is clearly a simplification. If E_2 is more similar to E_1 than E_L, the knee in the isotherm could occur at higher pressures and lead to a higher value of v_m. It is not unreasonable that the BET-measured surface area could be twice the actual surface area due to this artifact. As an example, the sorption of N_2 onto a finely ground mineral is shown in Figure 3.1. The slight hysteresis seen in the desorption leg for $P/P_{sat} > 0.5$ suggests that a small portion of the gas is entering pores or cracks in the crushed solid. Figure 3.1b shows the adsorption leg with the data for relative pressures between 0.05 and 0.35 regressed linearly to parameterize the BET equation. The slope is 1.31 and the y-intercept is 0.616. Use of these values in Equations 3.3 and 3.4 gives a monolayer volume of 0.519 $cm^3\ g^{-1}$ and a C value of 3.13. The molar volume of nitrogen gas is 24.5 L mol^{-1} at standard temperature and pressure and 6.413 L mol^{-1} at liquid nitrogen temperature (78 K), which

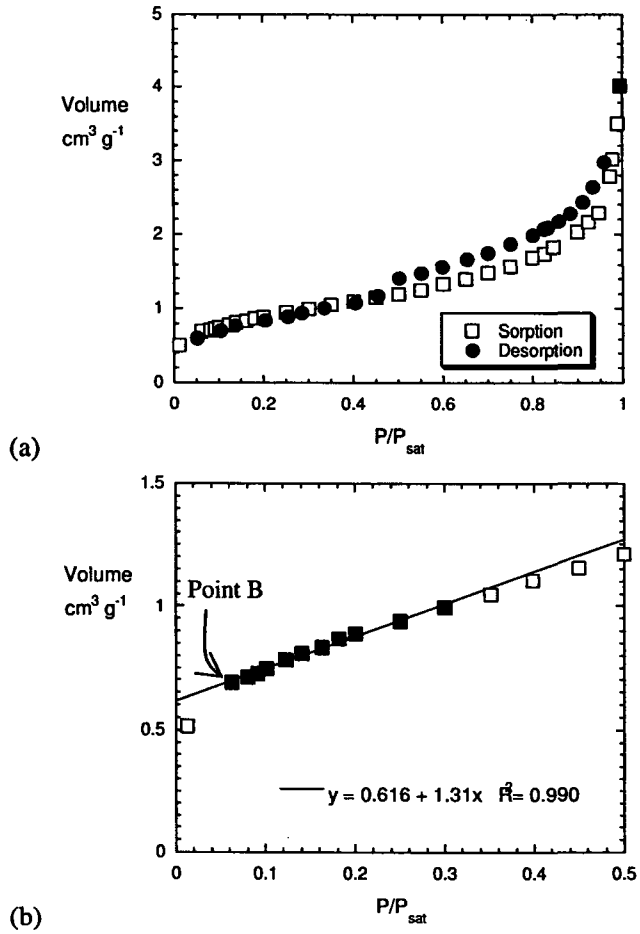

Figure 3.1. N_2 adsorption onto a mineral (a) sorption and desorption (b) linear fit to sorption data for $0.05 < P/P_{sat} < 0.35$. The open symbols were excluded from fit. Point B identifies the pressure at which the isotherm changes from being concave with the pressure axis as the first monolayer is completed to being linear as the second layer forms.

corresponds to 1.06×10^{-20} cm^3 $molecule^{-1}$. The monolayer volume of 0.519 cm^3 g^{-1} corresponds to a specific surface area of 7.90 m^2 g^{-1} solid.

3.2 Geometric Surface Area

The surface area of small particles is often estimated using a geometric approximation for a particular sieved size fraction. In this approach, the particles are modeled to have a simple geometry with dimensions related to the sieve mesh openings. For example, the particles can be modeled as cubes with an edge length or spheres with a diameter equal to the arithmetic average of the sieves used to isolate the fraction. The specific surface area (surface area/unit mass) can be calculated from the geometric surface area and volume of the average particle and the density of the material. For a spherical particle with diameter d and density ρ, the specific surface area is

$$\bar{S} = \frac{6}{d\rho} \tag{3.6}$$

For other particle shapes, different constants are used in the numerator. Constants for other shapes will be greater than 6, since the sphere provides the minimum surface area per volume.

The BET surface area is almost always greater than the geometric surface area, and the ratio is referred to as the surface roughness factor (λ). For non-porous materials, the surface roughness factor is on the order of 2-5 for properly modeled particles, but it can be much larger for porous materials. For example, White and Brantly (2003) reported a roughness factor of 110 for fresh biotite modeled as spherical particles. For some materials, the roughness factor includes internal surfaces in pores and capillaries. Adhering fines generated when the material is crushed can greatly increase the measured BET surface area and must be removed for an accurate measurement. The dissolution of fines will also dominate the initial dissolution in laboratory tests. The BET surface areas of several size fractions of crushed microcline measured by Holdren and Speyer (1987), Hodson et al. (1997), Hodson (1980), and Stillings and Brantley (1995) are reproduced in Figure 3.2 (Brantley and Mellott 2000). The function for the geometric surface areas of spheres of microcline (density = 2.56 g/cm^3) regressed to the pooled results is included in the plot. The sphere model (Equation 3.6) accurately represents the relationship between particle dimension and BET surface area when multiplied by a roughness factor of 7.

The role of the surface area in rates from laboratory measurements is to scale the response measured with a small specimen to larger field systems. However, the amounts of materials reacted in laboratory tests (and in the field) are related to the volume (or mass) that has reacted over the test interval, not the surface area *per se*. Although it is implicitly assumed that the volume (and mass) reacted is proportional to the surface area that relationship changes as the material dissolves. The fresh surfaces of particles prepared for laboratory tests are usually rougher than the reactive surfaces that are exposed on materials in the field. Crushed materials will have more high-energy surfaces than will weathered materials, including more fractured edges, a greater abundance of steps and crevices, and greater surface strain. Material at such sites on the surface will be more reactive than the bulk material and the surface will tend to become smoother as the particle dissolves. This is discussed further in Section 3.5. In addition, the mass of the specimen decreases as it dissolves. The effect of dissolution on the surface area will be negligible for large specimens but becomes significant for small particles less than about 100 micrometers. Based on how it is used, it is more important that the surface area used to calculate the dissolution rate represents the mass of material that has dissolved during the test duration than the initial surface area. Although the BET method probably provides a more accurate measure

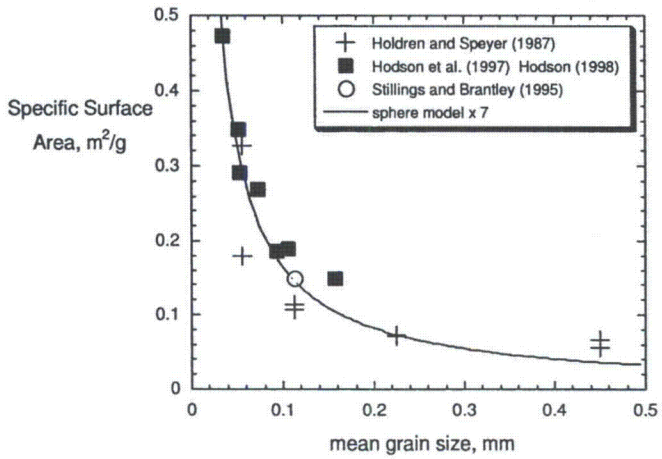

Figure 3.2. Data from Brantley and Mellott (2000): BET surface areas for various grain sizes of microcline.

of the surface area at any particular point of dissolution, the geometric surface area probably provides for a more accurate determination of the *volume (mass)* of material that has been dissolved during a test and is probably better suited for up-scaling laboratory rates to reaction in the field.

The volume of reacted material that is calculated using the geometric surface area is expected to represent the amount of dissolved material more accurately than the BET surface area. This is illustrated in Figure 3.3, where the medium and dark grey areas represent the initial and final particle shapes. The volume that dissolves is represented by the area between these perimeters. The BET areas measured before and after dissolution will provide measures of the irregular perimeters of the medium and dark grey areas, whereas the geometric areas determined based on the particle dimensions (e.g., from sieving) provide measures of the dashed and dotted circles that are drawn to approximate the particles before and after dissolution. Empirically (visually), the geometric approximation provides a poor estimate of both surface areas but a good estimate of the dissolved volume. Using the BET surface areas suggests too large a dissolved volume and

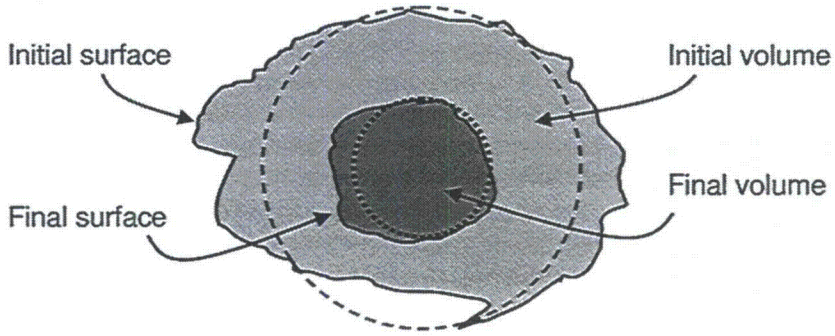

Figure 3.3. Illustration of particle surface area and volume with geometric approximation.

too high a dissolution rate. The final particle shape in Figure 3.3 is drawn to be smoother than the initial particle due to the preferential dissolution of rough edges, such that the roughness factor decreases as the particle dissolves. The roughness factor could increase if the porosity increased to a greater extent than the volume decreased as the particle dissolved. This would obviously complicate modeling of the dissolution behavior of the particle over time. Using the geometrical approximation (without the roughness factor) simplifies the calculations while accurately tracking the reacted volume and relating it to solution results by mass balance. This is discussed further in the following section.

3.3 Relationship between Particle Size and Specific Surface Area

Analyses of crushed glass shows a Gaussian distribution of particle sizes that is nearly centered within the range of sieve sizes 75-to-212 μm, as shown in Figure 3.4. Each point represents the fraction of particles within the small size range between points. The area fraction contributed by the particles within that size range is calculated by (1) modeling the particles as spheres with diameters given by the largest size in that range, (2) calculating the specific surface area for particles in each size range, (3) multiplying those specific surface areas by the fraction of particles in that size range, and (4) normalizing those products to 100%. Using the arithmetic average of the particle dimension (143.5 μm for the particles in Figure 3.4) to calculate the specific surface area will overestimate the total surface area slightly. This shows the important contribution of small particles to the initial test response. However, the surface area of small particles will decrease faster than that of large particles as the particles dissolve, so the relative contribution of small particles to the total surface area will decrease as the material dissolves. The surface area calculated with the average particle size within the size fraction will become more representative of the test conditions as more material dissolves.

Figure 3.5 shows a scanning electron photomicrograph of the crushed glass that was analyzed to generate Figure 3.4; the particles are clearly not spherical. However, the white circles drawn with diameters of about 143.5 μm show visually that the surface area of a sphere having that diameter is a reasonable representation of the surface area of an average particle. The surface roughness of crushed glass is expected to be similar to that determined for minerals crushed to similar sizes,

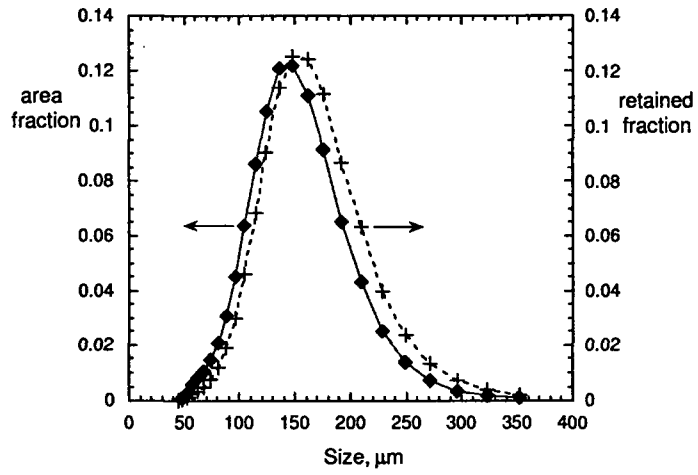

Figure 3.4. Particle number fraction (+) and area fraction (◆) for crushed and sieved glass based on measured particle dimensions assuming spherical particles.

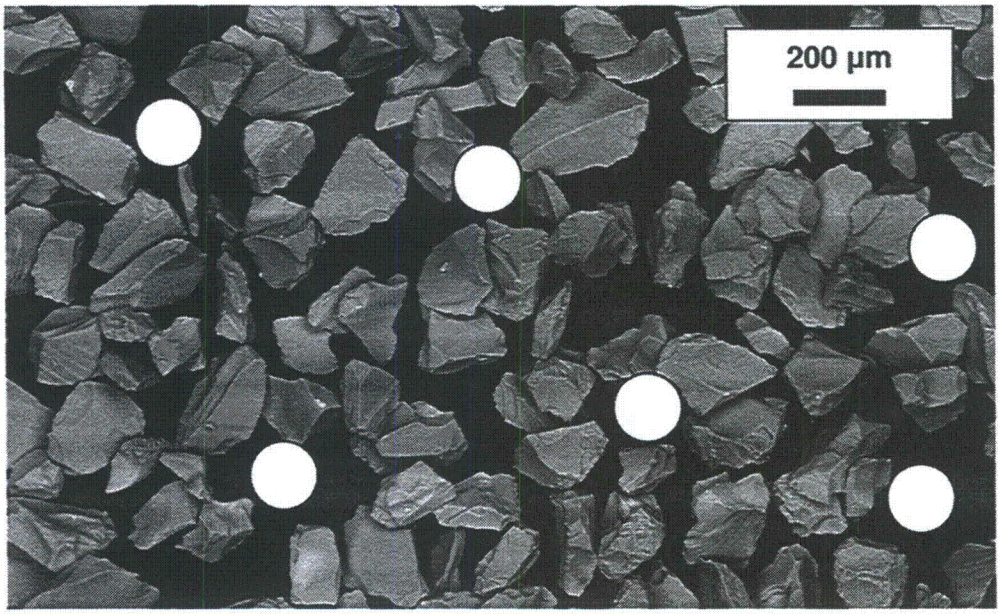

Figure 3.5. Photomicrograph of crushed glass and circles drawn with ~143.5 µm diameters to represent the modeling of particles as spheres.

which is about 7, since they are brittle materials. The surface roughness is expected to decrease as the material dissolves.

A simple method to take the change of surface area of crushed samples during the test into account is to model the particles as shrinking spheres (e.g., McGrail et al. 1997a). The decrease in surface area is related to the amount of material that has dissolved by calculating the final surface area of the reacted glass, S_f, from the mass of the sample at the end of the test interval as calculated from the dissolution rate and reaction time as:

$$S_f = S_o \bullet M^{1/3} \bullet m^{2/3} = \left\{\frac{6}{\rho \bullet d_o}\right\} \bullet M^{1/3} \bullet m^{2/3} \tag{3.7}$$

where ρ is the density of the material, S_o and d_o are the initial surface area and diameter of the glass particle, M is the initial mass of the sample, and m is the final mass of the sample. The final mass of the sample is calculated from the mass that has dissolved as

$$m = M - rate \times S_o \times t\,. \tag{3.8}$$

The fractional change in the surface area is

$$\frac{S_f}{S_o} = \frac{\left\{\frac{6}{\rho \bullet d_o}\right\} \bullet M^{1/3} \bullet m^{2/3}}{\left\{\frac{6}{\rho \bullet d_o}\right\} \bullet M} = \left(\frac{m}{M}\right)^{2/3}. \tag{3.9}$$

Analogous expressions can be derived for other particle shapes. A key point to be taken from Equation 3.9 is that the surface area decreases more slowly than the mass as the particles dissolve. This impacts the up-scaling of the area and mass dissolved and of the dissolution rate.

3.4 Effects of Crushing on Particle Surface

The near-surface regions of both crystalline and amorphous materials are damaged when crushed to generate particles for testing. Two major aspects of the disturbed surface region enhance dissolution relative to the bulk material: fracturing caused by tensile stress and plastic deformation caused by local compressive and shear stresses (Petrovich 1981). The relative importance of each depends on the mechanical properties of the material. Brittle fracture will be the dominant effect in brittle materials and contribute little to subsurface deformation, but microplastic deformation will generate a (relatively) thick disturbed layer in other materials. The disturbed surface can affect the dissolution kinetics of the mineral by (1) increasing the active surface area, (2) increasing the solubility, and (3) increasing the rate constant. The usual reason for crushing the test material is to increase the surface area to enhance the test response (e.g., to generate sufficiently concentrated solutions), and the measured dissolution rates are almost always normalized to the total surface area. The relationship between the density of active sites and the total surface area may depend on the particle size and the types and density of active sites will likely be affected by crushing. The contribution of the surface free energy to the molar free energy of the solid becomes significant for very small particles. This is referred to as the Kelvin effect or the Gibbs-Thompson effect. This effect is observed experimentally by the higher solubility of samples with fine material compared to samples with larger particles. The Gibbs free energy of the solid/solution interface and the size of the grains must be known to quantify the effect. The Ostwald-Freundlich equation adapts the Kelvin equation to solutions as

$$\frac{S(r)}{S(\infty)} = \exp\left(\frac{2\gamma\overline{V}}{R_g\, r\, T}\right) \tag{3.10}$$

where $S(r)$ is the solubility of grains with radius r and $S(\infty)$ is the solubility of large particles, γ is the Gibbs free energy of the solid/solution interface, $\overline{V}$ is the molar volume of the solid, R_g is the ideal gas constant, and T is absolute temperature. For example, the solubility of a material with a particle size of 25 nm with γ = 120 mJ m^{-2} will be twice that of large particles at room temperature (Petrovich 1981b). Although such small particles are not used in laboratory tests to measure dissolution rates, this quantifies the importance of removing fines from the crushed materials that are used. In addition, fracture edges (blade edges) and sharp points on crushed materials will have the same effect as minute particles on solubility. If r_1 and r_2 give the maximum and minimum radii of a surface feature, then Equation 3.10 can be written as

$$\frac{S(r_1, r_2)}{S(\infty)} = \exp\left[\frac{2\gamma\overline{V}}{R_g\, T}\left(\frac{1}{r_1} + \frac{1}{r_2}\right)\right]. \tag{3.11}$$

The solubility of a crystalline phase is usually lower than that of its amorphous form, for example, the solubility of quartz is lower than that of amorphous silica. When the structure of the near-surface region is disturbed by crushing, the solubility of material in that domain is increased. The more soluble domains control the metastable solubility of the specimen. The increased solubility due to the Kelvin effect implies an increase in the dissolution rate constant (Holdren and Berner 1979).

To relate the atomistic model for dissolution to the macroscopic (or mesoscopic) scale of laboratory experiments, the macroscopic rate constant k can be expressed as the product of the single-site dissolution rate constant k^* and the concentration of reactive sites n^*

$$k = k^* n^*. \tag{3.12}$$

From above, the value of k^* is sensitive to the particle size and the value of n^* may be sensitive to the particle size, although the effects are difficult to separate. Following Petrovich (1981), the free energy of a reactive site will depend on whether it is located on a large particle or a very small particle due to the Gibbs free energy of the solid/solution interface. Representing this difference in free energy as $\Delta G_{min}(r)$, it can be added to the free energy for reaction ΔG_r to produce the transition state relationship

$$\frac{k^*(r)}{k^*(\infty)} = \exp\left(\frac{\Delta G_r(r) - \Delta G_{\min}(r)}{k_g T}\right) \tag{3.13}$$

where k_g is the Boltzmann constant for the dissolution reaction at a single site. The effect of particle size on solubility is greater than the effect of particle size on the dissolution rate. The value of n^* is sensitive to the material surface, having lower values for low index crystal faces and higher values for high index faces. As dissolution proceeds, the average value of n^* will decrease as the more-reactive regions are consumed and the surface becomes dominated by less-reactive regions, that is, as the surface becomes smoother. This will also affect the values of k and ΔG_r, which will decrease as the surface relief approaches steady-state conditions on both the atomic and macroscopic scales. It is the dissolution kinetics under these steady-state conditions that should be used for comparisons with field behavior and for long-term predictions.

3.5 Relationship between Particle Size and Dissolution Rate

Holdren and Speyer (1987) measured the dissolution rates of various size fractions of several minerals. The results for plagioclase feldspars and alkali feldspars are provided in Tables 3.1 and 3.2. The results of dissolution tests with five size fractions of Hybla alkali feldspar are shown in Figure 3.6; note that the results for different size fractions are off-set in the y-direction for clarity. Tests with all size fractions were conducted with 4.75 g of feldspar in 475 mL of solution, so the exposed surface area was much greater in tests with smaller size fractions. The dissolution rate is reflected in the concentration of SiO_2. The dissolution rates based on the accumulation of dissolved SiO_2 are surprisingly similar for the four largest size fractions and only 1.5-times faster for the smallest size fraction (-400 mesh). The similarity is surprising because the available surface area is significantly different for the different size fractions. Although the results for the -400 mesh are shown with a linear fit, a quadratic fit is slightly better, which may reflect the loss of surface area as the material dissolves. Holdren and Speyer (1987) measured the surface areas of the various fractions with BET. They evaluated their data using the relationship

$$\text{rate}_{\text{bulk}}\ (\text{mol/s}) = \text{rate}\ (\text{mol/m}^{2m}\text{/s}) \times (\text{surface area, m}^2)^m \tag{3.14}$$

where $\text{rate}_{\text{bulk}}$ is the measured dissolution rate based on the amount of silica released into solution, rate is the intrinsic dissolution rate of the mineral with an undefined dependence on the surface area. These tests were intended to evaluate the assumption that the rate depends linearly on the surface area (i.e., $m = 1$). The units on the intrinsic rate must reflect the surface area dependence.

Table 3.1. Test Results from Holdren and Speyer (1987) for plagioclase feldspars

Size Fraction, mesh number	BET surface area, m^2/g	Geometric surface area, m^2/g	Roughness Factor[a]	Bulk rate, pmol Si/g/s
Evje Albite (density = 2.62 g/cc) at pH 3				
+30	0.034	—	—	4.11
-30 +50	0.036	0.035	1.03	4.79
-50 +100	0.049	0.070	0.70	5.71
-100 +200	0.066	0.140	0.47	8.07
-200 +400	0.154	0.281	0.55	6.96
-400	1.19	—	$\lambda_f = 4.3$	17.13
Mitchell Co. Oligoclase (density = 2.65 g/cc) at pH 3				
+30	0.065	—	—	3.63
-30 +50	0.079	0.035	2.24	5.13
-50 +100	0.09	0.071	1.27	6.14
-100 +200	0.128	0.141	0.91	5.39
-200 +400	0.334	0.284	1.18	2.71[b]
-400	0.889	—	$\lambda_f = 5.2$	10.11
Saranac Lake Andesine (density = 2.67 g/cc) at pH 3				
+30	0.110	—	—	6.83
-30 +50	0.119	0.036	3.34	8.33
-50 +100	0.134	0.071	1.88	8.78
-100 +200	0.21	0.142	1.47	8.39
-200 +400	0.386	0.286	1.35	11.39
-400	1.088	—	$\lambda_f = 6.3$	24.72
Crystal Bay Bytownite (density = 2.71 g/cc) at pH 3				
+30	0.099	—	—	79.2[b]
-30 +50	0.130[c]	0.036	3.60	27.8
-50 +100	0.127	0.072	1.76	27.8
-100 +200	0.214	0.145	1.48	45.8
-200 +400	0.473	0.290	1.63	79.2
-400	1.62	—	$\lambda_f = 7.1$	200
Grass Valley Anorthite (density = 2.74 g/cc) at pH 3				
+30	0.483[b]	—	—	300
-30 +50	0.619	0.037	16.94	381
-50 +100	0.700	0.073	9.58	429
-100 +200	0.757	0.146	5.18	514
-200 +400	1.02	0.294	3.47	597
-400	4.475	—	$\lambda_f = 10.6$	758

[a]Numerical values for arithmetic average of mesh opening dimension; values of λ_f from Anbeek (1992).
[b]Result excluded from plot in Figure3.7a.
[c]Reported value from Holdren and Speyer (1987) identified as being incorrect by Anbeek (1992).

Table 3.2. Test Results from Holdren and Speyer (1987) for alkali feldspars

Size Fraction, mesh number	BET surface area, m^2/g	Geometric surface area, m^2/g	Roughness Factor[a]	Bulk rate, pmol Si/g/s
Keystone Microcline, run 1 (density = 2.56 g/cc) at pH 3				
+30	0.060	—	—	2.53
-30 +50	0.067	0.034	1.96	3.38
-50 +100	0.073	0.068	1.07	4.11
-100 +200	0.114	0.137	0.83	3.19
-200 +400	0.327	0.274	1.19	1.78[b]
-400	1.488	—	$\lambda_f = 3.6$	8.53
Keystone Microcline, run 2 (density = 2.56 g/cc) at pH 3				
+30	0.060	—	—	3.24
-30 +50	0.067	0.034	1.96	3.93
-50 +100	0.073	0.068	1.07	3.94
-100 +200	0.114	0.137	0.83	3.43
-200 +400	0.327	0.274	1.19	1.78[b]
-400	1.488	—	$\lambda_f = 3.6$	7.03
Bancroft Microcline (density = 2.56 g/cc) at pH 2				
+30	0.045	—	—	3.98
-30 +50	0.056	0.034	1.64	4.69
-50 +100	0.072	0.068	1.05	5.42
-100 +200	0.107	0.137	0.78	4.6
-200 +400	0.179	0.274	0.65	3.65
-400	0.967	—	$\lambda_f = 3.2$	11.2
Perth Perthite (density = 2.58 g/cc) at pH 3				
+30	0.036	—	—	3.38
-30 +50	0.039	0.034	1.13	3.71
-50 +100	0.060[c]	0.069	0.87	4.19
-100 +200	0.089	0.138	0.65	4.03
-200 +400	0.277	0.276	1.00	1.68[b]
-400	1.221	—	$\lambda_f = 2.9$	4.07[b]
Hybla Alkali Feldspar (density = 2.56 g/cc) at pH 3				
-30 +50	0.05	0.034	1.46	4.44
-50 +100	0.072	0.068	1.05	5.62
-100 +200	0.108	0.137	0.79	5.23
-200 +400	0.176	0.274	0.64	4.21[b]
-400	0.881	—	$\lambda_f = 3.3$	8.19

[a]Numerical values for arithmetic average of mesh opening dimension; values of λ_f from Anbeek (1992).
[b]Result excluded from plot in Figure 3.7b.
[c]Reported value from Holdren and Speyer (1987) identified as being incorrect by Anbeek (1992).

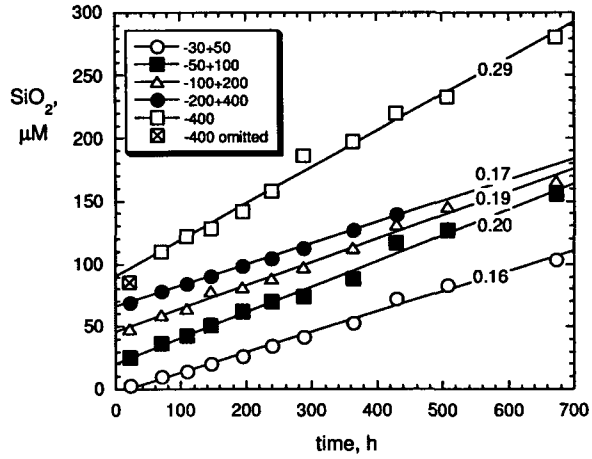

Figure 3.6. Results from Holdren and Speyer (1985): Dissolution of various size fractions of Hybla alkali feldspar at pH 3. Si release rates given on plot as µM/h. The numbers give slopes of fitted lines.

The tests were sampled by withdrawing 10 mL of solution (from the 1 L total solution volume) for analysis and replacing it with 10 mL fresh leachant to maintain a constant *S/V* ratio. This dilutes the solution (by about 1%) and complicates the accurate measurement of the dissolution rate; this is because the dissolution rate depends on the solution composition (see Ebert 2010, Section 3.3.3). In a static test, the *S/V* ratio determines the evolution of the solution chemistry as the material dissolves. Replacing a portion of the test solution with fresh leachant perturbs the solution chemistry, even though the *S/V* ratio is maintained, such that the solution composition does not accurately represent the amount of material dissolved. The difference may be small, but the impact under near-equilibrium conditions will be large. Nevertheless, the experimentally determined rates can be used to qualitatively assess the effects of the surface area and size fraction on the dissolution rate, even though the dissolution rate does not accurately represent the extent of dissolution.

The same masses were used in tests with different size fractions of a given material, but different amounts of the different materials were used. Unfortunately, only the masses of Grass Valley anorthite and the alkali feldspars were reported. The data for each material can be evaluated for the dependence on the relative surface areas, but the results for the various materials cannot be compared. The rate is actually reported as a bulk rate in units of pmoles Si/g mineral/s and plotted against the *specific* surface area in units of $m^2\ g^{-1}$. Holdren and Speyer (1987) measured the specific surface areas of each size fraction using the BET method. They express the relation between the surface area and the reaction rate as

$$\text{rate} = (\text{surface area})^m \tag{3.15}$$

and use log-log plots to determine values of *m*. However, they plot the log of the specific surface area, in which the total surface area is normalized to the mass of material, so that the relation between the bulk rate and the specific surface area is

$$\text{rate}_{\text{bulk}}\ (\text{mol}\ g^{-m}\ s^{-1}) = \text{rate}\ (\text{mol}\ g^{-2m}\ s^{-1}) * (\text{specific surface area, m}^2\ g^{-1})^m \tag{3.16}$$

where the mass and area terms in the expressions for the rate must reflect the areal dependence *m*.

Expressing Equation 3.16 in terms of the logarithms gives

$$\log \text{rate}_{\text{bulk}} \text{ (mol g s}^{-1}\text{)} = \log \text{rate (mol g}^{-2m}\text{ s}^{-1}\text{)} + m * \log \text{(specific surface area, m}^2\text{ g}^{-1}\text{)}. \quad (3.17)$$

The analyses by Holdren and Speyer (1987) neglect the first term on the right hand side of Equation 3.17, which is equivalent to assuming the per-area rate is constant and ascribing the full difference in the per-mass rate to the specific surface area. It is likely that a difference in the reaction affinity, which is also neglected, has a greater impact on the measured rate than does the specific surface area. The impact of the reaction affinity is discussed later. The geometric surface areas were calculated by modeling the particles as spheres having diameters equal to the arithmetic average of the size fractions using typical densities for the various minerals. This could not be done for the +30 mesh or -400 mesh size fractions because the maximum and minimum grain sizes, respectively, were not constrained. The surface roughness factor is the ratio between the BET specific surface area and the geometric surface area. These are summarized in Table 3.1 along with the specific surface areas measured with BET and the bulk rates. In his analysis of the Holdren and Speyer (1987) data, Anbeek (1992) calculated roughness factors assuming a uniform mass distribution between the upper and lower sieve mesh sizes, and then determined the maximum roughness factor for the material, which did not depend on the particle size fraction. Based on the dimensions of the size fraction shown in Figure 3.4, a uniform mass distribution is probably not a valid assumption.

Figure 3.7 shows the logarithm of the bulk rate plotted against the logarithm of the specific surface area. The bulk rate is reported in units of picomoles dissolved Si/gram feldspar/second. The results for the plagioclase feldspars are shown in Figure 3.7a and the results for the alkali feldspars are shown in Figure 3.7b. The rates are plotted against the BET specific surface areas and the regression slopes for each mineral are drawn as thin black lines with the value of the slope. A few data points[1] were excluded from the regressions as outliers. This lends some degree of subjectivity to the analysis. For example, in the case of Perth perthite, the result for the -200 +400 mesh size fraction is excluded to ensure a non-negative slope. Holdren and Speyer (1987) evaluated their data with regard to consistency with a slope of 1, and Figure 3.7 includes lines with slope of 1 (the heavy red lines) fit to the subsets of data that are consistent with that slope. As shown by Holdren and Speyer (1987) and evident in Figure 3.7, only subsets of data at small values of log *S* (larger mesh size fractions) are consistent with a slope of 1 for the plagioclase feldspars, and few data for the alkali feldspars are consistent with a slope of 1. There is no obvious reason to exclude the data at higher values of log *S* that are inconsistent. The average slope for the plagioclase feldspars (Figure 3.7a) is 0.41 and for the alkali feldspars (Figure 3.7b) is 0.24. Holdren and Speyer (1987, p 2317) concluded that "reaction rates are not related to the specific surface area of a given feldspar mineral *in any simple way*" (my emphasis), and that "reactions rates cannot be normalized to surface area in any simple or direct fashion." The greatest deviations occurred for the moderate size fractions. The differences in the results of duplicate tests with the Keystone microcline reflect the relatively small experimental uncertainty and the variances in the results of tests with other materials indicate that other factors are influencing the dissolution behavior. Note that the rates are normalized to the mass rather than the surface area, and that the relationship between mass and surface area varies with the size fraction.

[1] Crystal Bay bytownite dissolution rate for +30 mesh fraction is anomalously high and BET area for the -30 +50 mesh fraction is anomalously high; Mitchell Co. oligoclase dissolution rate of -200 +400 mesh fraction is anomalously low; Keystone microcline dissolution rates of -200 +400 mesh fraction are anomalously low in both runs; Perth perthite dissolution rate of -200 +400 mesh fraction is anomalously low.

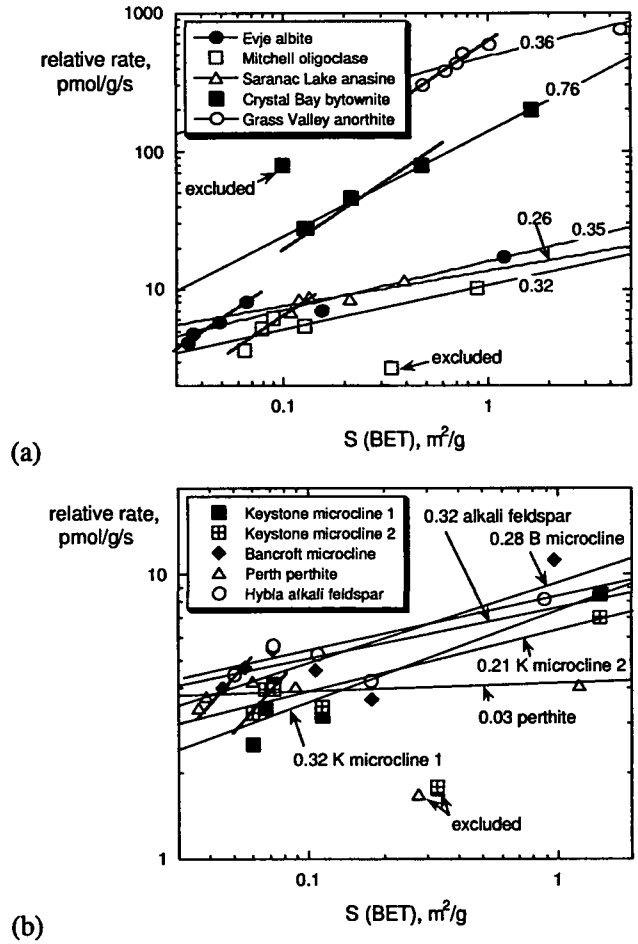

Figure 3.7. Results from Holdren and Speyer (1987): Relative dissolution rates as a function of BET surface area for different size fractions for (a) plagioclase feldspars and (b) alkali feldspars. The short lines show slopes of 1.0 fit to subsets of the data.

The data provided in Holdren and Speyer (1987) were further analyzed by Anbeek (1992a; 1992b) to quantify the effects of surface roughness and grain size on the dissolution rate. Anbeek (1992b, p. 3958) stated that "Holdren and Speyer (1985, 1987) tested the hypothesis that the experimental dissolution rates, normalized to BET-Ar surface area, are independent of the grain size. They found this to be approximately true at grain sizes > 75 μm." That is, for grains larger than 200 mesh.

At this point, it is worthwhile to discuss some of the nuances of what is meant by the dependence of reactivity on grain size. As mentioned above, atomistic models identify active sites that participate in reactions and include the concentrations of these sites in the rate law. Since these concentrations cannot be measured directly, they are usually assumed to be proportional to the total surface area. The question is whether the concentration of active sites remains constant as the material is crushed. Geometric models and BET measurements of the surface area of small particles both provide estimates of the total surface area, but neither provides the surface

concentrations of active sites. It is possible that the more active reaction sites are also preferential sorption sites. Dissolution tests provide a measure of the mass of a material that dissolves that can be related to the mass of material used in the test. The specific surface area of the starting material can be measured and used to calculate the initial surface area available in the test, but the concentration of active sites cannot be measured. Dissolution will result in the preferential loss of active sites and a decrease in their surface concentration. The initial dissolution rate may be significantly higher than the rate at longer test durations when the "activity" of the surface has decreased (e.g., when the surface has become smoother). The test response will decrease due to both the decrease in surface area and the decrease in the concentrations of active sites.

Another important aspect of the surface area measured by BET is that surfaces within all the pores that are accessible to the sorbing gas are included in the measured area. Although most of these pores will also be accessible to water, the extent of reaction within small pores will be limited by mass transport and may not contribute to the overall reaction progress as effectively as reaction at exposed surfaces. Some researchers refer separately to exterior and interior surface areas on porous materials and consider the surface roughness to represent the exterior surface. Insight into the relative amounts of interior and exterior surfaces can be gained from the hysteresis of adsorption/desorption cycles when measuring isotherms because desorption of gasses from pores is slower than desorption from exposed surfaces.

Anbeek (1992a, p. 1466) calculated surface roughness factors by assuming "equal sample masses at all grain sizes between the two sieve openings" and accounting for non-linear relationship at small grain sizes. His calculated values are included in Tables 3.1 and 3.2 as λ_f. The same value of λ_f was assigned to a material regardless of the sieve fraction, whereas the roughness factors calculated from the average mesh size and BET surface area generally increase with particle size. This is attributed to greater variance in the shapes of larger particles rather than the atomistic roughness of the surfaces. The values of λ_f in Tables 3.1 and 3.2 are about twice the roughness factors that were calculated for the -30 +50 mesh size fractions of all materials except the Green Valley anorthite, which is about 60% lower.

Figure 3.8 shows the rates measured by Holdren and Speyer (1987) plotted against the geometric specific surface area calculated based on the sieve sizes. The dependence of the bulk rate on the geometric specific surface area is weaker than the dependence on the BET specific surface area for most materials, and an inverse dependence is shown for many of the materials (the slopes of the fitted lines are given in the figures). This is probably a result of the more significant affinity effects that occur during the dissolution of smaller particles: The smaller particles provided much more surface area per gram material than the larger particles. When equal masses are reacted in the same solution volume, small particles generate more concentrated solutions and impose a lower reaction affinity than larger particles. This lowers the dissolution rate. Holdren and Speyer (1987) stated that the rates decreased initially, presumably due to the dissolution of fines. The greater number of particles in the tests with the -200 +400 mesh size material would likely contain more fines and high activity sites than the larger particles. These would generate higher solution concentrations that would lower the dissolution rate due to a lower reaction affinity. Therefore, the particle size affected these test results due to both the physical effects of different shapes and active site densities and the chemical effects of different reaction affinities during the test. The chemical effects are greatest in tests with small particles.

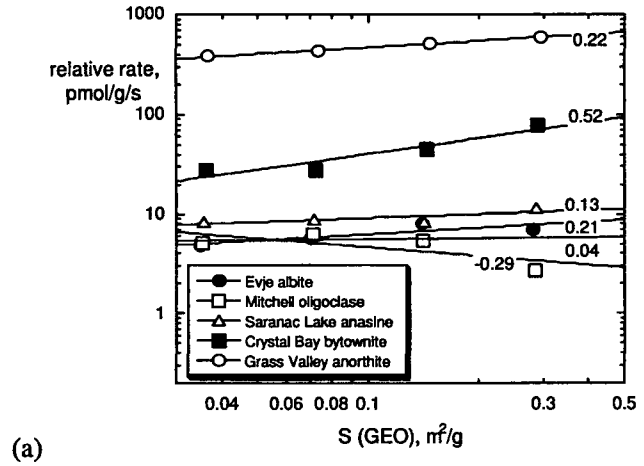

(a)

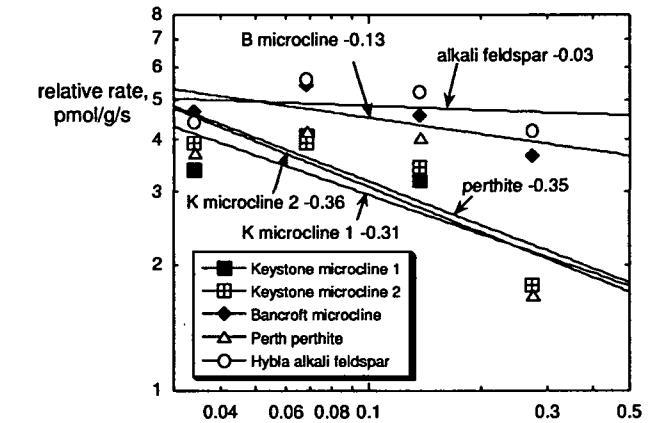

(b)

Figure 3.8. Data from Holdren and Speyer (1987): Bulk dissolution rates plotted versus the geometric specific surface area for spherical particles for (a) plagioclase feldspars and (b) alkali feldspars.

3.6 Comparing Surface Areas of Crushed and Monolith Specimens

An approach that can be taken with a material that is generally isotropic and dissolves primarily at flat surfaces is to compare the amounts dissolved from monoliths having measured macroscopic dimensions with the amounts dissolved from crushed material of a known size fraction under conditions in which the dissolution rates are expected to be the same. Such an experiment was conducted with a borosilicate glass dissolved at near the forward dissolution rate, where the effects of back-reaction were negligible. Under these conditions, the same dissolution rate (on a per area basis) should be determined with both test methods, so any difference can be attributed to the use of an incorrect surface area. Uncertainty in the geometric surface area of the monolith specimens is due to uncertainties in the measured dimensions and geometric model that is used. Uncertainty in the surface area of the crushed material is due to the highly irregular shape of each particle and the range of particle sizes within the size fraction (e.g., see Figure 3.4).

In addition, the test response is related to a reacted volume of the specimen, rather than the surface area *per se*. Although the surface area that is available for reaction may decrease or increase as the specimen dissolves, the available volume will always decrease. The dissolution rate determined from tests with monolithic specimens was 1.67 g $m^{-2}d^{-1}$. The rate measured for the crushed glass specimens was 1.64 g $m^{-2}d^{-1}$. This was calculated using a specific surface area of 0.021 m^2 g^{-1} for the -100 +200 mesh size fraction used in the test. (The density of the glass was 2.516 g cm^{-3} and the particles were modeled as spheres with a diameter d_o = 112.5 μm; see Equation 3.6.) The rate measured with the crushed glass is about 2% less than the rate measured with the monoliths. This may indicate the specific surface area is 2% too high, but the difference is well within the experimental uncertainty (the expanded uncertainty for the range measured with single-pass flow-through tests was ± 1.90 g $m^{-2}d^{-1}$ at the 95% confidence level).

Tests with monolithic and crushed glass show higher dissolution rates for microscopically rough surfaces, whether due to polishing scratches on monoliths or sharp fracture edges on crushed material. The dissolution rate of high energy sites is higher than that of flat surfaces. Most of the high energy sites are experimental artifacts and the dissolution rates of these sites do not represent the long-term dissolution behavior of glass. It is worth noting that the dissolution rates of finely polished glass surfaces do not represent long-term dissolution either. Tests have shown that a 600-grit surface finish represents glass dissolution well, whereas coarser finishes dissolve faster and smoother surfaces dissolve slower (Dussossoy et al. 1992). Presumably, a 600-grit finish simulates the texture glass achieves after the outer surface of the specimen has dissolved to relieve strain introduced during preparation of the particle. (The dissolution rates given in the preceding paragraph were for dissolution after the sharp edges of the crushed glass were dissolved and for monolithic specimens with a 600-grit surface finish.) This comparison provides confidence that the reactive surface area of a crushed material can be well-approximated based on the sieve mesh fraction and a geometric approximation of the particle shape. Unfortunately, the BET surface area of the crushed glass was not measured, so the relationship between the BET area, geometric area, and reactive surface area cannot be evaluated.

3.7 Relevance of the Particle Surface Area to Modeling Surface Disposal Systems

Pačes (1983) and Velbel (1985) suggested that the mineral surface areas in field systems contacted by groundwater contribute the most uncertainty to the dissolution rates calculated for field tests. The uncertainty in the surface area of test specimens is probably also a major contributor to the uncertainty in the rate determined from laboratory tests. On the atomic scale, the reaction potentials will vary between sites: atoms at what are referred to as high energy sites are not bound to the material as strongly as those at other sites and are more readily dissolved. Atoms at defect sites, such as points and blades generated by crushing, pits and crevices, steps and grain boundaries, etc., will react more readily than atoms that are part of a smooth surface. These variations cannot be distinguished at the mesoscale of laboratory tests, but the effect of large changes in the number of available high energy sites as the material dissolves can be detected. The dissolution rates measured with laboratory experiments are calculated to be proportional to the total surface area of the small particles used in the experiments, and are expressed on a per-area basis to allow for scaling to larger systems. This homogenizes the variations in the reactivities of various surface sites into an average for the total surface area, but the average will change as dissolution proceeds. The initial dissolution rate of crushed materials will be high due to the abundance of high energy sites on freshly prepared test material, but decreases as these sites dissolve. (This is discussed in detail in the following section.) The system then approaches near-to-steady-state conditions wherein the material dissolves at a rate

that is proportional to (1) the rate that advection or diffusion removes dissolved species from the vicinity of the specimen and (2) the concentration of reactive sites. The concentration of active dissolution sites is assumed to approach a steady state as the material dissolves. The steady-state concentration of reactive sites on the reacted material is expected to be lower than on the freshly prepared material, but could be higher than on test specimens prepared with very smooth surfaces, such as flame-annealed glass or low index faces of single crystal minerals. The continuous loss of surface area as the material dissolves will prevent the system from reaching steady state conditions on the atomic scale, but this may not be measurable in experiments conducted for only a few days under not-too-aggressive conditions.

A significant part of the uncertainty is whether the BET or geometric surface area better represents the reactive surface area of crushed materials. The roughness factor relating the geometric and BET surface areas indicates a 7-fold difference is typical for many minerals (see Figure 3.2). Although the BET surface area can be measured before and after a test, it is very difficult to quantitatively recover reacted small particles from a test to determine the actual surface area. That is, measuring the specific surface area of the reacted materials is not sufficient—it must be multiplied by final mass to calculate the surface area. The final surface area can be estimated from the solution composition in a static test or the rate measured in a dynamic test. The roughness factor will decrease as most materials dissolve, but can increase if the porosity increases. Because the surface area is used to scale the volume (mass) of material that is released into solution, this can lead to incorrectly calculated contaminant releases.

Although the majority of geochemists use the BET surface area to compute dissolution rates, several arguments presented here favor the use of the geometric surface area despite the higher degree of subjectivity (i.e., selecting the representative shape) because it can be used to better relate changes in the specimen surface area during the test to changes in the solution composition. The release of components into solution is proportional to the volume of material that dissolves, not the surface area. The dissolved volume may be better estimated using the surface area for a geometric particle shape than the measured surface area. The effects discussed in this section should be considered both when modeling surface disposal systems and when measuring release rates in laboratory tests. For example, crushing pure minerals or field samples for use in laboratory tests will introduce artifacts such as fractures and high-energy surface sites that dissolve faster than the bulk material. These effects are best avoided to reliably relate laboratory measurements to the system being modeled. The dissolution of sites generated as preparation artifacts will dominate the response in static tests if little material dissolves during the test and will provide a too-high calculated rate. The effect of surface artifacts can be neglected in dynamic tests by allowing a flowing system to reach a steady state or excluding the first few samplings of a solution exchange test when calculating the rate.

Whereas it is strongly expected that mineral surfaces in field systems will have been smoothed by weathering reactions over very long times, the exposed surfaces of waste materials in a disposal system will have been weathered for much shorter periods. Nevertheless, the surfaces of materials in the disposal system are expected to be much smoother than those generated by crushing materials for use in laboratory experiments, and the effects of surface roughness expected between laboratory and natural field systems are expected to contribute to differences between laboratory and disposal system to the same degree as field systems.

The insights provided by mineral dissolution are directly applicable to the dissolution of waste materials: the dissolution kinetics measured in laboratory tests is very sensitive to artifacts of specimen preparation. Although surface artifacts may be unavoidable, the effect on the dissolution rate that is determined from the laboratory test can be taken into account by (1)

recognizing the importance of the surface area assigned to laboratory samples and its impact on future use of the result and (2) conducting tests and utilizing test results in a manner that minimizes the contributions of the artifacts to the rate that is determined. This may involve allowing static tests to run long enough that the influence of preparation artifacts becomes insignificant, ensuring that dynamic tests have attained steady state conditions that are not influenced by the initial surface conditions, and demonstrating that the surface area used to normalize the test response is representative of the volume of material that has dissolved during the test. The last point addresses the fact that the rate measured in a laboratory test is expressed in units of moles per *area* per time even though the extent of dissolution depends on the reacted mass (or volume). The accuracy with which continued dissolution is predicted depends on the relationship between the assumed initial surface area and the volume that had reacted when the dissolution rate was measured.

4 Laboratory Tests

The use of various laboratory tests to measure material dissolution rates was discussed at length in the report for Part I of this study (Ebert 2010). A brief summary of a column flow-through test is presented as one of the test methods commonly used for measuring dissolution rates. The effect of the solution flow rate that is used in the column test on the dissolution rate and the approach to steady-state and equilibrium conditions are discussed in detail because much of the underlying physics and the mathematics used to model these laboratory tests are applicable to modeling and understanding mineral weathering field systems and waste materials in disposal systems. Other test results for specific minerals are presented for comparisons with mass-balance results to be discussed in Section 5.

4.1 Measurement of Dissolution Rates with Column Experiments

Figure 4.1 summarizes results from column flow-through tests with plagioclase (labradorite) conducted at 25°C by Taylor et al. (2000b). The material used in the test was crushed and sieved to isolate the 43 – 110 μm size fraction, which was then carefully washed to remove fines. Tests were conducted with an HCl solution at pH 3.08 that was pumped by a peristaltic pump upwards through the packed column and then collected for analysis; tests were conducted at several different flow rates. The results show (1) the transient rapid dissolution of the disturbed surface of crushed material through the first ~800 hours, (2) the congruent release of Si and Sr, and (3) the sensitivity of the steady-state Si and Sr concentrations to the solution flow rate in the test. Note that the steady-state Si and Sr concentrations are more sensitive to changes in flow at low flow rates (below 0.2 mL/h in samplings beyond 3000 hours) than changes at higher flow rates

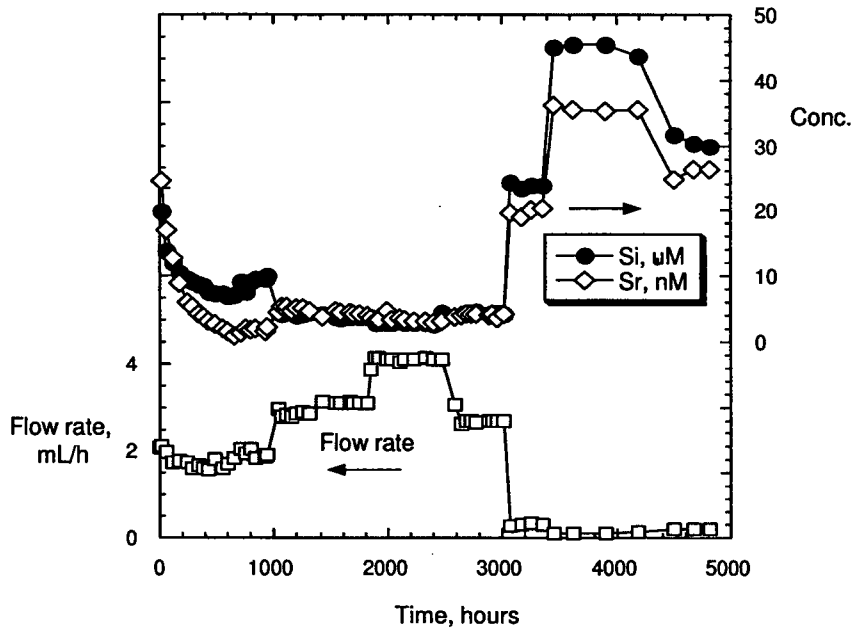

Figure 4.1. Results from Taylor et al. (2000b): Measured flow rate, Si, and Sr concentrations vs. *L/v* for 5.0 cm column tests with plagioclase.

(above 2 mL/h in samplings beyond 3000 yours). The steady-state concentrations are established by the dependence of the plagioclase dissolution rate on the solution chemistry, particularly the Si concentration.

4.1.1 Effect of Flow Rate in a Well-Mixed Reactor

Consider the reaction of a specimen with surface area S contained in a cell volume V that occurs when contacted by a solution passing through the cell at a flow rate F. The release rate of a component i as the material dissolves will depend on the affinity term and its dependence on the concentration of dissolved i, $C(i)$, and solubility product of the material K_{sp}. If the cell is a well-mixed reactor such that the concentration of i in the reaction cell is uniform, the variation in that concentration over time is the difference between the amount of i added by dissolution of the specimen and the amount of i removed from the cell due to flow:

$$\frac{dC(i)}{dt} = \frac{S}{V} k_f \left(1 - \frac{C(i)}{K_{sp}}\right) - \frac{F\,C(i)}{V} . \tag{4.1}$$

The first term on the right-hand side of Equation 4.1 gives the rate at which i is added to the solution in the cell (where the rate coefficient k_f represents the product of the intrinsic rate constant, pH dependence, and temperature dependence terms (see Section 2.3) and the second term give the rate at which dissolved i is removed from the cell due to the flow rate F. This model presumes no precipitation or sorption reactions occur to remove i from solution; additional terms would be required to take those processes into account. Under constant flow conditions, steady-state will occur when the rate at which i is added to the cell by specimen dissolution is the same as the rate i is removed from the cell by flow. The rate at which i must be added by dissolution of the specimen to maintain a steady-state concentration at a particular flow rate is determined by setting $dC(i)/dt = 0$ and solving for $C(i)^{ss}$. The dissolution rate necessary to maintain a steady-state concentration can be expressed in terms of the number of moles of i released under steady-state conditions $n(i)^{ss}$, which is simply the product of the cell volume and steady-state Si concentration

$$n(i)^{ss} = VC(i)^{ss} . \tag{4.2}$$

Expressing Equation 4.1 in terms of the number of moles of i and substituting Equation 4.2 gives

$$\frac{dn(i)^{ss}}{dt} = \frac{V\,dC(i)^{ss}}{dt} = V\left\{\frac{S}{V} k_f \left(1 - \frac{C(i)}{K_{sp}}\right) - \frac{F\,C(i)}{V}\right\} \equiv 0 . \tag{4.3}$$

Solving Equation 4.3 for $C(i)$ gives

$$C(i) = \frac{Sk_f}{F + Sk_f / K_{sp}} , \tag{4.4}$$

which can be substituted into Equation 4.3 to produce

$$\frac{dn(i)^{ss}}{dt} = \left(\frac{S k_f}{F + {Sk_f}/{K_{sp}}} \right) \bullet F \,. \tag{4.5}$$

The dissolution rate becomes independent of the flow rate only at the limit of very high flow rates, when the value of F (the flow rate) dominates the value of the denominator and Equation 4.5 reduces to

$$\frac{dn(i)^{ss}}{dt} = S k_f \,. \tag{4.6}$$

A threshold flow rate exists at which the material dissolves at the highest possible rate and further increases in the flow rate will not affect the reaction rate, although they will lower the steady-state i concentration. Lower flow rates will establish a unique steady-state condition for each value of F/S and a material dissolution rate corresponding to C_i^{ss}. In the limit of low (but non-zero) flow rates, the concentration of i will become proportional to the flow rate as:

$$\frac{dn(i)^{ss}}{dt} = K_{sp} F \,. \tag{4.7}$$

This rate expression does not depend on the dissolution kinetics of material dissolution, but is proportional to its solubility product. This simple well-mixed reactor model does not take into account mass transport effects, which will probably control the kinetics at very low values of the flow rate F. A steady state is not attained in a static system when $F = 0$ and dissolved components are not removed from the system by flow, and dissolution is controlled by the first term on the right-hand side of Equation 4.1.

4.1.2 Calculating Dissolution Rates for Column Tests

In a fluidized bed reactor, the surface area contacted by the solution is easily defined (ignoring for the moment the difference between the BET and geometrical surface areas) and independent of time (ignoring preparation artifacts). The solution in the reaction cell is assumed to be well mixed and the same at every location. In a packed column, the solution in the column is not well mixed through the length of the column. In the simplest case of plug flow, a concentration gradient exists along the length of the column but not laterally. Steady-state conditions can be attained in a column, but the steady-state concentration will vary continuously along the length of the column. An analogous dependence of the dissolution rate on the flow rate will exist at every point and the steady-state concentrations that are measured in the eluate exiting the column will depend on the column length. The solution at any point in a packed column will have only contacted the surface area in the column up to that point. The eluate solution that is collected for analysis will have contacted all the surface area, but not for its entire residence time in the column. In the analysis of the column tests, Taylor et al. (2000) followed Mogollon et al. (1996) to define an average surface area $\overline{S}$ as

$$\bar{S} = \frac{1}{L}\int_0^L S(x)\,dx \tag{4.8}$$

for points x through a column of length L. The average surface area is simply the total surface area, which is the product of the specific surface area and mass of material in the column, divided by the column length. The output concentration of component i is related to the mineral dissolution rate as

$$\Delta C_i = \frac{\beta_i\, k_{\text{mineral}}}{vV} L \bar{S} \tag{4.9}$$

where ΔC_i is the concentration accumulated in the flowing solution over the collection interval when the system is a steady state, v is the flow rate (m s^{-1}), V is the volume (liters) of solution in the column, $k_{mineral}$ (mol m^{-2} s^{-1}) the kinetic rate coefficient for mineral dissolution based on element i, and β_i is the stoichiometric coefficient of element i in the mineral. Solving Equation 4.9 for the rate coefficient gives

$$k_{\text{mineral}} = \frac{\Delta C_i\, vV}{\beta_i\, L\, \bar{S}}. \tag{4.10}$$

A dissolution rate can be calculated for any set of test parameters based on the eluent composition using Equation 4.10. To obtain a rate that is characteristic of the material, the eluate must represent steady-state conditions, and the measured rate will be a function of the flow rate and column length. The dissolution reaction for labradorite (Taylor et al. 2000b) can be written as

$$Na_{0.4}Ca_{0.6}Al_{1.6}Si_{2.4}O_8 + 1.6\ H_2O + 6.5\ H^+ \rightarrow 0.4\ Na^+ + 0.6\ Ca^{2+} + 1.6\ Al^{3+} + 2.4\ H_4SiO_4. \tag{4.11}$$

(The labradorite used by Taylor contained 12.9 ppm Sr substituted for Ca; this is excluded from Equation 4.11 for simplicity.) Figure 4.2 shows the steady-state Si concentrations (filled symbols, right-hand axis) from the pooled results of tests conducted in 3.5 cm and 5.0 cm columns at various L/v values (Taylor et al. 2000a). For a given column length, low L/v values represent high flow rates and high L/v values represent low flow rates. The solid line shows the limiting far-from-equilibrium rate that is approached at high flow rates. The steady-state concentrations measured at lower flow rates (solid symbols and right-hand axis) deviate negatively from the line representing the far-from-equilibrium limiting rate and approach the Si saturation limiting rate near to equilibrium as the flow rate approaches zero (i.e., as L/v becomes very large). The Si concentrations in Figure 4.2 have clearly not become independent of the flow rate and the Si solubility limit was not reached in these experiments. The dashed horizontal line is provided to illustrate the near-to-equilibrium rate limit. Longer columns or lower flows are required to attain higher L/v conditions and measure rates that approach the near-to-equilibrium limit. The open symbols in Figure 4.2 give the dissolution rates calculated with Equation 4.10 using the measured steady-state Si concentrations and parameters provided in Taylor (2000a, 2000b) for tests using 3.5 cm (open circles) and 5.0 cm (open triangles) long columns. These results show that steady-state conditions can be attained at any flow rate (see Figure 4.1) and a

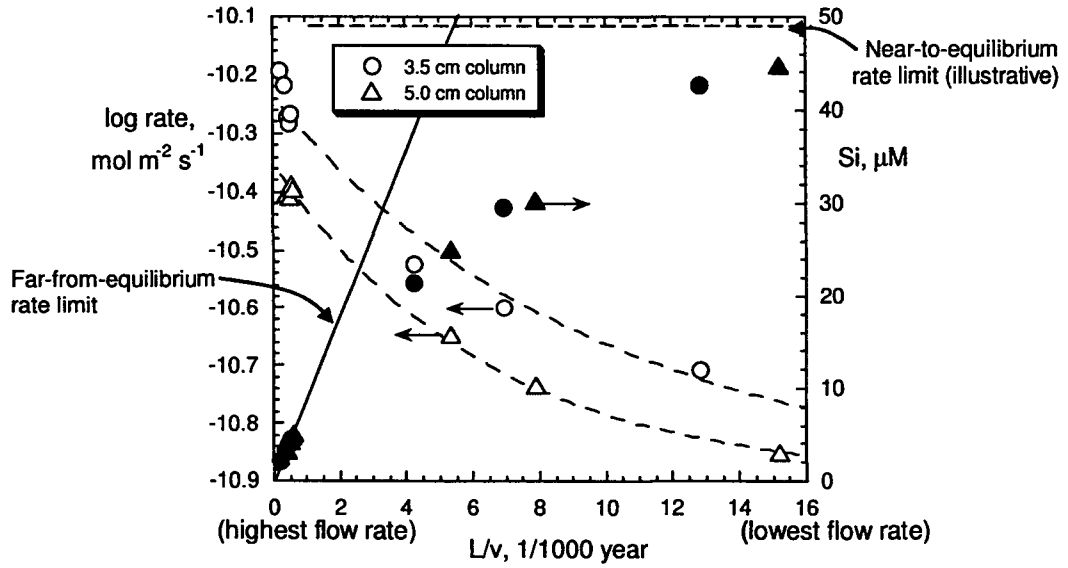

Figure 4.2. Results from Taylor et al. (2000b): Measured Si concentrations and calculated rates vs. L/v for tests conducted with $L = 3.5$ cm (filled circles) and $L = 5.0$ cm (filled triangles) columns. The solid line is fit to the low L/v data to show the far-from-equilibrium limit where the steady-state concentration is linear with the inverse flow rate (at very high flow rates) and the dissolution rate is constant.

dissolution rate can be calculated. However, the value of that rate will depend on the flow rate and column length except at extremely high or extremely low flow rates when far-from-equilibrium or near-to-equilibrium conditions exist (see Figure 4.2). This is the case for all column tests, and the effects of test parameters must be taken into account to determine intrinsic material properties.

Under far-from-equilibrium conditions, as the value of L/v approaches zero (at very high flow rates) and the dissolved Si concentration approaches zero, the dissolution rate is about 6.3×10^{-11} mol m^{-2} s^{-1}. Dissolution slows as the Si concentration increases with higher values of L/v (at very low flow rates) and the solution approaches equilibrium with labradorite. As in Equation 2.6, the term $fn(\Delta G_r)$ is used to quantify the effect of the deviation from equilibrium on the rate. The steady-state conditions provide a single value of the ion activity product (Q), which can be divided by the solubility product of the mineral (K_{sp}) to calculate ΔG_r for the system

$$\frac{\Delta G_r}{RT} = \ln\left(\frac{Q}{K_{sp}}\right). \tag{4.12}$$

Taylor et al. (2000b) fit their data using a rate law with a nonlinear dependence on the free energy [note that Equation 9 in Taylor et al. (2000b) has an error in the sign of the second term] as

$$rate_{diss} =$$

$$-k_{labradorite}\left\{0.76\times\left[1-\exp\left(-1.3\times10^{-17}\times\frac{|\Delta G_r|^{14}}{RT}\right)\right]+0.24\times\left[1-\exp\left(-0.35\times\frac{|\Delta G_r|}{RT}\right)\right]\right\}. \quad (4.13)$$

The test results fitted with Equation 4.13 are shown in Figure 4.3. The group of data at values $L/v < 1$ is modeled to be essentially independent of ΔG_r (represented by the first ΔG_r term raised to the 14th power—this value was determined from an empirical regression) and the data at values $4 < L/v$ are modeled to have a first-order dependence on ΔG_r (represented by the second ΔG_r term). This significant difference in the dependence of the dissolution rate in terms of ΔG_r occurs for only a factor of four increase in L/v, which could occur due to longer flow paths or lower flow rates in the column or in a natural system.

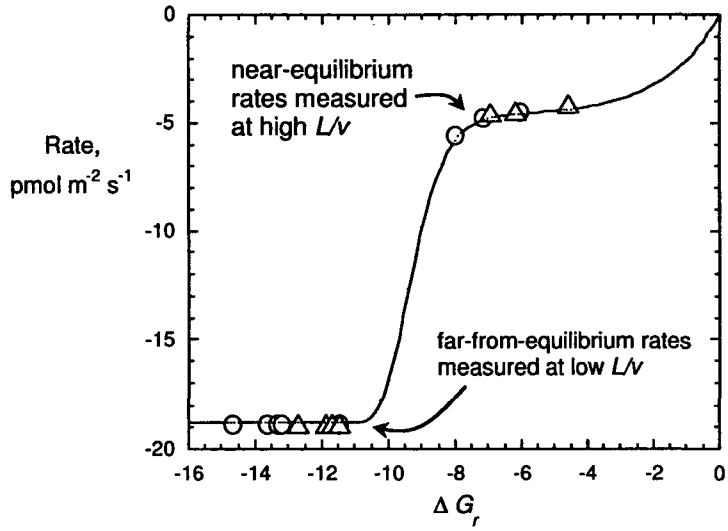

Figure 4.3. Results from Taylor et al. (2000b): Measured dissolution rates plotted against calculated ΔG_r and fit with nonlinear rate law. (Note that dissolution rates are assigned negative values in this plot, per convention. Tests at low flow rates provide high values of L/v and tests at high flow rates provide low values of L/v.)

Based on Figures 4.2 and 4.3, the effective value of L/v in a laboratory test can have a significant effect on the dissolution rate that is measured, even though the system attains steady state. The values of the test parameters L and v do not affect the rate, *per se*; rather, they are test parameters that influence the steady-state solute concentration that is attained at the end of the column, which, in turn, affects the measured rate. Each steady condition provides a single datum on a plot such as Figure 4.3 and the steady-state rates can differ by several orders of magnitude as equilibrium conditions are approached (i.e., as ΔG_r approaches zero).

As will be discussed in the next section, the mass-balance calculations used to estimate field weathering rates are based on an assumption that a steady state relationship exists between the ground water and the minerals it contacts. The steady-state concentrations are measured directly and then used to calculate the dissolution rate using Equation 4.10 (or an equivalent form). That

calculation does not explicitly account for the effect of the chemical affinity term on the dissolution rate.

Whereas generally constant flow paths can be imposed on laboratory measurements by using uniformly-sized particles, fixed flow rates, and fixed column lengths, the flow rates and flow paths in natural systems will vary spatially and temporally. In most cases, naturally-occurring precipitation, glacial melt, snow, or ground water movement in an aquifer will establish the flow rate that is measured for the field system, and most of these sources will vary over time. The naturally-occurring influx can be augmented by irrigation in small catchment studies to maintain a more constant flow or measure the effects of flow rate on the system behavior. Transport in the field occurs through a variety of fractures and regions having different porosities. The relative contributions of mineral dissolution in large fractures, tight fractures, and various pore channels may vary with the flow rate: high flow rates are expected to be dominated by dissolution of minerals exposed in large fractures. Flow rates will also affect the groundwater compositions and mineral dissolution rates. With reference to Figure 4.3, field dissolution can occur at relatively high rates near the far-from-equilibrium plateau at high flows, at rates near zero at very low flows, or anywhere on the steep portion of the curve in between these extremes at moderate flows.

4.2 Effects of Secondary Phase Formation in Static Tests

The effect of secondary phase precipitation on the dissolution rate of a mineral of interest can be complicated and difficult to quantify. The results of two studies of simple systems are described in detail in this section to present an experimental approach and the associated uncertainties. Coupling of the dissolution and precipitation reactions is proposed to be an important factor affecting mineral dissolution in the field that is absent in laboratory tests used to measure the dissolution rates of individual minerals. The coupling affects both the thermodynamics and kinetics of the system under near-equilibrium conditions, including the kinetics of nucleation and maturation of secondary phases. The later further complicates the comparison of laboratory and field studies. The tests described in this section provide useful examples of the relationship between the free energy and dissolution rate as near-equilibrium conditions are approached in a system with two minerals.

As an example of the coupling of dissolution and precipitation reactions, the dissolution of sanadine ($K_{1.00}Na_{0.03}Al_{0.99}Si_{3.00}O_8$) in a 0.1 molal sodium bicarbonate solution at 300°C and pH 9 in static tests conducted by Alekseyev et al. (1997) is presented and discussed. The dissolution reaction is written as

$$\underset{\text{sanadine}}{xKAlSi_3O_8} + 8xH_2O = xK^+ + xAl(OH)_4^- + 3xH_4SiO_4 \qquad (4.14)$$

and the precipitation reaction as

$$yNa^+ + yAl(OH)_4^- + 2yH_4SiO_4 = \underset{\text{analcime}}{yNaAlSi_2O_6} + 5yH_2O, \qquad (4.15)$$

where x and y are the numbers of moles of sanadine dissolved and analcime precipitated, respectively. The coupled reactions are written as

$$\underset{\text{sanadine}}{xKAlSi_3O_8} + yNa^+ + (8x\text{-}5y)H_2O = \underset{\text{analcime}}{yNaAlSi_2O_6} + xK^+ + (x\text{-}y)Al(OH)_4^- + (3x\text{-}2y)H_4SiO_4. \qquad (4.16)$$

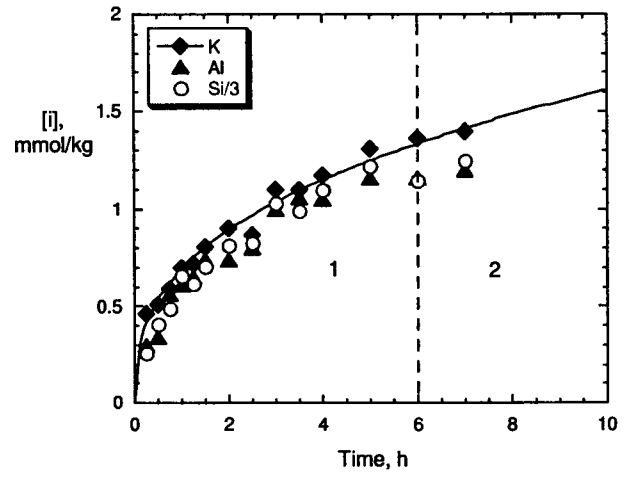

(a)

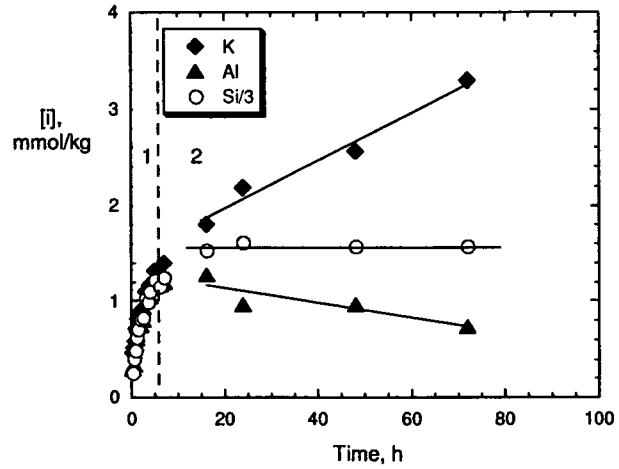

(b)

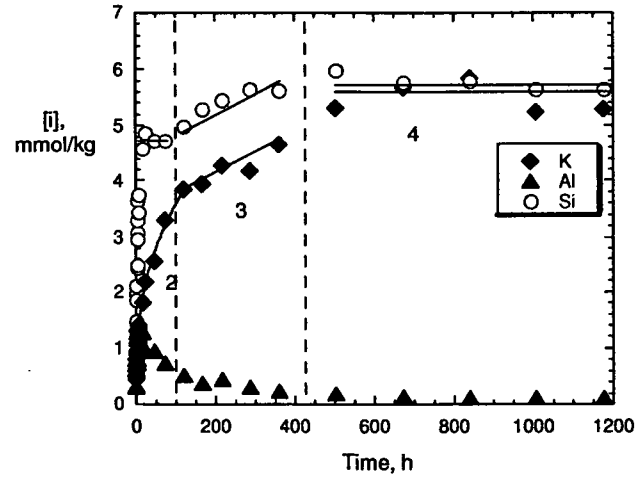

(c)

Figure 4.4. Results from Alekseyev et al (1997): Solution concentrations of K^+, Al, and Si in experiments with sanadine through (a) 10 hours, (b) 100 hours, and (c) 1200 hours.

Only sanadine is present initially and analcime forms after the dissolution of sanadine has progressed to super saturate the solution. (The formation of analcime is favored over the formation of albite under these test conditions.) Figure 4.4a shows the measured solution concentrations of Al, K^+, and Si for samplings during the first 10 hours of reaction, where the measured Si concentrations have been divided by 3 to show that the congruency of the sanadine dissolution is consistent with the stoichiometry in Equation 4.14 through the first 5 hours. The results at 5, 6, and 7 hours show constant Al and Si concentrations and increasing K^+ concentrations. The subsequent samplings through 72 hours are presented in Figure 4.4b and show the K^+ concentration continues to increase, the Al concentration decreases, and the Si concentration is constant. The dashed line suggests the K^+ release follows the same trend established during the first 7 hours through 72 hours. Between 100 and about 400 hours, the release of K^+ slows and the release of Si increases such that the K^+ and Si concentrations increase at the same rate, as shown in Figure 4.4c. The Al concentration continues to decrease. At 500 hours and longer (results are provided by Alekseyev et al. (1997) through 1848 hours), the concentrations of Al, K^+, and Si remain essentially constant.

The reaction of sanadine in sodium bicarbonate is observed to proceed through four stages: congruent dissolution prior to the precipitation of analcime, incongruent dissolution as analcime is initially nucleated, incongruent dissolution as the analcime crystals ripen, and no measurable dissolution when the system equilibrates. Sanadine dissolves stoichiometrically during the first 5 hours of the reaction (Stage 1). A power-law fit to the K^+ release is shown in Figure 4.4a (the fitted equation is $[K^+] = 0.69\ t^{0.36}$). Precipitation of analcime is first detected after 6 hours and begins the second stage (Stage 2). The extent of precipitation is such that all of the Si released by sanadine dissolution is consumed by the precipitation of analcime. The lack of change in the Si concentration during Stage 2 indicates that the stoichiometry in Equation 4.16 for the coupled reactions is $3x - 2y = 0$, where x and y are the numbers of moles of sanadine that dissolve and analcime that precipitate, respectively, so that $y = 1.5x$. Also, from the stoichiometry in Equation 4.16, 1.5 moles of analcime precipitate for every mole of sanadine that dissolves when the sanadine dissolution rate and the analcime precipitation rate are equal. These conditions result in a net consumption of 0.5 moles of Al per 1.5 moles of analcime formed.

Stage 3 occurs between about 120 and 400 hours during which time the K^+ and Si concentrations increase at the same rate. The stoichiometry of the coupled reactions indicates that equal amounts of sanadine dissolve and analcime precipitate ($x = 3x - 2y$) and there is no change in the Al concentration. The release of K^+ in Stage 3 is slower than would be predicted by extrapolating the trend in Stage 2, which indicates precipitation of analcime is now limiting the dissolution rate of sanadine. The system appears to have reached equilibrium after 400 days (the beginning of Stage 4), based on the constant K^+ concentrations and the equal amounts of Si and K^+ ($x = y = 0$).

Alekseyev et al. (1997) examined the solids of reacted sanadine and precipitated analcime particles that had been recovered from some tests using a scanning electron microscope and noted the surface morphologies and size ranges of the precipitated analcime crystallites. These were used to estimate the surface area of the precipitated analcime. Figure 4.5 shows the relative number of precipitated analcime crystallites having measured dimensions that were formed after reaction times of 16, 24, 72, 120, 168, 216, and 504 hours. The size distribution of between 40 and 70 crystallites was measured for each test. With regard to the previous discussion of the solution results, test durations of 16, 24, and 72 hours are in Stage 2, durations of 120, 168, and 216 hours are in Stage 3, and the test duration of 504 hours is at the beginning of Stage 4. Small crystallites had formed within16 hours, but did not increase in size significantly through 72 hours (throughout Stage 2). Most of the small crystallites had been replaced by larger crystals after 120 hours, at the same time the solution composition changed from Stage 2 to Stage 3. As

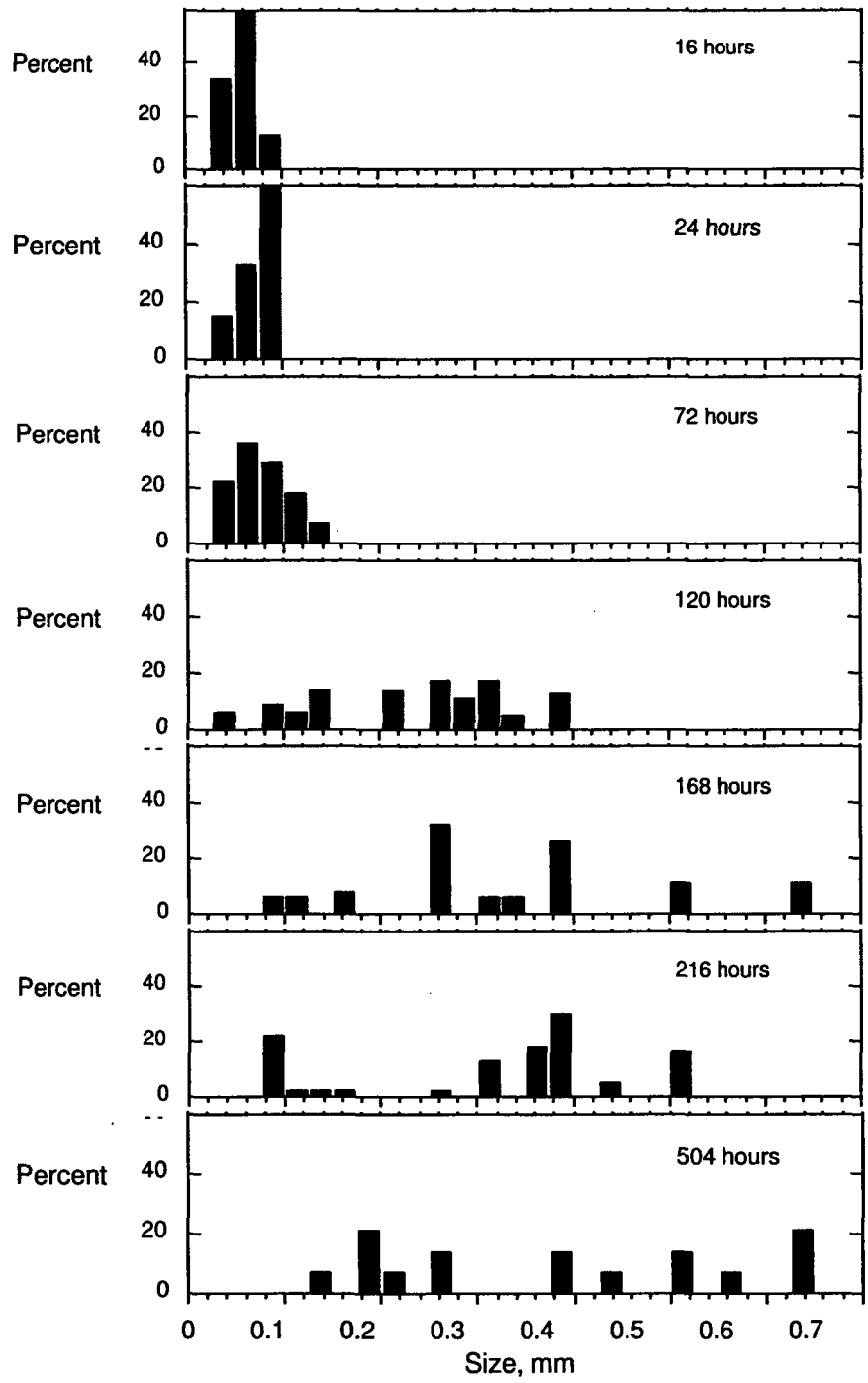

Figure 4.5. Results from Alekseyev et al (1997): Dimensions and size distributions of analcime crystallites after different reaction times. Reaction times of 16, 24, and 72 hours are in Stage 2, 120, 168, and 216 hours are in Stage 3, and 504 hours is in Stage 4.

discussed in Section 3, smaller crystallites have much higher specific surface areas (area per mass) and higher solubilities than larger crystals, so the system became stabilized by the formation of large crystals to replace small cystallites. Similar size distributions were observed for tests run at 168, 216, and 504 hours, with no obvious difference as the solution evolved from Stage 3 to Stage 4. A small number of small crystallites (< 0.2 mm) were detected at all test durations. Figure 4.6 shows the estimated number of analcime crystallites and calculated total surface area at different reaction times (the geometric surface area was calculated by assuming spherical particles with diameters equal to the measured particle sizes). The decrease in surface area occurring between 72 hours, which is the last data point in Stage 2, and 120 hours, which is the first data point in Stage 3, is a factor of 2.5. The surface area of precipitated analcime remains essentially constant at reaction times of 120 days and longer.

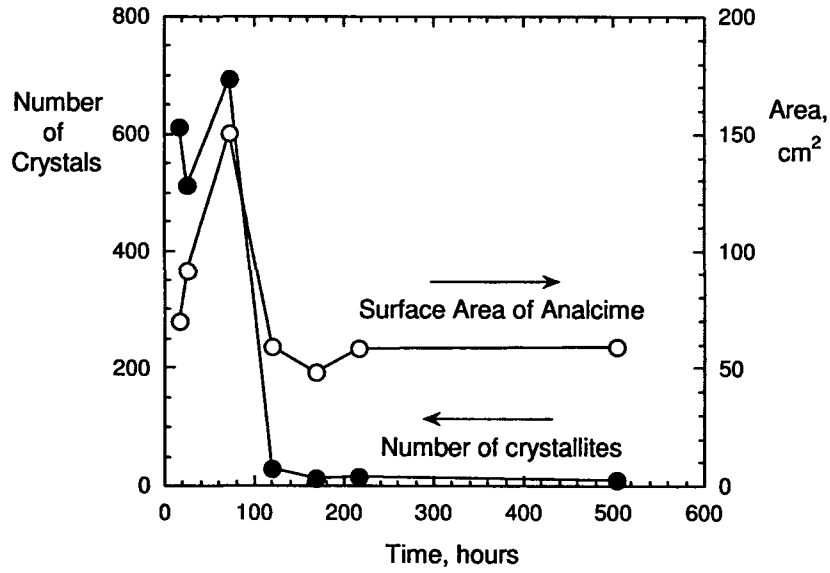

Figure 4.6. Results from Alekseyev et al (1997): Numbers (solid symbols) and total surface areas (open symbols) of analcime crystallites formed after different reaction times.

Consumption of Al and Si from solution due to the precipitation of analcime increases the dissolution rate of sanadine by increasing the affinity term (1 - Q/K_{sp}) for sanadine dissolution. The effect is most pronounced during the first four days that analcime is precipitating, when many small crystallites nucleate. The sanadine dissolution rate is not affected by the formation of the small crystallites in Stage 2, based on the continued release of K^+ following the same trend as in Stage 1. The Si concentration remains constant (at steady state) in Stage 2 and the Al concentration decreases as the sanadine dissolution and analcime precipitation occur at the same rate. The uninterrupted release of K^+ suggests that the analcime precipitation rate is not affecting the sanadine dissolution rate in Stage 2. The effect of analcime precipitation on sanadine dissolution changes as the many small crystallites of analcime formed initially are replaced by fewer large crystals and the total surface area of analcime decreases as a result. This slows the sanadine dissolution in Stage 3 relative to the rate in Stage 2, based on the slower increase in the K^+ concentration. The Si concentration in Stage 3 increases above the transient steady-state concentration observed during Stage 2 and the Al concentration continues to decrease to very low concentrations. In Stage 3, it appears that the precipitation of analcime is not able to consume the

Si that is released as sanadine dissolves. The increasing Si concentration slows the dissolution rate as the solution approaches saturation. The precipitation rate of analcime is probably limited by both the decreasing availability of Al in the solution and lower surface area of analcime. The change in solution behavior in transitioning from Stage 3 to Stage 4 is assumed to indicate a nearly equilibrated system; there is no obvious change in the size or abundance of analcime crystals between Stages 3 and 4.

These tests provide a useful data base for demonstrating the relationship between the free energy and the dissolution rate as near-equilibrium conditions are approached in a system with two phases. Alekseyev et al. (1997) estimated the dissolution rates at different points of the reaction by determining the tangents of curves drawn with neighboring points. The Gibbs free energy values were calculated using values of Q/K based on the measured solution compositions and independent equilibrium experiments conducted with sanadine, albite, and analcime (see Alekseyev et al. 1997). The sanadine dissolution rates for the full set of experiments are plotted against the Gibbs free energy in Figure 4.7a, where the open symbols denote test results prior to analcime precipitation and the filled symbols denote test results after analcime precipitated. The first test result (after 15 minutes) provides an estimate of the "far-from-equilibrium" rate under these test conditions and has a calculated Gibbs free energy of -12.1 kcal/mol. Subsequent samplings show a steep ascent towards the "near-to-equilibrium" rate. The kink in the trend after about 2 hours (between ΔG values of -4.1 and -2.9 kcal/mol) gives a plateau analogous to that shown for labradorite in Figure 4.3, which was modeled using a non-linear free energy dependence. It was suggested by Alekseyev et al. (1997) that this may indicate dissolution of two different surface sites. Another kink occurs between about 7 and 16 hours, which corresponds to the transition between Stage 1 and Stage 2 behavior seen in the solution results and the initial precipitation of analcime. This is most likely a real change in mechanism wherein the reaction controlling the system changes from the dissolution reaction in Equation 4.14 to the coupled reaction in Equation 4.16. Figure 4.7b shows both the sanadine dissolution and analcime precipitation rates near equilibrium on an expanded scale. The black solid curves drawn for sanadine dissolution in Figures 4.7a and 4.7b represent the fit regressed to the full data set for sanadine dissolution reported by Alekseyev et al. (1997) as

$$\frac{R_{sanadine}}{S} = -500\left[1-\left(Q/K_{sp}\right)^{0.16}\right]^{1.4} \tag{4.17}$$

The fit to the initial results (open symbols) is good, but it does not represent sanadine dissolution when analcime is precipitating beyond 7 hours (filled symbols). The blue dashed curves in Figures 4.7a and 4.7b show the fit to the linear model

$$\frac{R_{sanadine}}{S} = -500\left[1-\left(Q/K_{sp}\right)^{1}\right]^{1} \tag{4.18}$$

which fits the far-from-equilibrium conditions (not shown) but is not consistent with the approach to equilibrium or the coupling with analcime precipitation near equilibrium. The use of separate free energy terms is probably required to account for the change(s) in the mechanism as the system evolves toward equilibrium.

The sanadine dissolution rates and analcime precipitation rates calculated by Alekseyev et al. (1997) for tests run between 6 hours and 1845 hours are plotted in Figure 4.7b. The results for

sanadine dissolution after 6 hours and 120 hours of reaction are identified to orient the changes in dissolution behavior from congruent dissolution in Stage 1 to incongruent dissolution in Stage 2 and from Stage 2 to Stage 3 behavior, respectively. Analcime precipitation is fastest at 6, 7, and 16 hours, and the degree of supersaturation with respect to the reaction in Equation 4.15 is highest at 16 and 24 hours. Note that the sanadine dissolution rate decreases in the 48, 72, and 120 hour tests even though the free energy remains nearly constant at $\Delta G = -12.1$ kcal/mol. Furthermore, the free energy for sanadine dissolution becomes more negative beyond 120 hours (i.e., favoring dissolution), but the dissolution rate continues to decrease. The sanadine dissolution rate is clearly not linearly related to the free energy for the dissolution reaction in Equation 4.14 beyond about 120 hours. Instead, the dissolution rate of sanadine is affected by the precipitation rate of analcime.

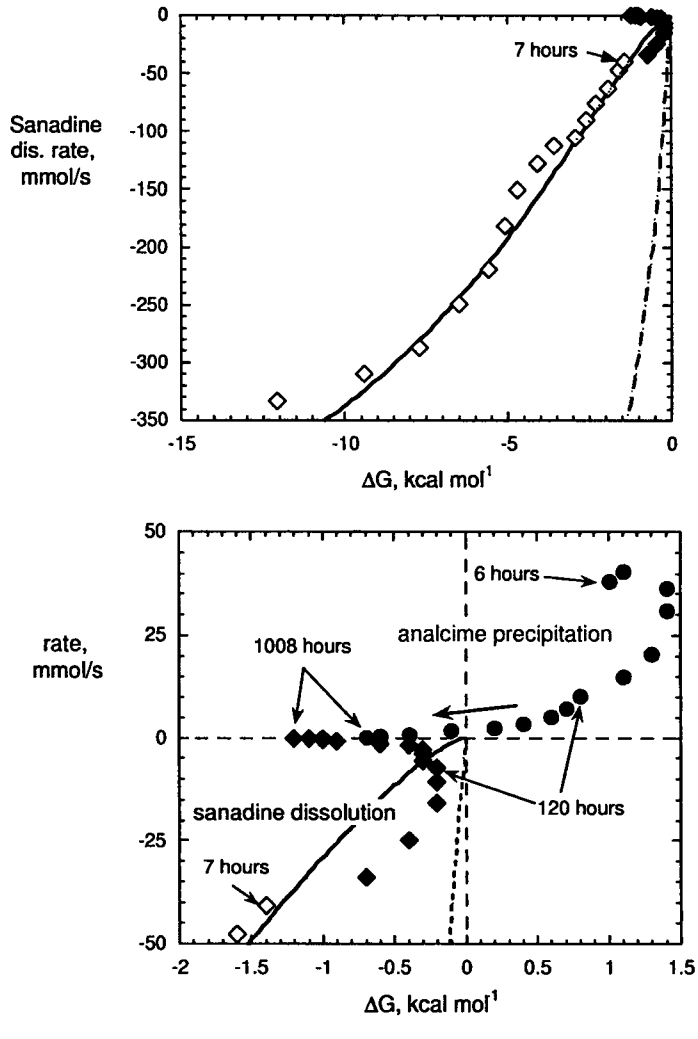

Figure 4.7. Results from Alekseyev et al (1997): (a) Sanadine dissolution rate vs. Gibbs free energy and (b) Sanadine dissolution rate and analcime precipitation rate vs. Gibbs free energy from 6 to 1845 hours.

The free energy driving analcime precipitation decreases from a maximum value at 24 hours of $\Delta G = 1.3$ kcal/mol, to $\Delta G = 0.8$ kcal/mol at 120 hours, and then $\Delta G = 0.2$ kcal/mol at 360 hours. After 504 hours, the calculated free energies for analcime precipitation and sanadine dissolution are $\Delta G = -0.1$ kcal/mol and $\Delta G = -0.6$ kcal/mol, respectively, indicating the system is not at equilibrium. The free energy calculated for sanadine dissolution (Equation 4.14) represents the rate-controlling mechanism during the first 72 hours, then analcime precipitation controls the system through about 360 hours, then the coupled reaction given in Equation 4.16 describes the system as it approaches equilibrium.

This example shows the importance of alteration phase formation on the dissolution rate of a primary phase when the reactions are coupled. The effect can be more significant than just that of a common solution. That is, not only does the precipitation of analcime affect the dissolution rate of sanadine through the value of Q, K_{sp} now represents the coupled reactions rather than the dissolution of sanadine alone. This is shown in the following example.

Another system studied by Alekseyev et al. (1997) was the dissolution of low albite and precipitation of sanadine in a 0.1 molal potassium bicarbonate solution. The dissolution and precipitation reactions are written as

$$\underset{\text{albite}}{x\text{NaAlSi}_3\text{O}_8} + 8x\text{H}_2\text{O} = x\text{Na}^+ + x\text{Al(OH)}_4^- + 3x\text{H}_4\text{SiO}_4 \qquad (4.19)$$

and

$$y\text{K}^+ + y\text{Al(OH)}_4^- + 3y\text{H}_4\text{SiO}_4 = \underset{\text{sanadine}}{y\,\text{KAlSi}_3\text{O}_8} + 8y\text{H}_2\text{O}, \qquad (4.20)$$

where x and y are the numbers of moles of albite dissolved and sanadine precipitated, respectively, and the coupled reactions are written as

$$\underset{\text{albite}}{x\text{NaAlSi}_3\text{O}_8} + y\text{K}^+ + (8x\text{-}8y)\text{H}_2\text{O} = \underset{\text{sanadine}}{y\,\text{KAlSi}_3\text{O}_8} + x\text{Na}^+ + (x\text{-}y)\text{Al(OH)}_4^- + (3x\text{-}3y)\text{H}_4\text{SiO}_4. \qquad (4.21)$$

The solution results are shown in Figures 4.8a, 4.8b, and 4.8c for short, intermediate, and long reaction times. As seen in Figure 4.8a, the release rates of Na^+, Al, and Si are high initially (Stage 1) but decrease to very low rates between about 5 hours and 24 hours (Stage 2). The releases are essentially congruent in Stage 1 and Stage 2. The Si concentration decreases between 24 and 48 hours, then remains nearly constant through about 168 hours (Stage 3). Precipitated sanadine is first detected after 24 hours. The Al concentration decreases slightly and the Na^+ concentration increases slightly in Stage 3. Consistent with the stoichiometry of the coupled reactions, the slope of the Na^+ increase is twice that of the Al decrease. The Na^+ concentration increases rapidly beyond 200 hours, whereas the Al and Si maintain their Stage 3 concentrations. The release of Na+ is linear through about 1400 hours. The Na^+ release coincides with the precipitation of sanadine and the constant Al and Si concentrations are consistent with the stoichiometry in Equation 4.21 for the coupled reactions.

The measured rates for albite dissolution and sanadine precipitation are plotted against the calculated free energies in Figures 4.9a and 4.9b. The curves drawn for albite dissolution in Figures 4.9a and 4.9b represent the regression fit by Alekseyev et al. (1997) using a rate equation that is non-linear in the free energy dependence

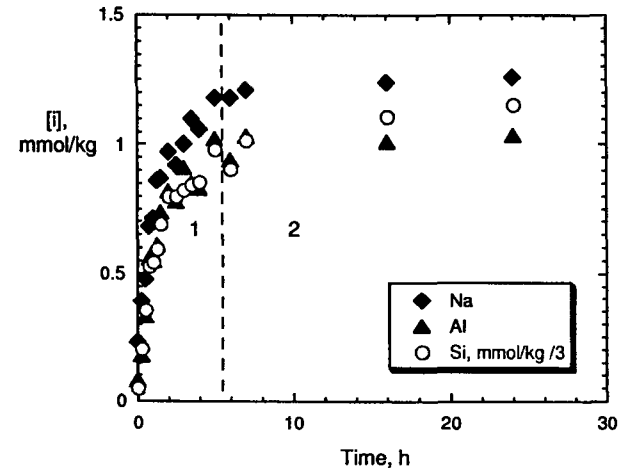

(a)

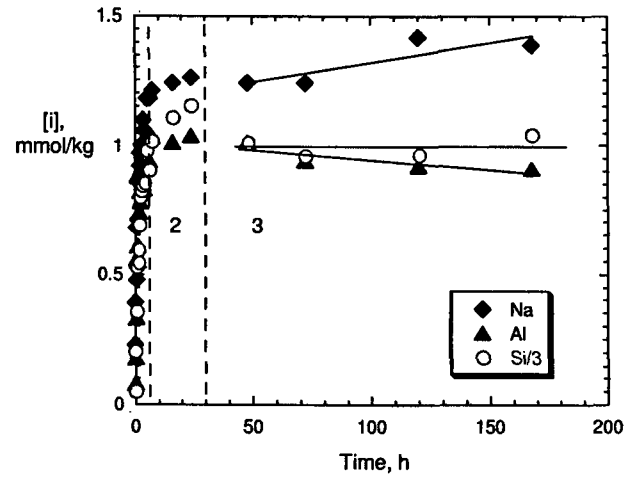

(b)

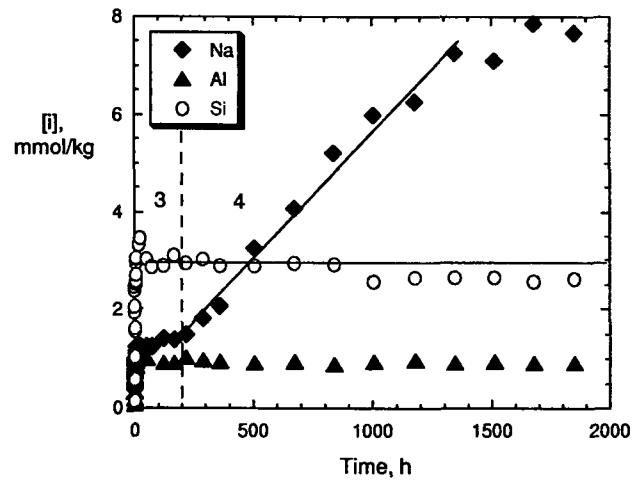

(c)

Figure 4.8. Results from Alekseyev et al (1997): Solution concentrations of Na^+, Al, and Si in experiments with albite through (a) 30 hours, (b) 200 hours, and (c) 2000 hours.

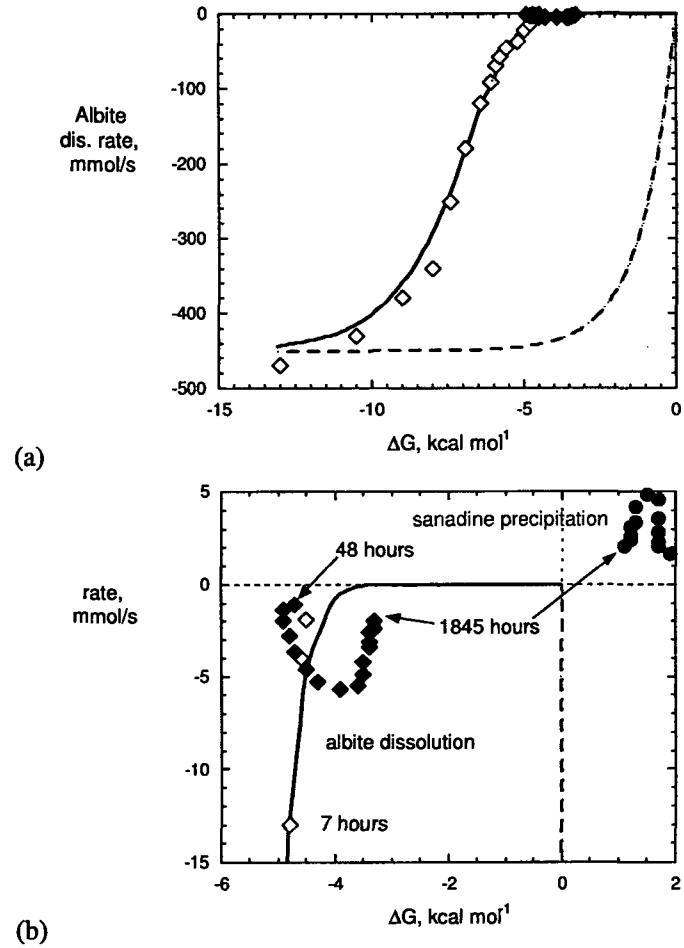

Figure 4.9. Results from Alekseyev et al (1997): (a) Albite dissolution rate vs. Gibbs free energy and (b) albite dissolution rate and sanadine precipitation rate vs. Gibbs free energy from 7 to 1845 hours.

$$\frac{R_{albite}}{S} = -450\left[1-\left(Q/K\right)^{0.76}\right]^{90}. \tag{4.22}$$

The fit is good over the first 24 hours prior to the precipitation of sanadine (open symbols in Figure 4.9a), but it is not a good fit after sanadine precipitates (filled symbols). The dashed (blue) curves in Figures 4.9a and 4.9b show the fit to the linear model

$$\frac{R_{sanadine}}{S} = -450\left[1-\left(Q/K\right)^{1}\right]^{1}, \tag{4.23}$$

which fits the far-from-equilibrium conditions but is not consistent with the approach to equilibrium or coupling with sanadine precipitation.

In this system, the solution becomes supersaturated with respect to sanadine after 1.5 hours, based on the calculated ΔG values, but sanadine crystallites are not detected until after 48 hours. The values of ΔG for albite dissolution become more negative than the 24-hour value for tests between 48 and 216 hours and the dissolution rate increases between 48 and 504 hours, and then become smaller again to form a loop in the rate vs. ΔG plot. The free energy values for sanadine precipitation continue to decrease over time. The albite dissolution rate is seen to be correlated with the sanadine precipitation rate: increasing between 48 and 504 hours and decreasing thereafter. In fact, the rates are equal after 9 days and beyond.

These examples illustrate the potential importance of other phases on the dissolution behavior of a phase of interest under near-saturation conditions. (The effects are negligible under far-from-equilibrium conditions.) The precipitation of a secondary mineral will affect the dissolution rate of a primary mineral through the concentrations of common species even if the precipitation rate does not control the coupled rate. The dissolution rate of a mineral will be higher when the possibility of secondary mineral precipitation is excluded because the equilibrium solution composition will be attained faster. In the first example, the experimentally-measured dissolution behavior of sanadine would have been different if the Na content of the test solution was higher or at a lower pH where analcime precipitation was not favorable. Although analcime formed as a secondary phase in these tests, it could have been added at the beginning of the test. The observed behavior would likely have been different, since nucleation, growth, and ripening of analcime embryos would not be required and Stages 2 and 3 might not have been observed. Instead, the system would have evolved to equilibrium (Stage 4) at a rate depending on the relative surface areas of the two phases.

In the second example, dissolution of albite had nearly ceased until the precipitation of sanadine caused an increase in the dissolution rate by consuming Al and Si. The albite dissolution rate appears to be controlled by the precipitation rate of sanadine thereafter. The system moved away from albite equilibrium when sanadine first precipitated and the albite dissolution rate increased. The system then moved towards equilibrium after 504 hours, presumably as the sanadine crystallites matured, although equilibrium was not attained after 1845 hours.

4.3 Effects of Intermediate Phases

The results of Alekseyev et al (1997) showed correlations between the solution compositions, the dissolution of the primary phases, and the precipitation of secondary phases. Differences in dissolution and precipitation rates of different minerals will cause the evolution of the solids assemblage and composition to lag behind the evolution of the solution chemistry. As a groundwater flows through a natural system, it interacts with many phases that may dissolve or precipitate to modify the groundwater composition. Changes in the solution chemistry could result in saturation of another phase, which could precipitate to further change the solution composition. The precipitation of a less stable phase could compete with the precipitation of a more stable phase. The following example shows the effect of forming an intermediate phase on the dissolution rate of a primary phase when the solution is far from equilibrium.

Batch dissolution experiments were conducted by Fu et al. (2009) in which albite was dissolved in a ~0.20 molal KCl solution acidified to pH 3.0 with HCl at 200°C and 300 bars. The albite was ground and sieved to isolate the 50–100 μm size fraction, which was washed repeatedly with acetone and then with water to remove fines. The specific surface area was determined to be 0.13 $m^2 g^{-1}$ with BET analysis. Tests were conducted with 1.5 g albite in 40 mL solution. Albite dissolution is incongruent and results in the formation of kaolinite by the reaction

$$\underset{\text{albite}}{NaAlSi_3O_8} + H^+ + 0.5H_2O \rightarrow \underset{\text{kaolinite}}{0.5Al_2Si_2O_5(OH)_4} + Na^+ + 2SiO_2. \quad (4.24)$$

Albite dissolution consumes H^+ and releases Na^+ and SiO_2 to solution (at a 1:2 mole ratio) and the solution composition is expected to evolve accordingly. The solution compositions measured for six samplings over time are given in Table 4.1. Analysis of the reacted solids after 5 days (solids recovered from separate experiments) and after 78 days (the 1872-hour sampling in these tests) revealed the formation of boehmite (AlOOH) in addition to kaolinite. The formation of boehmite occurs through the reaction

$$\underset{\text{albite}}{NaAlSi_3O_8} + H^+ \rightarrow \underset{\text{boehmite}}{AlO(OH)} + Na^+ + 3SiO_2. \quad (4.25)$$

Table 4.1. Evolution of solution composition during albite dissolution

Sample	Time, h	Concentration, mmoles/kg						pH	
		Cl^-	K^+	SiO_2	Na^+	Ca^+	Al^{3+}	25°C	200°C
	0	198.3	204.0	NA	NA	3.72	NA	3.0	3.1
1	24	197.5	202.8	0.31	0.42	0.12	0.01	3.2	3.3
2	216	198.7	201.1	1.46	1.13	0.21	0.003	3.5	3.6
3	456	196.8	197.8	1.70	2.04	0.43	0.08	4.1	3.7
4	816	167.9	204.3	1.35	1.86	0.16	0.03	4.2	4.0
5	1368	199.5	197.0	4.18	3.72	0.30	0.01	4.9	4.5
6	1872	199.4	196.5	3.75	1.91	0.35	0.001	4.9	4.7

Figure 4.10a shows the evolution of the solution concentrations of Na^+ and SiO_2 overlaying the mineral phase diagram. The solution composition measured in Sampling 1 lies in the boehmite field whereas the compositions of subsequent samplings lie in the kaolinite field. (A separate experiment showed boehmite to form within 5 days.) Within the first 216 hours, boehmite that was formed initially begins to convert to kaolinite by the reaction

$$\underset{\text{boehmite}}{AlO(OH)} + 0.5H_2O + SiO_2 \rightarrow \underset{\text{kaolinite}}{0.5Al_2Si_2O_5(OH)_4}. \quad (4.26)$$

The initial solution composition is dominated by the leachant used in the experiment and evolves towards compositions in the albite field as albite dissolves. The precipitation of first boehmite and then kaolinite provide metastable systems that affect the albite dissolution rate.

The evolution of the Al, Na^+, and SiO_2 concentrations over time are plotted in Figure 4.10b to help interpret Figure 4.10a. The rates of Na^+ and SiO_2 increases are greater between the first and second samplings than between subsequent samplings and the release of Al decreases except between the second and third sampling when it increases by a factor of 27. The initial dissolution of albite adds Na^+, Al^{3+}, and SiO_2 to solution with negligible amount of product phases precipitating. Between the first and second sampling, boehmite precipitates to consume Al^{3+} from solution, but little kaolinite forms. Between the second and third samplings, boehmite becomes unstable and begins to dissolve and release Al^{3+} into solution, and the Al^{3+} concentration increases due to the dissolution of both albite and boehmite. The relatively high Al^{3+} concentration moderates the dissolution rate of albite, which is reflected by the nearly steady-state SiO_2 concentrations in the second, third, and fourth samplings when the boehmite and albite

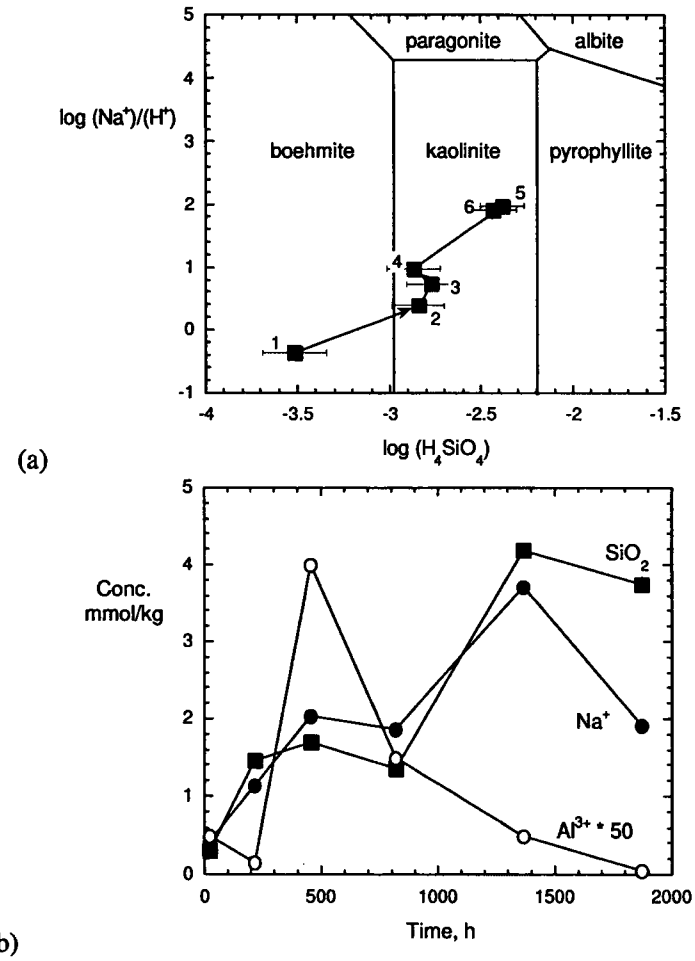

Figure 4.10. Results from Fu et al. (2009): Solution concentrations plotted (a) on Na_2O-Al_2O_3-SiO_2-H_2O-HCl phase diagram and (b) against test duration.

dissolution rates are coupled. As seen in Figure 4.10b, this results in upward migration on the phase diagram parallel to the boehmite-kaolinite phase boundary, which occurs because Na^+ is released and H^+ is consumed by albite dissolution. The Na^+ and SiO_2 concentrations increase significantly between samplings 4 and 5 and the Al^{3+} concentration continues to decrease (see Figure 4.10b). This places the solution composition far from the boehmite/kaolinite boundary (see Figure 4.10a), but boehmite is still detected after the sixth sampling and the solution is not in equilibrium with the solids. The solution concentrations of Al^{3+}, Na^+, and SiO_2 all decrease between the fifth and sixth sampling, albeit only slightly. This may indicate that kaolinite precipitation has become faster than albite dissolution and that the solution is being driven to equilibrate with a mixture of kaolinite and the remaining boehmite.

This simple example demonstrates the impact even an intermediate phase can have on a weathering system. The rate of the overall process as measured by the release or uptake of dissolved silica $rate_{Si\ r/u}$ can be calculated from the individual reactions

$$rate_{Sir/u} = \frac{\sum_n \frac{\Delta m_{Si,n}}{\beta_n}}{t}, \tag{4.27}$$

where $\Delta m_{Si,n}$ is the change in the number of moles of silica as it is either dissolved or consumed by each of the n reactions contributing to the overall process (absolute value), and β_n accounts for the stoichiometry of SiO_2 in each reaction. For the dissolution of albite discussed above, the first three samplings reflect the dissolution of albite to form boehmite by the reaction in Equation 4.25, in which 3 moles of SiO_2 are released per mole albite dissolved. The SiO_2 concentration is 1.70 mmol/kg after 456 hours, and the test was conducted with 40 g of solution. Using Equation 4.27, the albite dissolution rate and the boehmite precipitation rate are

$$rate_{Sir/u} = \frac{\left(\frac{0.04\,kg \times 1.70\times10^{-3}\ moles\,SiO_2\,kg^{-1}}{3\ moles\,SiO_2\ per\ mole\,albite\,dissolved}\right)}{1.64\times10^{6}\ sec} = 1.38\times10^{-11}\ mol\cdot s^{-1}. \tag{4.28}$$

The specific surface area of the albite was 0.13 $m^2\ g^{-1}$ and 1.5 g was used in the experiment, so the initial surface area was 0.195 m^2, and the dissolution rate was 7.08 x 10^{-11} mol $m^2\ s^{-1}$. If the formation of boehmite had not been detected and if it was assumed that albite was dissolving to form kaolinite directly during the first 456 hours by the reaction in Equation 4.24, the albite dissolution rate would have been calculated to be 1.06 x 10^{-10} mol $m^2\ s^{-1}$, which is 50% higher. Boehmite becomes unstable between samplings 4 and 5, and albite dissolution results in the direct formation of kaolinite according to the reaction in Equation 4.24, in which 2 moles SiO_2 are released per mole albite dissolved. Assuming the same solution volume, the rate calculated for the reaction between samplings 4 and 5 is double the initial rate

$$rate_{Sir/u} = \frac{\left(\frac{0.04\,kg \times (4.18-1.35)\times10^{-3}\ moles\,SiO_2\ kg^{-1}}{2\ moles\,SiO_2\ per\ mole\,albite\,dissolved}\right)}{1.99\times10^{6}\ sec} = 2.85\times10^{-11}\ mol\cdot s^{-1}. \tag{4.29}$$

The precipitation rate of kaolinite between samplings 4 and 5 is calculated to be half that of albite because one mole kaolinite is formed per 2 moles dissolved albite and per 4 moles dissolved SiO_2

$$rate_{Sir/u} = \frac{\left(\frac{0.04\,kg \times (4.18-1.35)\times10^{-3}\ moles\,SiO_2\ kg^{-1}}{4\ mole\,SiO_2\ per\ mole\,kaolinite\ precipitated}\right)}{1.99\times10^{6}\ sec} = 1.42\times10^{-11}\ mol\cdot s^{-1}. \tag{4.30}$$

If the solution had not been sampled until 1368 hours of reaction and the SiO_2 concentration was 4.18 mmol/kg, the calculated albite dissolution rate would have been 1.13 x 10^{-11} mol s^{-1} and the specific rate 5.81 x 10^{-11} mol $m^{-2}\ s^{-1}$, based on the initial BET surface area of 0.195 m^2.

The solution concentration of SiO_2 is affected by the dissolution of primary phases and the precipitation and dissolution of both transient and stable secondary phases as the mineralogy of the system evolves. The solution concentration of Na^+ is not directly affected by the precipitation

of boehmite in the albite system being considered here. If the solution concentration of Na^+ is used to monitor the extent of dissolution instead of SiO_2, the average dissolution rate between 0 and 456 hours is 4.97×10^{-11} mol m^{-2} s^{-1}. This is 3.6-times the rate based on the SiO_2 concentration for the same duration. The average dissolution rate between 0 and 1368 hours is 3.02×10^{-11} mol s^{-1} (1.55×10^{-10} mol m^{-2} s^{-1}), but the average rate between 0 and 1872 hours based on Na^+ is only 1.13×10^{-11} mol s^{-1} (5.81×10^{-10} mol m^{-2} s^{-1}). The decrease in rate between 1368 and 1872 hours reflects the decrease in Na^+ concentration due to consumption by the precipitation of boehmite, albite, or another phase. In a more complex system, some of the Na^+ could be removed from solution by ion exchange (e.g., with another feldspar) or other uptake mechanism. The use of any single component to monitor the extent of reaction requires consideration of possible effects of competing reactions on the measured solution concentrations. Differences in dissolution and precipitation rates, and also differences in the exposed surface areas, will cause the evolution of the solids composition to lag behind evolution of the solution chemistry. The disequilibrium between the solution composition and the solids, even in a static system, adds uncertainty to the prediction of both.

4.4 Relevance of Evolving Dissolution Behavior to Surface Disposal Systems

The primary issue presented and discussed in this section is the differences in the dissolution rates and behaviors of a material that can occur under far-from-equilibrium and under near-to-equilibrium conditions. Changes in the dominant reaction sites and the impact of coupled reactions, such as the precipitation of secondary phases can occur as equilibrium between the primary phase and the solution is approached. Relevant to surface disposal systems are (1) the observations of the different behaviors due to solution composition and interactions with other phases (which are already present or precipitate), (2) the experimental methods used to measure the dissolution behavior, and (3) the modeling approaches used to interpret the experiments.

The majority of laboratory tests address material dissolution under far-from-equilibrium conditions in which the affinity effect due to species released during the dissolution of the material is minimized so that the effects of temperature, pH, specific solutes, and the composition of the dissolving material can be quantified and included in the dissolution model. However, as shown by the examples discussed above, the dissolution kinetics can change significantly as equilibrium is approached due to changes in the predominant dissolution sites or the influence of other reactions. Analytical models that represent dissolution behavior well under far-from-equilibrium conditions may not accurately represent the behavior of coupled systems of primary and secondary materials under near-equilibrium conditions. Understanding the dissolution behavior over the full range of environmental conditions is crucial to forward modeling approaches (such as reactive transport modeling) in order to take into account the wide range of possible reaction conditions and contaminant release rates that can occur. It is also important for understanding the relationship between measured laboratory rates and the rates inferred from field studies.

It is generally assumed that value of the affinity term must decrease to near zero before affinity effects become significant based on a linear rate law. However, Figures 4.7a and 4.9a show that solutions only slightly more concentrated than far-from-equilibrium conditions can result in much lower dissolution rates (solid black curves fitting the test results) than would be predicted by using a linear rate law (dashed blue curves). It is likely that differences in the effects of the solution concentration on field and laboratory systems have a much greater impact than have been assumed in the past based on a linear rate law. Field systems include a large array of phases that

interact as sources and sinks for the solutes in migrating groundwater. The effects of other phases will probably be negligible under far-from-equilibrium conditions used in many laboratory experiments to measure mineral dissolution rates, but will be significant under the near-equilibrium conditions that exist in most natural environments. The behavior of a particular mineral may also be different in the presence of other phases in the field than when isolated in a laboratory test. The interactions will be strongest under conditions very near to equilibrium, but the influence of other phases may also be significant in more dilute solutions.

In a surface disposal system with different areas of high and low effective porosity that is exposed to weather changes, the contact of various surfaces by run-off water, large volumes of perched water, and small volumes of static pore waters, coupled with the effects of intermittent contact during wet/dry cycling can impose a wide range of solution conditions on exposed surfaces. They range from the far-from-equilibrium conditions provided by run-off water to the nearly-saturated conditions generated in water trapped in non-connected pores and cracks. The release of contaminants from various phases in the disposal system will be affected by the spatial and temporal extents of the water contact conditions and the dynamics of water flowing through the system, including wet/dry cycling and the occasional flushing of otherwise stagnant pore waters. The weathering behaviors of phases exposed to these different environments could be very different and a range of laboratory test methods and test conditions would be required to characterize contaminant release under each of the full range of possible weathering conditions. Near-equilibrium behavior and interactions with neighboring phases will be important in stagnant environments but not in open environments exposed to high flow rates. Alteration products are expected to overgrow the primary phases and may restrict their continued alteration in stagnant environments, but not necessarily in open environments. Release of contaminants from stagnant locations may require flooding events to overcome the transport limitations, whereas release from open environments would be coupled with the advective currents.

Measuring dissolution behaviors under near-saturation conditions is experimentally difficult because small differences must be measured in concentrated solutions and the dissolution rates are low. Static tests and dynamic tests conducted in nearly saturated solutions can provide near-saturation conditions. A testing approach similar to that discussed in Section 4.2 can be used to study weathering under saturated conditions under very aggressive test conditions that differ significantly from the natural system (e.g., at much higher temperatures and pressures). The dynamic method discussed in Section 4.1 can also be used and provides a simple system that could be used to represent a disposal system. This method requires long durations, long columns, and very low flow rates. The approach to equilibrium could be accelerated by generating nearly saturated solutions and alteration phases in separate tests and tracking changes in the solution and the surface conditions that occur when the fresh material of interest is added to the system. These are research methods that may not be practical for characterizing all of the phases that must be considered when modeling a disposal system.

The composition of a flowing ground water may remain far from equilibrium with the materials it flows over and through, depending on the flow rate and flow path, but the solution is expected to evolve towards equilibrium as the flow path increases or flow rate decreases, albeit very slowly. The evolution of the solution chemistry in a static system that was discussed in Section 4.3 also applies to flowing ground water. The disposal system can be modeled as a column through which water flows and contacts various and dispersed phases. Water may contact a phase of interest only occasionally and only for a short time as it flows through the column, but a small amount of material will dissolve each time it is contacted. The dissolved components will be transported by the water to the next location where the phase is encountered and the interaction will be a little different because of the different solution chemistry. Of course, the groundwater composition

will be affected by interactions with other phases it contacts, so the interactions of different phases can occur over space and time. This process can be modeled conceptually in the same way as the small-scale column experiments discussed in Section 4.1. Migration of contaminants that are released from a particular phase through the column may be interrupted by sorption or the precipitation of a phase that sequesters the contaminant, or by an interruption of advection by the evaporation of the water. These effects can be modeled by mass transport equations through the retardation and advection terms; this is discussed in the following section.

5 Mass Balance Approach

The majority of the field-based mineral dissolution rates to which rates measured in the laboratory are compared have been determined (inferred) by applying mass balance analyses to measurements of surface or groundwater compositions. The mass balance approaches used by several researchers are described in detail in this section for two purposes: to evaluate the uncertainties in the inferred mineral dissolution rates that are compared with rates measured directly in the laboratory and to present and evaluate the mathematical and analytical tools used for mass balance analyses that could be applied to assessments of surface disposal systems. The first purpose is the topic of this report and the second will be the main topic of a future report.

Mass balance modeling is a bookkeeping exercise in which additions and removals of key species from solution by various processes over time are estimated to explain the change from a known initial composition to a known final composition. Application of the mass-balance approach in the field study of weathering within a catchment involves (1) defining the volume of interest, (2) measuring the fluxes of solutes into and out of that volume, (3) identifying the likely sources and sinks within the volume, and (4) determining the dissolution and precipitation rates (or release and uptake rates) of those sources and sinks that are consistent with the measured fluxes.[2] The results can include identifying the minerals responsible for changes in the composition of the water passing through the volume of interest and the dissolution and precipitation rates of those minerals. Most studies apply the mass balance requirement to components dissolved in the water exiting a watershed or aquifer, and those studies will be the primary focus of this discussion. Alternative methods include tracking the evolution of mineral assemblages in a regolith and changes in groundwater composition with depth (e.g., Maher et al. 2004).

Although early studies utilized characterizations of the ground water composition whereas most current studies address solute fluxes, the mass balance approach is the same. The concentration of soluble species such as Na^+, K^+, Ca^{2+}, Mg^{2+}, and SiO_2 (H_4SiO_4) in stream water can all be used to monitor the extents of mineral dissolution/precipitation reactions, but the relationships that are determined will usually be different because not all species are present in all minerals, some species participate in sorption and desoption reactions, and different species are sequestered in product phases to various extents. In most cases, mean annual concentrations are used to "average" the effects of daily and seasonal variations in the complex hydrochemical processes that occur in the system of interest. An important factor for stream waters is the mixing of base-flow water with occasional storm flows. The concentration variation due to storm flow can be taken into account as (Johnson et al. 1969)

$$C_{c,discharge} = \left(\frac{1}{1+\beta D}\right)\left(C_{c,soilwater} - C_{c,precipitation}\right) + C_{c,precipitation}, \quad (5.1)$$

where $C_{c,\,dscharge}$ is the annual discharge concentration of c, $C_{c,soilwater}$ is the concentration in ground water, $C_{c,\,precipitation}$ is the concentration in rain water, D is the stream discharge (runoff), and β is an empirical parameter defined as the ratio of the fluid residence time in the system to the initial volume of soil water. As an example, value $\beta = 1 \times 10^{-4}$ ha day L^{-1} was determined for Na^+, Mg^{2+}, SiO_2, SO_4^{2-} and Cl^-, and a value $\beta = 1 \times 10^{-5}$ ha day L^{-1} was determined for H^+, Al, and Ca^{2+} for Hubbard Brook in New Hampshire (Johnson et al. 1969). Components in the former group of

[2] A catchment is a region for which the incoming and outgoing waters can be quantified.

elements were diluted with increases in the discharge and components in the latter group were concentrated, which reflects their relative abundances in the soil water and precipitation. The annual discharge concentration approaches the soil water concentration, $C_{c,\ soilwater}$, for low runoff volumes and concentration in rain water, $C_{c,\ precipitation}$, for high runoff. The flux of solute c in the discharge fluid, $Q_{c,\ discharge}$, is

$$Q_{c,\,discharge} = C_{c,\,discharge} \times \frac{V}{S\,t}, \tag{5.2}$$

where V is the volume of fluid, S is the surface area of the watershed, and t is time. For a reservoir volume of interest, the conservation of mass in terms of fluid flux can be operationally defined using a steady state assumption as

$$Q_{c,\ wet} + Q_{c,\ dry} + Q_{c,\ desorption} + Q_{c,\ weathering} + Q_{c,\ bio-decay} = Q_{c,\ discharge} + Q_{c,\ bio-uptake} + Q_{c,\ sorption} \tag{5.3}$$

where

$Q_{c,\ wet}$ = input flux due to wet precipitation
$Q_{c,\ dry}$ = input flux due to dry deposition
$Q_{c,\ desorption}$ = input flux due to desorption from rocks and soil
$Q_{c,\ weathering}$ = net output flux due to weathering of rocks and soil
$Q_{c,\ bio\text{-}decay}$ = input flux due to biological decay
$Q_{c,\ sorption}$ = uptake flux due to sorption on rocks and soil
$Q_{c,\ bio\text{-}uptake}$ = uptake flux to biomass

Note that other terms are often included in the flux balance to take into account anthropogenic inputs, suspended solids, etc. Those were excluded in the analyses considered in this report. Rearranging Equation 5.3 in terms of $Q_{c,\ weathering}$ produces

$$Q_{c,\,weathering} = Q_{c,\ discharge} - \left(Q_{c,\,wet} + Q_{c,\,dry}\right) + \left(Q_{c,\,bio-uptake} - Q_{c,\,bio-decay}\right) + \left(Q_{c,\,sorption} - Q_{c,\,desorption}\right) \tag{5.4}$$

Knowledge of the input fluxes due to wet and dry atmospheric deposition, the net effect of the biota, and the net effect of ion exchange (e.g., through partition coefficients), the net input of component i due to the dissolution and precipitation of phases in the rock and soil can be estimated from the discharge composition and flux. Precipitation, runoff, and evapotranspiration (ET) data for many watersheds on granitic rocks have been compiled by White and Blum (1995) in their evaluation of climate effects on chemical weathering. Solutes become more concentrated due to ET, and it may be difficult to distinguish the effect of ET from the extent of weathering based on concentration alone. However, "watershed solute fluxes are not susceptible to ET effects" (White and Blum 1995). Application of the mass-balance method is described and evaluated using the approaches and results available in several literature sources.

Bowser and Jones (2002) listed five restrictions to the mass-balance method:

- The number of plausible phases included in the model must be equal to the total number of analyzed solute species in water,
- The solute species considered are restricted to those elements whose stoichiometric coefficients in the minerals are well-known or definable from direct mineralogical or mineral-chemical analysis (that is, not trace elements such as Mn, Zn, Co, Ni, Cu, etc.),

- Precise mineral-chemical definition is not always possible, especially in mechanically mixed, clastic aquifers and sedimentary rock-dominated terrains
- Analytical solutions to mass-balance analyses do not always provide unique results, and
- Mineral dissolution is controlled by its inherent rate, effective surface area, reaction temperature, and closeness to equilibrium, not simply to the modal abundance.

The requirement that the same number of phases and constituents are needed to solve the mass-balance equations for the mass-transfer coefficients calls for insight to eliminate some of the potential phases from consideration based on known behaviors, although similar or related phases can be modeled with a single fictive phase having a composition representing a composite. A model for selecting preferred pathways in inverse modeling using information theory was recently developed (Dai et al. 2010).

Several examples of mass-balance calculations are presented in the following sections. The results of studies by Velbel and Pačes have been cited in many publications as examples of the discrepancy between the dissolution rates measured in the field and in the laboratory, and these are reviewed in detail to evaluate the modeling approaches and methods used to quantify the systems. The work of Drever and coworkers represents combinations of laboratory controls applied to natural systems and the use of natural specimens in laboratory tests. Recent work by Zhu and coworkers show the application of mass-balance methods to aquifers that are not affected by the same uncertainties as the catchment systems studied by others. The methods used by these researchers are evaluated in this report both with regard to extracting mineral dissolution rates and for potential use in modeling surface disposal systems.

5.1 Velbel

Velbel (1985, 1986) applied the mass balance approach to the Coweeta watershed in the southern Blue Ridge of North Carolina. The mass balance values were determined from the difference in compositions of the stream outputs from seven control watersheds and rain input, which was measured previously by Swank and Douglass (1977) and expressed as moles per hectare per year. The unit of hectare is commonly used to measure geological areas, such as lakes; 1 ha = 10,000 $m^2 \approx 2.5$ acres. As described in Velbel (1985), six sources and sinks were considered: "the weathering of three major weatherable rock-forming minerals (biotite mica, almandine garnet, and plagioclase feldspar), and the uptake of mineral nutrients by the forest biota," plus the precipitation of gibbsite and kaolinite. However, the formations of gibbsite [$Al(OH)_3$] and kaolinite [$Al_2Si_2O_5(OH)_4$] do not affect the tracked elements (Na, K, Mg, and Ca) and these were later excluded from the mass balance calculations. The mathematical approach of Velbel is examined in detail to evaluate and demonstrate the general method for applying mass-balance on the field scale.

5.1.1 Mass-Balance Calculation

Consider a single catchment of interest that is fed by a number of reservoirs λ and drains into a number of reservoirs μ. Assume there are ϕ mineral phases that contain the species of interest c in catchment i, including primary and secondary phases. If the chemical compositions of the waters entering and exiting catchment i are known and the compositions of the reactant minerals and product phases are known, equations representing the conservation of mass can be written for each elemental constituent. The change in the mass of element c in the volume (reservoir) of interest i over time is

$$\frac{dm_c}{dt} = \sum_{l=1}^{\lambda} Q_{l\to i}^{c} \; - \; \sum_{m=1}^{\mu} Q_{i\to m}^{c} \; + \; \sum_{j=1}^{\phi} Q_{j,i}^{c} \tag{5.5}$$

where there are λ input reservoirs feeding water bearing c into reservoir i at a flux $Q_{l\to i}^{c}$ from reservoir l, and μ output reservoirs that are fed by water bearing c flowing from reservoir i at a flux $Q_{i\to m}^{c}$ to reservoir m, and ϕ phases containing element c that dissolve or precipitate to contribute or remove c from solution by reaction j, all of which affect the mass of c present in reservoir i at any time. The flux of c from reservoir l to reservoir i is a function of the amount of c in the water in reservoir l and the water flow rate

$$Q_{l\to i}^{c} \; = \; \left(\frac{\partial m_c}{\partial w_{l,i}}\right)\left(\frac{dw_{l,i}}{dt}\right) \tag{5.6}$$

and, likewise, the flux of c from reservoir i to reservoir m is

$$Q_{i\to m}^{c} \; = \; \left(\frac{\partial m_c}{\partial w_{m,i}}\right)\left(\frac{dw_{m,i}}{dt}\right). \tag{5.7}$$

The difference in the sums of the individual fluxes can be calculated from the measured concentrations and is denoted as Δm_c.

$$\sum_{m=1}^{\mu} Q_{i\to m}^{c} \; - \; \sum_{l=1}^{\lambda} Q_{l\to i}^{c} \; = \Delta m_c \, . \tag{5.8}$$

The source/sink term within reservoir i can be written

$$Q_{i,j}^{c} \; = \; \left(\frac{\partial m_c}{\partial m_j}\right)\left(\frac{dm_j}{dt}\right). \tag{5.9}$$

The first term is simply the stoichiometric coefficient of constituent c in phase j, which can be represented as $\beta_{c,j}$. The second term represents the dissolution or precipitation rate of phase j, which can be represented as α_j. Substituting Equations 5.8 and 5.9 into Equation 5.5 gives

$$\frac{dm_c}{dt} = \sum_{j=1}^{\phi} \alpha_j \, \beta_{cj} - \Delta m_c \, . \tag{5.10}$$

At steady state (and only at steady state), Equation 5.10 reduces to

$$\sum_{j=1}^{\phi} \alpha_j \beta_{cj} = \Delta m_c \ . \tag{5.11}$$

Such a mass-balance equation can be written for each of the constituents c being tracked. Values of α_j can be calculated if the assemblage of reacting and precipitating phases is known, including the phase compositions, and Δm_c is measured. Equation 5.11 can be applied to field systems by defining Δm_c in terms of either composition or flux, which affects the units of α_j: concentration differences give rates with dimensions moles per unit volume of water and flux differences give rates with dimensions moles per unit area of watershed per unit time. The use of concentrations does not allow for the calculation of mineral weathering rates. The number of moles of a material that dissolve defines a reacted volume. Comparisons with laboratory rates require transforming volumes of reacted minerals to weathering rates and estimating the reactive surface area of the mineral in the natural system. The field rate in terms of the area of the watershed was expressed in terms of mineral surface area by Velbel (1986) as:

$$\alpha_j \left(\frac{V_j}{A_j}\right)\left(\frac{V_r}{A_r}\right)\left(\frac{1}{V_r}\right) = \alpha_j^m \tag{5.12}$$

where V_j and A_j are the volume and surface area of mineral j, V_r is the volume and surface area of rock that is weathered *per surface area of watershed*, A_r is the area of rock *per surface area of watershed* that is weathered, and α_j^m is the field rate based on the surface area of mineral j. The unit analysis suggests that this formulation is in error. Instead, the rate based on catchment area can be multiplied first by the ratio of catchment area-to-mineral area and then by identities for the mineral and catchment volumes, as shown on the left-hand side of Equation 5.12, and then rearranged as shown on the right-hand side of Equation 5.13.

$$\alpha_j \left(\frac{A_r}{A_j}\right)\left(\frac{V_j}{V_j}\right)\left(\frac{V_r}{V_r}\right) = \alpha_j \left(\frac{V_j}{A_j}\right)\left(\frac{V_r}{V_j}\right)\left(\frac{A_r}{V_r}\right) \tag{5.13}$$

The catchment and rock are assumed to be equivalent. To solve Equation 5.12, Velbel (1986) considered each of the terms in parentheses. The surface area of a geometric particle is related to its volume by its dimension as

$$\frac{A_j}{V_j} = \frac{b_j}{d_j} \tag{5.14}$$

where d_j is the dimension and b_j is a shape factor for a particle of phase j. For spherical particles, d is the diameter and b is 6. For cubic particles, d is the edge length and b is 6. For disk-shaped particles, d is the diameter and b can be expressed in terms of d.

The modal abundance (see below) of mineral j in fresh rock, N_j, is assumed to be equal to the modal abundance of mineral j in weathered rock (weathered rock is referred to as saprolite). The

modal abundance is determined from analysis of several exposed surfaces, and the abundance based on volume is assumed to be the same as the abundance based on surface area.:

$$\frac{V_j}{V_r} = \frac{V_j}{V_s} = N_j \,. \tag{5.15}$$

The volume of weathered rock is the product of the catchment area and mean thickness of the weathering profile, so the volume per unit watershed area is the mean thickness of the saprolite layer, z_s.

$$\frac{A_r}{V_r} = \frac{1}{z_s}. \tag{5.16}$$

Substituting Equations 5.14, 5.15, and 5.16 into Equation 5.13 gives

$$\alpha_j \frac{d_j}{b_j} \frac{1}{N_j} \frac{1}{z_s} = \alpha_j^m \,. \tag{5.17}$$

Equation 5.17 agrees with the equation used by Velbel (1986) to estimate the field-based weathering rates and the unit analysis gives the correct units for the mineral dissolution rate

$$\left(\frac{mol}{m^2 \text{ catchment } yr}\right)\left(\frac{m \text{ mineral}}{unitless}\right)\frac{1}{\left(\frac{m^3 \text{ mineral}}{m^3 \text{ rock}}\right)}\frac{1}{(m \text{ catchment})} = \frac{mol}{m^2 \text{ mineral } yr}. \tag{5.18}$$

5.1.2 Modal Analysis

The stoichiometry of the minerals and their modal abundances were estimated from petrographic and mineralogical analyses. Modal analysis is a method used to quantify the volume contents of minerals in a complex rock based on the analyses of thin sections. The minerals in the thin section are first identified (or characterized sufficiently for recognition during the analysis) by surveying the thin section. The abundance of each phase is then determined by tallying the number of times each phase is seen in the cross hairs during a large number of viewings (typically 300) made at either random or regular intervals across the area of a thin section. Additional thin sections are then analyzed and included in the tally for better fidelity to the source. The results of the modal analysis performed by Velbel (1985) for 18 sections of rock from Coweeta watershed 27 are shown in Table 5.1.

Table 5.1. Modal petrography of Coweeta group rocks (Velbel 1985)

Phase	Volume %	Phase	Volume %	Phase	Volume %
Quartz	61.6	Muscovite	12.9	Epidote	0.1
Biotite	11.6	Plagioclase	8.3	Staurolite	0.9
Garnet	1.9	Opaques	1.4	K-feldspar	0.6

5.1.3 Results

The fluxes and abundances used in the calculations are summarized in Table 5.2. Note that the fractional abundances (rather than percentages) are given in Table 5.2, and that there is a factor of two discrepancy in the abundance of biotite in the two references. This may be due to a difference in the stoichiometry used in the calculation. Dissolution of quartz and muscovite was assumed to be negligible (see Table 2.2).

Table 5.2. Values used in Calculations for Coweeta Watershed (Velbel 1986)

Element c	Flux Δm_c, (mol $m^{-2} s^{-1}$)	Mineral j[a]	Modal abundance N_j
Na	7.0×10^{-10}	biotite	0.058
K	2.0×10^{-10}	almandine	0.019
Mg	4.4×10^{-10}	plagioclase	0.083
Ca	1.8×10^{-10}	—	—

[a]From Velbel 1985:

Based on the mineral dissolution rates on a per hectare basis, Velbel estimated the saprolitization rates for each mineral to range between 3.8 and 15 cm per 1000 years (ky) for a weathering depth of 20 feet. Which primary mineral must be completely weathered to form saprolite is related to the susceptibility of the resulting weathered rock to erosion. Comparison with the denudation rate, which was measured separately, suggests that a rate corresponding to complete weathering of all three minerals is required for saprolite formation, which is the lowest rate (3.7 cm ky^{-1}) based on the mineral dissolution rates and abundances. The dissolution rates calculated by Velbel (1986) for mineral dissolution on a per watershed area and on a mineral surface area basis, and also the rates of profile development (saprolitization), are summarized in Table 5.3. A value of $d = 1$ mm was used as the characteristic dimension of all minerals: biotite was modeled as 1-mm diameter spheres, plagioclase as 1-mm cubes, and almandine as disks 1-mm in diameter and 0.2 mm thick.

Table 5.3. Results of Mass Balance Calculations for Coweeta Watershed (Velbel 1986)

	α_j mol m^{-2} watershed s^{-1}	*Saprolitization rate* m s^{-1}	α_j^m mol m^{-2} mineral s^{-1}
biotite	5.92×10^{-10}	1.50×10^{-12}	5.98×10^{-14}
almandine	8.73×10^{-10}	5.05×10^{-12}	1.26×10^{-12}
plagioclase	9.66×10^{-10}	1.17×10^{-12}	3.18×10^{-13}

5.2 Pačes

Pačes (1983) performed the mass balance using the Na^+ concentration of forested and agricultural catchments in the Trnávka river basin and the Elbe river basin (for two different years) in the former Czechoslovakia. In addition to the dissolution of minerals in the rock, he took into account runoff, fixation in biomass, input from fertilizers, and input form atmospheric precipitation.

5.2.1 Mass-Balance Calculation

In the approach of Pačes (1983), the 1-dimensional conservation of mass expression for the solute of interest *i* (neglecting dispersive processes) was written as

$$\frac{\partial m}{\partial t} = F - P\frac{\partial q}{\partial t} - v\frac{\partial m}{\partial x} \tag{5.19}$$

where F is the net input of species i into the system of interest, m is the concentration of that species in the system, q is the concentration of the species i in the mineral phases that are dissolving within the system, v is the ground water velocity ($v = \partial x/\partial t$), and P is a conversion factor that converts the system property from units of per unit mass dissolving mineral to units of per volume ground water. That term is calculated as

$$P = \lambda\,\sigma\frac{(1-p)}{p}, \tag{5.20}$$

where λ is the mass fraction of dissolving minerals in the rock, σ is the density of the rock without pores, and p is the porosity of the water-saturated rock (Pačes 1983). The conversion factor P has the units kg m^{-3}. The last term gives the ratio of the volume of rock to volume of water in the pores of the rock. The units for terms in Equation 5.20 are

$$\frac{\textit{mass}\ \text{mineral}}{\textit{mass}\ \text{rock}}\frac{\textit{mass}\ \text{rock}}{\textit{volume}\ \text{rock}}\frac{\textit{volume}\ \text{rock}}{\textit{volume}\ \text{water}}. \tag{5.21}$$

Assuming a constant mineral dissolution rate k and surface area S gives

$$\frac{\partial q}{\partial t} = Sk. \tag{5.22}$$

At steady state,

$$0 = F - PSk - \frac{dm}{dt}, \tag{5.23}$$

which after rearranging and integrating produces

$$m = Ft - PSkt. \tag{5.24}$$

Pačes (1983) defined the specific wetted surface area in the catchment $\hat{s}$ as

$$\hat{s} = \frac{SP}{n}, \tag{5.25}$$

where n is the fraction of the rock surface occupied by minerals releasing the species of interest. The term $\hat{s}$ has units m^2 rock m^{-3} water-saturated rock. Substituting this expression into Equation 5.24 and rearranging gives

$$k = \frac{m - Ft}{n\hat{s}t}. \tag{5.26}$$

Note that the term Ft accounts for inputs and uptakes occurring over the analyzed time period for all sources other than mineral dissolution or precipitation. This gives the mineral dissolution (or precipitation) rate in terms of concentration and is appropriate for either laboratory or field measures of the rate.

An expression converting the rate from a per catchment area basis to a per mineral area basis that is equivalent to Equation 5.13 was derived by Pačes (1983) as

$$\bar{k} = \frac{\overline{Q_r}}{n\,\hat{s}\,H\,p} \tag{5.27}$$

where $\bar{k}$ is the field rate constant for mineral dissolution, in units mol m^{-2} y^{-1}, $\overline{Q_r}$ is the rate constant in units of per area of the catchment, n is the fraction of rock occupied by the mineral, $\hat{s}$ is the specific wetted surface area of rock [see Section 5.5 and the Appendix in Pačes (1973)], in m^2 m^{-3}, H is the mean thickness of permeable rock, in m, and p is the porosity of the (water-saturated) rock. Unit analysis of Equation 5.27 gives the desired units for the mineral dissolution rate (after conversion of years to seconds):

$$\frac{mol}{m^2 \text{mineral } y} = \frac{\left(\frac{mol}{m^2 \text{ catchment } yr}\right)}{\left(\frac{m^2 \text{ mineral}}{m^2 \text{ rock}}\right)\left(\frac{m^2 \text{ wetted rock}}{m^3 \text{ water}}\right)(m \text{ catchment})\left(\frac{m^3 \text{ water}}{m^3 \text{ rock}}\right)}. \tag{5.28}$$

This is similar to the equation used by Velbel (1986), except the wetted surface area and porosity of the rock are used in the calculation instead of the entire surface area.

5.2.2 Results

The dissolution rates are $\overline{Q_r}$ = 21±12, 55±24, 69, and 210 mol m^{-2} catchment yr^{-1} for the four catchments analyzed by Pačes. The values used to calculate the mineral dissolution rates by using Equation 5.27 are summarized in Table 5.4. All of the Na^+ was assumed to be released during the weathering of oligoclase (feldspar). The values of the wetted surfaces $\hat{s}$ used in these calculations were the average of two limiting values: 2.0×10^5 m^2 m^{-3} for fractured rock with smooth walls and 1-mm-wide joints and 1.2×10^6 m^2 m^{-3} for fractured rock with smooth walls and 0.01-mm-wide joints (see also the appendix in Pačes 1973). Pačes (1983) compared his field-derived rates with the dissolution rates that had been measured in laboratory tests. The rate measured by Busenberg and Clemency (1976) for oligoclase at 25°C was 1.7×10^{-12} mol m^{-2} s^{-1}. This rate may be too high because they did not use a lower limit to the particle sizes in those tests.

Table 5.4. Characteristic values for catchments used by Pačes (1983)

Catchment	H, m	p	Na_2O, percent	$\hat{s}$, m^2m^{-3}	n for oligoclase	Dissolution rate, mol m^{-2} s^{-1}
Trnávka river basin						
Forested	8.19	0.24	2.60	2.0×10^5	0.19	8.9×10^{-15}
Agricultural	8.11	0.23	1.98	1.6×10^5	0.14	4.2×10^{-14}
Elbe river basin						
in 1892	100	0.3	1.9	1×10^5	0.14	5.2×10^{-15}
in 1976	100	0.3	1.9	1×10^5	0.14	1.6×10^{-14}

Oxburgh et al. (1994) measured the dissolution rate to be about 1×10^{-12} mol m^{-2} s^{-1} in laboratory tests, which is consistent with the rate measured by Busenberg and Clemency (1976). Pačes (1983) adjusted the calculated rates to first account for clays masking half the oligoclase surface and then for the top 1 m of the regiolith not reacting (e.g., not being contacted by water). This leads to increased rates in the agricultural catchment of the Trnávka river basin from 4.2×10^{-14} mol m^{-2} s^{-1} to 8.4×10^{-14} mol m^{-2} s^{-1} due to the decrease in the accessible surface area and then to 6.8×10^{-13} mol m^{-2} s^{-1} due to exclusion of the top 1 m of the regiolith; these are 2-fold and 16-fold increases, but still a factor of two lower than the laboratory rate.

5.3 Drever and Others

Drever and students conducted several studies in which field weathering conditions were controlled and carefully monitored and laboratory tests were conducted with materials carefully collected from the field site. These studies provide a more complete data base for evaluating field weathering and laboratory tests that include mineral interactions. Consider first the study summarized in Swoboda-Colberg and Drever (1993). Six small plots in Maine were stripped of soil (the organic horizon) and irrigated with HCl solutions having pH values of 2, 2.5, and 3 (60 L per week for about six months) and the groundwater was collected in tension lysimeters placed at 25-cm and 50-cm depths. The compositions and sizes of the minerals in the soil were measured, and the mineral dissolution rates were calculated based on the solution compositions and soil characteristics. Soil samples were reacted in laboratory flow-through tests using HCl solutions that matched the pH values attained in the field tests, which were 2 to 2.5 pH units higher than the irrigating solutions. The soil was separated into light-mineral and heavy-mineral fractions that were tested separately The dissolution rates measured in the laboratory tests were up to 400-times faster than those calculated for weathering in the field. The authors attribute the difference in rates to (1) incomplete wetting of minerals in the field, (2) microclimes in pores that result in lower dissolution rates, (3) differences in surface characteristics in the field and laboratory, and (4) the dissolution rate not scaling with the geometric surface area.

A subsequent study was performed on a small (39 m^2) catchment in Rocky Mountain National Park, CO, that is located above the timberline in a bedrock knoll. The catchment included a 15.5 m^2 pocket of soil and the outflow was constrained to a small crack. The water was sampled weekly or biweekly between July and September for five consecutive years (Clow 1992). In addition to rain water, the site was irrigated with demineralized water to achieve a more continuous flow than occurred naturally. The amounts of rainfall and irrigation were similar during each year, but differed between years. The difference between the amounts of water input by rain and irrigation and the amounts collected in the outflow was used to estimate the

Table 5.5. Weathering Reactions

$1.15\ \text{biotite} + 0.10\ Ca^{2+} + 0.49H_4SiO_4 + 1.21\ O_2 + 2.13\ CO_2 + (0.73 + n)H_2O \rightarrow$ $\text{smectite} + 0.76Mg^{2+} + 0.81K^+ + 1.28FeO(OH) + 2.13HCO_3^- + 0.21TiO_2$	(A)
$1.39\ \text{chlorite} + 0.10\ Ca^{2+} + 0.32K^+ + 0.31\ H_4SiO_4 + 1.78\ O_2 + 3.74CO_2 + nH_2O \rightarrow$ $\text{smectite} + 2.13Mg^{2+} + 3.53FeO(OH) + 3.74\ HCO_3^-$	(B)
$\text{oligoclase} + 1.27CO_2 + 4.82H_2O \rightarrow$ $0.64\ \text{kaolinite} + 0.27Ca^{2+} + 0.73Na^+ + 1.46H_4SiO_4 + 1.27HCO_3^-$	(C)
$2\ \text{microcline} + 2CO_2 + 11H_2O \rightarrow \text{kaolinite} + 2K^+ + 4H_4SiO_4 + 2HCO_3^-$	(D)
$\text{kaolinite} + 5H_2O \rightarrow 2Al(OH)_3 + 2H_4SiO_4$	(E)
$\text{calcite} + H_2O + CO_2 \rightarrow Ca^{2+} + 2HCO_3^-$	(F)
$xNH_4^+ + yNO_3 + (x\text{-}y)HCO_3 \rightarrow \text{organic-N}$	(G)
$Fe_2S + 3.75O_2 + 3.5H_2O \rightarrow Fe(OH)_3 + 4H^+ + 2SO_4^{2-}$	(H)

evapotranspiration losses. Mass balance calculations were performed using an existing mineral data base for the region and the set of reactions given in Table 5.5 (Mast et al. 1990, Clow 1992).

Soil samples were analyzed to determine the mineral abundances in four size fractions by using optical microscopy and scanning electron microscopy with X-ray emission spectroscopy (Clow 1992, Clow and Drever 1996). Overall, the soil contained 25% quartz, 21% oligoclase, 20% microcline, 19% biotite/chlorite, and 15% others, by mass. The biotite and chlorite phases were intergrown and "others" included opaque, polymineralic, and unidentified grains. The specific surface area of the bulk material was measured in each size fraction and the oligoclase, microcline, and biotite/chlorite fractions that were separated from the 106–208 μm size fraction.

The amount of each species *i* released to solution by weathering was calculated from the amounts measured in the solutions entering and exiting the catchment and the changes in the amounts stored in the soil solution as

$$\text{atmospheric input } (i) + \text{weathering inputs } (i) = \text{outflow } (i) + \text{changes in soil storage } (i). \quad (5.29)$$

Changes in the amounts taken up or released from biota were assumed to be negligible and are excluded from Equation 5.29. The annual atmospheric inputs were taken from data collected by the National Atmospheric Deposition Program/National Trends Network at a near-by location and rain gauges at the study site and the controlled irrigation. Figure 5.1a presents the mean concentrations from precipitation (open symbols) and in the outflow (filled symbols) for the five year duration of the study. The vertical bars represent the average annual discharge rates, which are the differences between the sum of the inputs from precipitation and irrigation minus the loss due to evapotranspiration for each year. The solution concentrations are not very sensitive to the amount of water passing through the catchment. The similarities in solution concentrations suggest that transport effects such as sorption remain nearly constant.

The mass-balance results are summarized in Table 5.6 (Clow 1992). The extents of mineral dissolution (i.e., the weathering flux values) and the change in the amounts stored in soil were

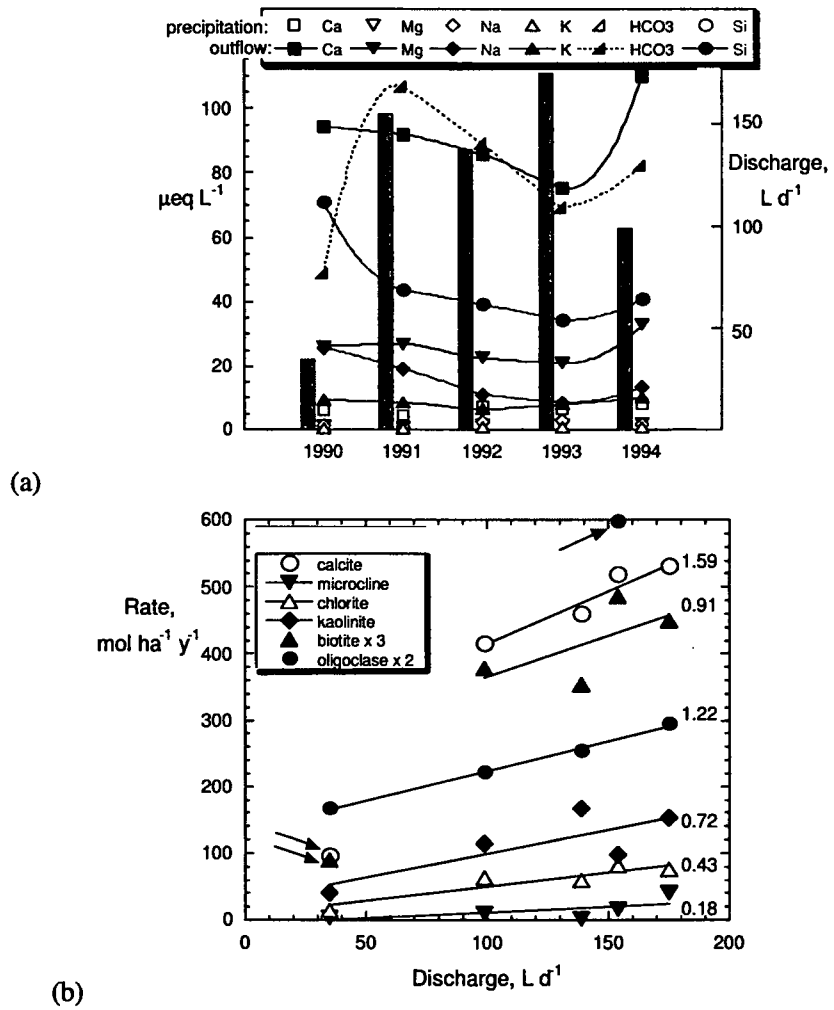

Figure 5.1. Results from Clow and Drever (1996): (a) Average annual concentrations (symbols) and discharge rates (bars), and (b) estimated annual mineral dissolution rates at different discharge rates (see text).

adjusted to best match the calculated net composition of the outflowing solution. This was done by first matching particular dissolved elements to the likely source phase based on the phase composition and geochemical insights. For example, the Mg in the outflowing solution was attributed to the conversion of biotite and chlorite to smectite (Reactions A and B). In addition to releasing Mg, Reaction A consumes Ca, Si and CO_2 and releases K, Fe, and HCO_3^-. Reaction B consumes Ca, Si and CO_2 and releases K, Fe, and HCO_3^- to solution. The inventories of the elements being tracked were adjusted based on the stoichiometries of the reactions. Inputs due to mineral dissolution were subtracted from the inventory of the output solution. (The inventory of Ca was not adjusted for these reactions and was not addressed.) The entire Na inventory in the outflowing solution was assigned to result from the weathering of oligoclase to form kaolinite (Reaction C) and all of the K to the conversion of microcline to kaolinite (Reaction D). Because these reactions do not release enough Si to match the measured output, Clow (1992) assumed an unidentified aluminosilicate phase (similar to kaolinite) degraded to an amorphous aluminum

Table 5.6. Mass-balance results for 1991, in mmoles (Clow 1992, Table 21)

	Si	**Ca**	**Na**	**Mg**	**K**	**HCO_3^-**	**H^+**	**NH_4^+**	**NO_3**	**SO_4^{2-}**	**mmoles reacted**
Outflux in surface water	399	421	179	124	78	978	0	0	52	63	—
Change in amount stored in soil	-26	-15	-25	-11	-4	-40	0	0	2	-10	—
Influx by precipitation	0	-15	-7	-3	-2	0	-84	-54	-96	-47	—
Net Outflow	373	391	147	110	-72	938	-84	-54	-42	6	—
Biotite → smectite reaction A Chlorite → smectite reaction B	58	—	—	-110	-56	-385	—	—	—	—	106 53
Amount remaining:	*431*	*391*	*147*	*0*	*16*	*553*	*-84*	*-54*	*-42*	*6*	
Oligoclase → kaolinite reaction C	-294	-54	-147	—	—	-256	—	—	—	—	201
Amount remaining:	*137*	*337*	*0*	*0*	*16*	*297*	*-84*	*-54*	*-42*	*6*	
Microcline → kaolinite reaction D	-31	—	—	—	-16	-16	—	—	—	—	16
Amount remaining:	*106*	*337*	*0*	*0*	*0*	*282*	*-84*	*-54*	*-42*	*6*	
$amAlSiO_4 \rightarrow amAl(OH)_3$	-106	—	—	—	—	—	—	—	—	—	53
Amount remaining:	*0*	*337*	*0*	*0*	*0*	*282*	*-84*	*-54*	*-42*	*6*	
Nitrogen assimilation reaction G	—	—	—	—	—	12	—	54	42	—	
Amount remaining:	*0*	*337*	*0*	*0*	*0*	*294*	*-84*	*0*	*0*	*6*	
Pyrite (FeS_2) oxidation reaction H	—	—	—	—	—	—	-12	—	—	-6	3
Amount remaining:	*0*	*337*	*0*	*0*	*0*	*294*	*-96*	*0*	*0*	*0*	
$H^+ + HCO_3^- \rightarrow H_2CO_3$	—		—	—	—	96	96	—	—	—	
Amount remaining:	*0*	*337*	*0*	*0*	*0*	*390*	*0*	*0*	*0*	*0*	
Calcite dissolution reaction F	—	-337	—	—	—	-673	—	—	—	—	337
Amount remaining:	*0*	*0*	*0*	*0*	*0*	*-284*	*0*	*0*	*0*	*0*	

hydroxide and provided the Si necessary to match the outflow concentration. The remaining Ca content was attributed to calcite dissolution, which also contributed bicarbonate, and sulfate was attributed to pyrite dissolution.

Weathering rates were calculated based on the estimated amounts of each mineral dissolved, the exposed surface area in the catchment, and the reaction time. The fluxes used to calculate the dissolution rates are the products of the measured concentrations and the discharge rates. The mineral surface areas measured in the various size fractions provided a per-volume surface area that was readily scaled to the area (volume) of soil in the catchment. It was assumed in these calculations that all exposed mineral surface area was contacted by ground water, even though the soil was only fully saturated during the summer of 1993. The surface area was also assumed—implicitly—to remain constant over the duration of the study. The rates reported by Clow and Drever (1996) for collections during 1991 on the catchment and mineral scales are:

Biotite	1.6×10^{-10} mol ha^{-1} yr^{-1}	1.2×10^{-14} mol m^{-2} yr^{-1}
Calcite	5.2×10^{-10} mol ha^{-1} yr^{-1}	
Chlorite	8.1×10^{-11} mol ha^{-1} yr^{-1}	
Kaolinite	9.8×10^{-11} mol ha^{-1} yr^{-1}	
Microcline (K-spar)	1.7×10^{-11} mol ha^{-1} yr^{-1}	2.0×10^{-14} mol m^{-2} yr^{-1}
Oligoclase	3.0×10^{-10} mol ha^{-1} yr^{-1}	3.2×10^{-13} mol m^{-2} yr^{-1}

Figure 5.1b shows the mineral dissolution rates on the catchment scale estimated from mass balance analyses performed for waters collected during the summer for five consecutive years. Except for one outlying rate for each of calcite, biotite, and oligoclase (located by the arrows), the rates increase linearly with the discharge rate with very similar dependencies for both rapidly and slowly dissolving minerals (e.g., calcite and chlorite, respectively). The same mineral surface areas were used in the mass balances for each year.

The dissolved chemical load in the ground water is known to be diluted with increasing discharge and has been explained to be the result of the replacement or mixing of soil water with rain water (Johnson et al. 1969). However, the results in Figure 5.1a show that relatively constant concentrations were maintained over a wide range of discharge rates. Either the dissolution rates or the reacting surface areas had increased with the amount of water flowing through the catchment. Clow and Drever (1996) suggested that increased fluxes were due to increased flushing and diffusion during the wet years. That is, the relative contributions of surfaces in cracks, pores, and dead-end channels, all of which may be diffusion limited, were greater during the high flow rate events. They considered the system to contain separate domains with macropores that support rapid flow and domains with micropores that are more resistant to flow.

However, the average discharge rate varies only by a factor of 6, which may or may not be enough to affect the contributions of the two flow paths. An alternative explanation is that the mineral dissolution rates are responding to the solution composition in the same way that the solution flow rate affects the dissolution rate in flow-through laboratory tests. From the simple model used to quantify the effects of flow rate on the mineral dissolution rate (see Section 4.1.1), the dissolution rate becomes proportional to the flow rate at low flow rates. At very low flow rates, the dissolution rate becomes independent of the surface area of the dissolving phase, and the dissolution rate becomes limited by the saturated solution. Below a certain low flow rate, the dissolution rate becomes proportional to the product of the flow rate and the solubility product of the dissolving phase. Of course, the steady-state conditions used to model the effects of flow rate and used to determine dissolution rates in dynamic tests such as single-pass flow-through and column tests are not achieved in the field system, where the groundwater flow rate varies

throughout the year. Nevertheless, the qualitative effect of the solution flow rate on the mineral dissolution rates is observed in the results plotted in Figure 5.1b. The linearity of the rates (neglecting the few outliers located by arrows) also suggests the flow path does not change with the discharge rate.

Clow and Drever (1996) also conducted laboratory tests using soil samples taken from the catchment. Tests were conducted with a flow-through reactor (fluidized bed) and a column (gravity flow) at 19°C with ammonium acetate/acetic acid buffers. Only the <2-mm size fraction was used in the tests, and various subsamples were treated to remove soluble salts, organic matter, iron oxides, etc. Tests in the fluidized bed reactor were conducted at pH 4, pH 4.7, and pH 5.6 at a flow rate of 6.2 ± 0.6 mL h^{-1} (0.149 L d^{-1}) and the column tests were conducted at pH 5.6 at a flow rate of 5.3 ± 1.5 mL h^{-1} (0.127 L d^{-1}).

Similar to the mass balance analysis, the dissolution rates of individual minerals within the sample grains were determined from the steady-state solution concentrations of elements specific to the composition of each mineral and the estimated exposed surface area. For example, the biotite dissolution rate was determined based on the releases of Mg and Si, and the measured amount of biotite in the specimen relative to other silicates, such as oligoclase and microcline. The dissolution of stable minerals such as quartz was assumed to be negligible. From the column test with the 106-208 μm size fraction of soil, the dissolution rate of oligoclase was determined to be 2.2 x 10^{-13}, 1.7 x 10^{-13}, and 1.3 x 10^{-12} mol m^{-2} s^{-1} based on Si, Al, and Na, respectively. The rate based on Si is probably the most accurate. The dissolution rate of biotite based on Mg release was 6 x 10^{-14} mol m^{-2} s^{-1}. The dissolution rates of minerals in the same soil sample measured in the fluidized bed reactor at pH 5.6 were 1.8 x 10^{-12} and 1.9 x 10^{-12} mol m^{-2} s^{-1} for oligoclase based on Si and Na, respectively, and 9 x 10^{-14} mol m^{-2} s^{-1} for biotite based on Mg.

The dissolution rates estimated from the field studies and measured in laboratory tests using soil from the catchment were summarized by Drever and Clow (1996); these results are reproduced in Table 5.7. Drever and Clow (1996) attribute the generally higher dissolution rates in the

Table 5.7. Comparison of mineral dissolution rates from mass-balance calculations and laboratory tests, in pmol m^{-2} s^{-1}

Conditions	Oligoclase	Biotite	Microcline
Field Measurements			
Low-flow rate (34 L d^{-1} in 1990)	0.09	0.002	0.006
High-flow rate (154 L d^{-1} in 1991)	0.32	0.012	0.020
Column Reactor			
Unfractionated, treated soil	0.22 ± 0.04	0.06 ± 0.01	
Crushed granite	0.22 ± 0.03	0.03 ± 0.01	
Fluidized Bed Reactor			
Feldspar concentrate	1.70 ± 0.20		0.58 ± 0.14
Biotite concentrate		0.12 ± 0.02	
Unfractionated, treated soil	1.84 ± 0.48	0.09 ± 0.02	
Unfractionated, untreated soil	1.93 ± 0.31	0.09 ± 0.04	

laboratory tests to the lower average temperature: 7 to 11°C in the field compared to 19°C in the laboratory tests. Using an activation energy of 7.1 kcal mol^{-1} (14 kJ mol^{-1}), the higher temperature used in the laboratory tests increases the rate by factors of 2.0 and 2.8.

The column tests were conducted to compare the dissolution rate of the field soil, which was not crushed, with the dissolution of a crushed granite (45-1000 μm size fraction) having a similar mineral composition. The results show no effect of crushing on the column test results. The feldspar and biotite concentrates refer to subsamples of solids that were separated by specific gravity and magnetism to measure the specific surface areas of the component phases. Laboratory tests were conducted to measure the interactions of several dissolving phases. Finally, subsamples of the soil were treated to remove iron oxide coatings and destroy organics. Separate laboratory tests were conducted with these subsamples. Neither the treatments nor the isolation of phases had a significant effect on the dissolution rates.

Note that the primary effects of crushing the granite are expected to be the generation of high-energy surface sites and surface strain. If the column test is conducted until steady state is attained, the effects of the perturbed surface will have dissipated. The early data provided by Clow (1992) did show an initial rate that was 10-times higher than the steady-state rate for the soil samples. This may have been the result of a too low flow rate when the test was initiated (the flow rates were not reported for each sampling) or a surface effect.

While Drever and Clow (1996) discounted the effect of chemical affinity on the dissolution rates from the perspective of solution saturation, their results show the less obvious but not less important effect of chemical affinity operating through the solution flow rates used in the laboratory tests and probably also in the discharge rates of the field tests. The flow rates used in the fluidized bed and column tests were essentially the same, but the mineral surface areas contacted in the reactors were probably very different. Clow (1992) did not report the sample masses used in the tests, but the nature of the test method makes it likely that a greater sample mass and a much greater surface area was available for reaction in the column reactor. As discussed previously with regard to calculating the dissolution rate from flow-through tests, the dissolution rate at steady state is proportional to the ratio of the flow rate and surface area. Proper comparisons require consideration of both the flow rate and the surface area. That the dissolution rates measured in the column tests were about 8-times lower than those measured in the fluidized bed reactor should be expected because of the higher steady-state concentrations of dissolved mineral components (primarily dissolved silica) attained in the column experiment due to more exposed surface area and lower flow rates. The relative areas exposed in the catchment and laboratory tests would need to be linked with the effective flow rates to compare the mineral dissolution rates.

The flow rates used in the column and fluidized bed reactor tests were 0.13 and 0.15 L d^{-1}, which are about 230- to 1200-times slower than the discharge rates from the catchment of 35 and 154 L d^{-1}. The approximate volume of the soil in the catchment based on the reported area and mean depth was 4.65 m^3, whereas the approximate volume of soil used in the column was probably on the order of 100 cm^3 (1×10^{-4} m^3) based on the reported flow rate of 5 mL h^{-1} and residence time of 2-4 hours, with an assumed column porosity of 20%. The fluidized bed tests were probably conducted with about 5 cm^3 of material. The mineral surface area available in the catchment is about 40,000-times greater than in the column test and even greater than in the fluidized bed reactor, so the *F/S* ratios in both laboratory test methods will be significantly higher than that in the catchment. From the earlier discussions regarding the effects of the *F/S* ratio, the reaction conditions applied in both laboratory measurements are much more aggressive than the conditions in the catchment and result in higher dissolution rates.

5.4 Zhu and Others

As another example of applying inverse modeling, mass balancing was applied to an aquifer within the saturated Navajo sandstone at Black Mesa, Arizona (Zhu 2005). This study differed from those discussed above in that the mass balance approach was applied to water samples collected from wells rather than run-off. The locations of the wells and path of groundwater flow were used to estimate the chronology. Groundwater was sampled from 28 wells and archived rock chips that had been collected when oil and gas exploration wells were drilled and several outcrop samples were obtained and used to characterize the mineralogy. The groundwater ^{14}C ages and recharge rates had been determined previously by Zhu (2000) and two flow paths have been identified. Sixteen wells were in flow path 1 and 12 wells were in flow path 2. The minerals included in the analysis are listed in Table 5.8.

Table 5.8. Phases used for inverse mass balance model

Mineral	Composition	M_j, mmol/L		
		#1	#2	#3
Calcite	$CaCO_3$	-0.15	-0.15	-0.15
Halite	NaCl	0.01	0.01	0.01
Gypsum [a]	$CaSO_4 \cdot 2H_2O$	0.04	0.04	0.05
Smectite [b]	$K_{0.27}Ca_{0.15}(Mg_{1.005}Al_{1.26})((Al_{0.36}Si_{3.64})O_{10}(OH)_2$	-0.06	-0.06	-0.06
Muscovite [a]	$KAl_3Si_3O_{10}(OH)_2$	0	0.02	0.02
K-feldspar [a]	$KAl_3Si_3O_8$	0.02	0	0
Plagioclase [a]	$Ca_{0.38}Na_{0.62}Al_{1.38}Si_{2.62}O_8$	0.26	0.26	0.26
Na-Ca exchanger	$Ca^{2+} + 2NaX = 2Na^+ + CaX_2$	-0.72	-0.72	-0.72
Silica [b]	SiO_2	-0.08	-0.04	0
Kaolinite	$Al_2Si_2O_5(OH)_4$	-0.14	-0.16	-0.16

[a]Only allowed to dissolve.
[b]Only allowed to precipitate.

Changes in the compositions of groundwater taken from wells along each flow path and the groundwater age were used to define the solute fluxes. The dissolution rate of each mineral j was calculated as

$$R_j = \frac{M_j}{S_j \, \Delta t} \tag{5.30}$$

where R_j is the dissolution rate, M_j is the moles of mineral j reacted per liter groundwater, Δt is the time span for the reaction, and S_j is the surface area of the mineral per liter groundwater. The groundwater from the first well of the flow path was used as the starting point and the evolution tracked from that composition. Changes in the groundwater composition between successive wells were modeled in terms of the dissolution or precipitation of the basis set of minerals by using the PHREEQC computer program (Parkhurst and Appello 1999). Based on chemical insights, gypsum, muscovite, K-feldspar, and plagioclase were only allowed to dissolve, whereas smectite and amorphous silica were only allowed to precipitate. The other phases were allowed to either dissolve or precipitate. Even with these restrictions, several reaction paths were found to be consistent with the evolution of the groundwater compositions and these provided optional

values of M_j. Preferred paths were determined using insights gained from analyses of the mineral samples. Table 5.8 includes the values of M_j for three possible paths for the changes measured in the groundwater compositions in going from well 08T-541 to well Kayenta #5 due to the reactions of specific phases. Positive values indicate dissolution reactions and negative numbers indicate precipitation. Model #1 was preferred based primarily on the dissolution of K-feldspar. Once the values of M_j were determined, they were used with the values of S_j and Δt to determine the mineral dissolution or precipitation rates as the groundwater was transported between wells. For example, the travel time from well 08T-541 to well Kayenta #5 was 21,000 years (Zhu 2000).

The dissolution rates of K-feldspar and plagioclase determined by inverse mass balance modeling for transport between each well are shown in Figure 5.2. The rates were determined using the BET surface areas measured for particles from six core samples. The specific surface area was calculated using the equation

$$S_j = \frac{\varphi_j \, 10^3 \, \rho_j \, s_j}{\theta} \tag{5.31}$$

where φ_j and ρ_j are the volumetric abundance and density of mineral j, s_j is the measured BET specific surface area, and θ is the porosity of the aquifer; the constant 1000 is included to adjust the water volume from liters to m^3. The uncertainty bars were calculated by Zhu (2005) using the propagation of errors method for Equations 5.30 and 5.31. The uncertainties are about 80% of the rates and are dominated by contributions of mass transfer and the surface area. The overall average dissolution rates are 1.1×10^{-18} mol m^{-2} s^{-1} for the K-feldspar and 9.4×10^{-17} mol m^{-2} s^{-1} for the palagonite, the composition of which is similar to oligoclase.

The measured pH values of the 50 groundwater samples were in the range pH 7.4 to pH 10.2, with an average of pH 8.71 and median pH 8.6. Although the computed dissolution rates are the averages for transport over several kilometers between wells and cannot be ascribed to particular conditions, it is appropriate to compare these rates with laboratory rates measured in neutral to

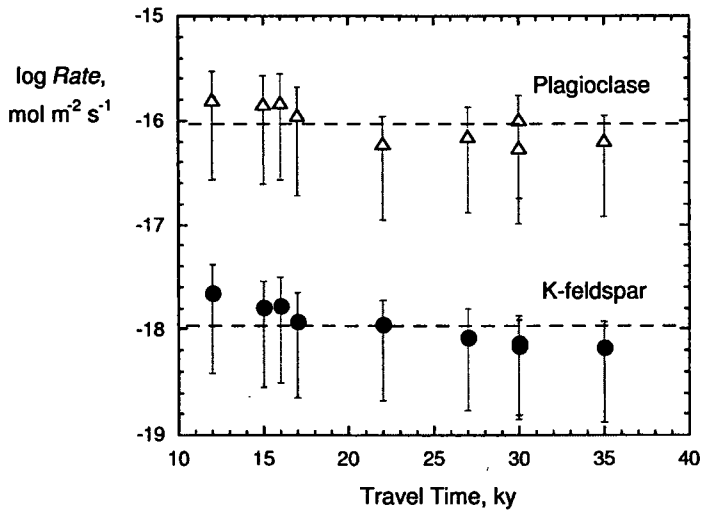

Figure 5.2. Dissolution rates of K-feldspar and plagioclase determined by inverse mass balance modeling. The dashed lines are drawn at the average values.

slightly alkaline solutions. Likewise, the temperature was found to vary from 15 to 35°C over the period analyzed (Zhu 2005). Using an activation energy of 55 kJ mol^{-1} (Blum and Stillings 1995), increasing the temperature from 15 to 35°C increases the rate by a factor of 5.2. Oxburgh et al. (1994) measured the dissolution of oligoclase $Ca_{0.31}Na_{1.27}Al_{1.93}Si_{5.02}O_8$ (based on their reported composition) at several pH values using a mixed flow reactor. The rates are specific to the single flow that was used, but are expected to be characteristic. Previously measured rates of similar feldspar minerals (at near room temperature and based on the release of Si) were summarized by Mast et al. (1987; Figure 9) and Oxburgh et al. (1994), and the pooled results are plotted in Figure 5.3a. The dissolution rates appear to be independent of pH over the range pH 4 to pH 10, with an average of 2×10^{-12} mol m^{-2} s^{-1}. The results of tests with K-feldspar conducted at 25°C in several laboratories have been summarized by Blum and Stillings (1995, Figure 5) and reproduced in Figure 5.3b for rates in the units of mol m^{-2} s^{-1}. Different symbols represent measurements made by different researchers; see Blum and Stillings (1995) for individual references. The dissolution rate of K-feldspar is more sensitive to the pH than is the dissolution rate of plagioclase. The results from Schweda (1989) and from McClelland (1950), as presented by Blum and Stillings (1995) and shown by the filled and open circles, respectively, are well-fit by lines with slopes -0.49 and -0.29 in acidic solutions and 0.77 in alkaline solutions. A "U-shaped" pH dependence is observed for many silicate minerals and glasses wherein the rate

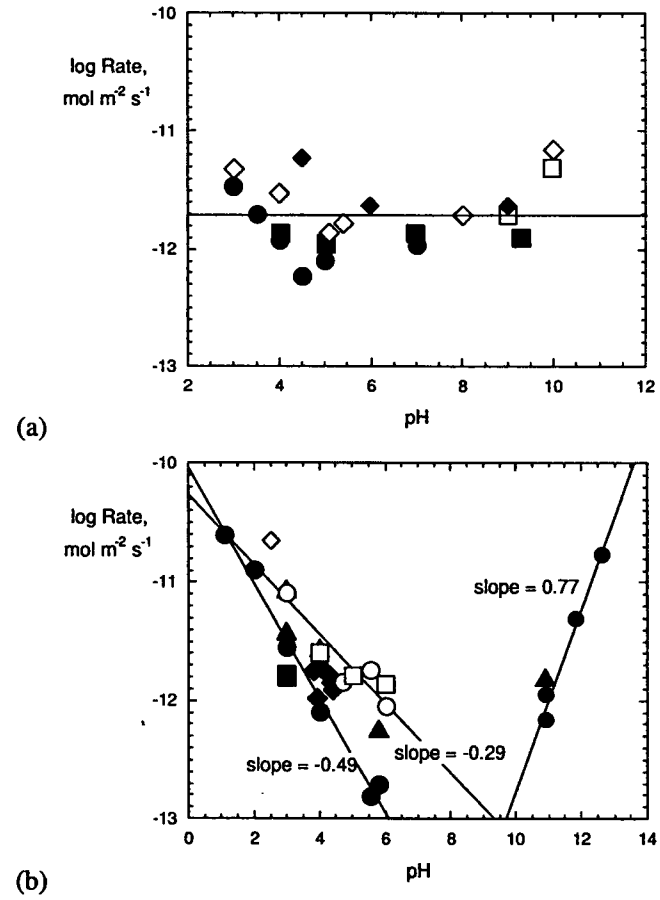

Figure 5.3. Dissolution rates of (a) oligoclase and (b) K-feldspars at various pH values.

decreases with pH in acidic solutions, is independent of pH in neutral solutions, and increases with pH in alkaline solutions (e.g., Kump et al. 2000). The scatter in both sets of results at neutral pH values obfuscates any pH dependence.

The calculated, measured, and modeled dissolution rates of K-feldspar at pH 6 are summarized in Table 5.9. Zhu (2005) cited laboratory rates of 3.2×10^{-13} mol m^{-2} s^{-1} and 3.2×10^{-12} mol m^{-2} s^{-1} for K-feldspar and plagioclase, respectively, although the data suggest slightly lower rates. Nevertheless, the field rates determined by inverse mass balance modeling are 10,000- to 100,000-times lower than the laboratory rates. All rates are relative to the BET surface area. Using the smaller geometric surface area will result in higher dissolution rates but not affect the differences significantly because the particles were of similar size. The specific surface areas of particles from six core samples ranged from 0.44 to 0.88 m^2 g^{-1} after the clay coatings had been removed, with an average value of 0.69 m^2 g^{-1}. Zhu used a geometric specific surface area of 0.02 m^2 g^{-1}, which implies the surface roughness factor is 35. For comparison, Mast and Drever (1987) used a specific surface area of 0.116 m^2 g^{-1} for the prepared -100 +200 mesh (75–150 μm) size fraction used in their tests and Oxburgh et al. (1994) used a specific surface area of 0.02 m^2 g^{-1} for the same size fraction. Differences in the specific surface areas contribute at least a factor of five uncertainty to the rate comparisons. The rates from the mass-balance are about five orders of magnitude lower than the laboratory rates.

Table 5.9. Dissolution rates for K-feldspar and plagioclase, mol m^{-2} s^{-1}

	K-feldspar	Plagioclase	Reference
Field rate	1.1×10^{-18}	9.4×10^{-17}	Zhu 2005
Laboratory rate	3.2×10^{-13}	3.2×10^{-12}	Zhu 2005
Laboratory rate	$1.5–8.9 \times 10^{-13}$	—	Blum and Stillings 2005
	—	2.0×10^{-12}	Mast and Drever 1987 and Oxburgh et al. 1994

5.5 Wetted Surface Area

Perhaps the most challenging aspect of mass-balance calculations for field studies is estimating the surface areas of minerals that are contacted by ground water. The available surface area is estimated based on modal analysis of representative particles taken from the regolith and the measured particle size distributions. The volume between particles, which is the pore volume, is a characteristic of the rock. Pačes (1973) described a geometric model that can be used to estimate the surface area of a mineral in an open fracture that is contacted by water, referred to as the "specific wetted surface area." The wetted specific surface area is defined as

$$\tilde{S} = \frac{S}{\phi}, \tag{5.32}$$

where S is the surface area of the mineral in 1 L of rock filled with water and ϕ is the porosity of the rock. The model used to determine $\tilde{S}$ follows:

Consider the fracture between two rocks A and B having an average width d. If both A and B have smooth surfaces, then the contacted surface area S is simply

$$S = \frac{2V_T}{d}, \tag{5.33}$$

where V_T is the volume of the fracture. The roughness of the walls in the fracture can be represented by n cubes having edge length d that occupy a portion of the volume V_T. Figure 5.4 shows a side view of such a fracture. The total volume of the fracture between the walls of rocks A and B is

$$V_T = W + nr^3, \tag{5.34}$$

where W is the volume of water in the fracture. Now consider the portion of the fracture containing 1 L of ground water (W = 1 L) and calculation of the corresponding surface area $\tilde{S}$, which is referred to as the wetted specific surface area (i.e., specific to 1 L ground water). The surface area in the fracture (i.e., the sum of the surfaces of A and B) that is contacted by water is

$$\tilde{S} = \frac{2W}{d} + \frac{2nr^3}{d} + 4nr^2 - pnr^2. \tag{5.35}$$

The first term gives the surface area contacted by water on the smooth portions of the fracture (without the cubes) in Figure 5.4. The second term gives the sum of the areas on the bottoms of the cubes on rock A and the tops of the cubes on rock B. The third term gives the areas on the four sides of the cubes in the lateral direction. The fourth term accounts for the faces of cubes on the periphery of the unit cell, such as the cube on the far right edge of rock B in Figure 5.4. In the limit of no roughness (n = 0), the wetted specific surface area is

$$\lim_{n \to 0} \tilde{S} = \frac{2W}{d}. \tag{5.36}$$

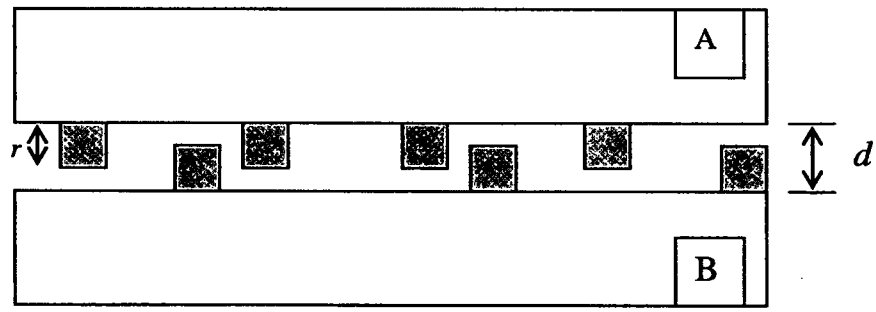

Figure 5.4. Schematic illustration of fracture with rough surfaces.

The roughness of the fracture ρ can be described by the ratio of the values of r and d

$$\rho = \frac{r}{d}, \tag{5.37}$$

where the maximum roughness occurs when $\rho = 0.5$. At that limit (see Pačes 1973), the wetted specific surface area is

$$\lim_{\rho \to 0.5} \tilde{S} = \frac{12W}{d} - 2d\left(\frac{2W}{d}\right)^{1/2}. \tag{5.38}$$

In the limit of smooth surfaces, the wetted specific surface area is

$$\lim_{\rho \to 0} \tilde{S} = \frac{6W}{d}. \tag{5.39}$$

For a 1 mm wide fracture containing 1 L of water, the limiting values of the wetted specific surface areas for smooth and rough surfaces are:

Smooth surface ($n = 0$, where n is number of cubes used to simulate roughness of fracture surfaces):

$$\tilde{S} = \frac{2W}{d} = \frac{2 \times 1000\, cm^3}{0.1\, cm} = 2 \times 10^4\ cm^2 \tag{5.40}$$

Smooth surface ($\rho = 0$, where ρ is the ratio of the roughness of the fracture surfaces to the fracture width):

$$\tilde{S} = \frac{6W}{d} = \frac{6 \times 1000\, cm^3}{0.1\, cm} = 6 \times 10^4\ cm^2 \tag{5.41}$$

Rough surface ($\rho = 0.5$):

$$\tilde{S} = \frac{12W}{d} - 2d\left(\frac{2W}{d}\right)^{1/2} = \frac{12 \times 1000\, cm^3}{0.1\, cm} - 2 \times 0.1\, cm \left(\frac{2 \times 1000\, cm^3}{0.1\, cm}\right)^{1/2} = 1.2 \times 10^5\ cm^2 \tag{5.42}$$

This simple model gives an order-of-magnitude estimate of the effects of surface roughness and crack width on the surface area that may provide useful initial insights regarding the exposed surface areas of rubble piles having a wide range of particle and void sizes. For example, the tortuous water pathways can be modeled as rough fractures as in Figure 5.4 with appropriate values of ρ and n in order to simplify the mathematics. Application of this approach to surface piles will be further evaluated in a later study.

5.6 Temperature

The Arrhenius equation quantifies the effect of temperature on a single elementary reaction step and usually also the combined effect on coupled processes. The effect of temperature on the dissolution of minerals in laboratory tests has been reviewed by White et al. (1999). As in the studies described herein to show the general approaches used to evaluate field behavior, the mean annual temperatures (local, regional, or global) are used in applying the Arrhenius equation for most geochemical model calculations. However, since the rate depends exponentially on the inverse temperature, using the arithmetic average temperature (i.e., the mean annual temperature) in the Arrhenius equation will not give the mean rate. This issue was discussed by Lasaga et al. (1994), and their analysis is worth repeating here. Assume that the seasonal variation in temperature is sinusoidal as

$$T = \overline{T} + \Delta T \sin(2\pi t) \tag{5.43}$$

where $\overline{T}$ is the average temperature, ΔT is the maximum annual variation in temperature, and t is time, in years. The time-averaged rate constant from the Arrhenius equation is determined as

$$\overline{k} = A \int_0^1 \exp\left\{\frac{-E_a}{R\left[\overline{T} + \Delta T \sin(2\pi t)\right]}\right\} dt \,. \tag{5.44}$$

The rate constant calculated from the Arrhenius equation for the average temperature is

$$k = A \exp\left(\frac{-E_a}{R\overline{T}}\right). \tag{5.45}$$

Note that

$$k \neq \overline{k} \,. \tag{5.46}$$

"The result of the nonlinear relation between temperatures and rates is that the mean of the function in [Equation 5.45] is not equal to the function evaluated at the mean temperature" (Lasaga et al. 1994, p. 2373). The temperature that provides the time-average rate constant, the so-called kinetic average temperature, will depend on the both the effective activation energy, E_a, and the amplitude of the annual temperature variation, ΔT. For an activation energy of 20 kcal mol^{-1} and an amplitude of 10°C, the kinetic average temperature is about 2.8°C higher than the average temperature. This results in 40% increase in the rate for an average annual temperature of 15°C.

5.7 Relevance of Mass Balance Models to Surface Disposal Systems

Several aspects of the approaches used in mass balance models for natural systems are relevant to modeling surface disposal sites and provide valuable tools that can be used in other modeling approaches. These include modal analyses of phase distributions, the mathematical treatments

and simplifications used to model large-scale systems, and the approaches for taking seasonal variations into account. Simple modifications of the governing equations used in mass balance models to include porosity and water saturation extend their use to unsaturated systems. The mathematics for separating the dissolution inputs in the mass transport equations and modeling mineral surface areas and wetted areas are directly applicable to modeling surface disposal systems. Many of the techniques used to collect data in field studies are also applicable to the characterization of surface disposal systems, including lysimeters, which are discussed in the next section.

In addition, qualitative insights regarding the relative importance of various processes and aspects of hydrology are provided, in part due to the observed discrepancies with values measured for individual processes, such as the dissolution rates discussed in this report. Mass balance models for field systems and the data bases that support them can fill an important role for confirming and calibrating forward models. The limited amount of site-specific geochemical and hydrological information available for most disposal systems must be supplemented to develop predictive forward rate models. Inverse modeling with mass balance calculations may provide valuable insights utilizing a limited data base that can then be used to support forward modeling. If no data are available, collecting the smaller amount of field data that is needed to support qualitative inverse modeling may be possible, whereas the more detailed studies needed to support quantitative forward modeling (e.g., the reactive transport models discussed in Section 7) are more likely to be cost prohibitive.

6 Field Tests

Field tests have been conducted in which materials are buried in test plots and allowed to corrode under natural or sometimes modified or supplemented environmental conditions. Field tests provide a more realistic simulation of the materials interactions and mass transport effects than can be achieved in laboratory tests, but at the cost of poorer control of conditions and poorer collection of solutions (or sometimes loss of solutions). The use of lysimeters allows for closer monitoring of the reaction conditions and collection of solution samples during the test. Surface analyses of recovered test materials usually provide the key evidence regarding the extent of corrosion. The earliest field tests with glass waste forms were conducted at Chalk River, Canada, in sand (Walton and Johnson 1981). Other field tests have been conducted at Ballidon, England, in limestone (Newton 1985), Mol, Belgium, in clay (e.g., Van Iseghem 1990), Stripa, Sweden, in granite (e.g., Werme et al. 1985), and at WIPP, New Mexico, in salt (Wicks 1986). Various glasses (including glasses with radionuclides) and sometimes other materials, such as steel, were either buried directly or arranged around a heating element in a "pineapple slice" (or other configuration) and exposed to natural ground water or prepared solutions. In some designs, solution was retained and samples collected for analysis throughout the test period. Field tests with borosilicate waste glasses have been reviewed by Wicks (1992) and in DOE (1994 chapter 4).

The study of some natural analogue materials is considered a field test in the broadest sense because the extent of weathering under assumed conditions over an estimated duration is used to calculate an effective degradation rate. For the purpose of this report, the characterizations of materials recovered from the waste site being evaluated (e.g., Veblen 2004) are not considered field tests because they are not used to provide kinetic information regarding degradation rates from past exposure in the field. The use of such studies for modeling future performance will be discussed in a subsequent report.

6.1 Natural Analogues

The term "natural analogue" refers both to an occurrence of materials or processes resembling those expected in a geological waste repository (Côme and Chapman 1986) and the methodology used to study and assess such materials and processes (IAEA 1989; ASTM 2009). The scientific method of analogy uses inference from resemblances to imply further similarity (Ewing 1987; Petit 1992a). The method is useful for judging the veracity of process models when direct demonstration and validation are impossible and for evaluating the range of conditions to which the model can be applied.

Examinations of naturally weathered materials have been used extensively by geochemists to study the corrosion processes in terrestrial and marine environments, by archeologist to age-date artifacts, and in the waste management community as natural analogues for radioactive waste materials, particularly waste glass. Studying the alteration of materials that has occurred over thousands to millions of years provides insights that can be utilized in projecting alteration behavior far into the future. The use of natural analogue materials enhances confidence in the validity of waste form performance models for calculating long-term durability in two ways. First, the processes that drive degradation reactions in natural environments can be used to develop mechanistic models and estimate corrosion kinetics. Second, the corroded materials and corrosion products can be used to calibrate laboratory tests designed to accelerate the corrosion process. That is, if a test method can be shown to reproduce the extent of corrosion of a glass or

mineral and generate the same corrosion products that resulted from natural weathering during the previous million years, then application of that same test method to a waste form having a similar composition is expected to result in an extent of corrosion representing weathering for a million years into the future.

The use of natural glasses as analogues for radioactive waste glass was proposed by Ewing and coworkers (Ewing et al. 1979) and several reviews of the alteration phase analysis, field studies, and modeling efforts are available (Adams 1984; Chapman 1984; Ewing 1987; McKenzie 1990; Jercinovic 1992; Ewing 1992; Petit 1992b; and Luo et al. 1998). Perhaps the most extensive application of natural analogues has been the use of natural glasses including tektites, rhyolithic (obsidian) glasses, and basaltic glasses as analogues for waste glass. These are aluminosilicate glasses that contain the same major components of nuclear waste glasses.

Tektites are glassy materials formed when rock, sand, or soil is melted by meteoric impact. Fields of strewn tektites are found in Australia, Europe, Africa, and North America. Weathered tektites have been recovered from deep-sea cores and sub-aerial environments (e.g., Glass et al. 1984). Weathered tektites collected from the Cretaceous/Tertiary boundary (e.g., Sigurdsson et al. 1991) provide key evidence implicating the impact from a large meteor as the cause of extinction of large dinosaurs.

Rhyolithic glasses (obsidian) are formed as the outer surfaces of magmas cool rapidly. Obsidian was used by ancient peoples as cutting tools and weaponry in the Pacific Rim, North and South America, and the extent of weathering has be used by archeologists to age-date obsidian artifacts (e.g., Friedman and Smith 1960). The interaction of water with both tektites and obsidians has been used as an analogue for interactions of water with waste glass (Mazer et al. 1992).

Basaltic glasses are also of volcanic origin and occur at the surfaces of cooled magmas having basaltic compositions. The silica content of many basalts is similar to that in borosilicate waste glasses, and basalts may be the most-studied analogues. Weathering of basalt glass produces a range of alteration products referred to collectively as palagonite (e.g., Jercinovic and Ewing 1987), and many of the same phases form during the corrosion of basalt glass and waste glass, for example: analcime, chabazite, garronite, gibbsite, gyrolite, hydrotalcite, kaolinite, lizardite, phillipsite, smectite, thomsonite, and tobermorite (Ewing and Jercinovic 1987; Byers et al. 1986; Byers et al. 1987). The role of basalt weathering in continental and deep sea environments has been studied as a potentially important sink for atmospheric CO_2 (Brady and Gílason 1997). The corrosion of ancient man-made glasses is also studied from the perspective of conservation (e.g., Vandiver 1992) and as analogues for waste glasses (Strachan 2003).

In many cases, the chemistry of the solution in which the material corroded can be inferred from the adjacent environmental materials (e.g., soils and sediments) and the assemblage of alteration phases. However, the understanding of the corrosion process and comparisons to corrosion models are often limited to analysis of the solids due to difficulties in obtaining an analogue material still contacting the surrounding media, since the materials are often artifacts collected many years earlier for reasons other than weathering studies. Laboratory experiments and modeling can play an important role in the analogue studies, for example, by confirming the sequence of mineral formation under the assumed corrosion conditions.

Many analogue studies have been conducted as part of radioactive waste disposal programs, such as the Nopal I uranium deposit in the Sierra Peña Blanca of northern Mexico. The naturally occurring mineral uraninite, which is chemically similar to uranium oxide spent nuclear fuel, has been oxidized under conditions similar to those at Yucca Mountain, Nevada. This system

provided a representative system for studying the corrosion of spent fuel and the transport of contaminants (e.g., Murphy and Pearcy, 1992; Pearcy et al. 1994). Studies related to this system and other systems and processes relevant to slags and concrete are being evaluated in greater detail and will be discussed in a later report. These include several studies sponsored by the U.S. NRC, studies of the obsidian/tuff interface at the Valles, New Mexico, site (Stockman et al. 1994), the sandstone uranium deposits of Meghalaya (Bajpai and Narayan 2008), the Steenkampskraal monazite mine in South Africa for colloidal transport (Jarvis et al. 1997), and many other process analogue sites that have been summarized by Simmons (2002).

6.2 Lysimeter Studies

A lysimeter is a device that is used to constrain the percolation of water to an isolated column of soil and is commonly used to measure the interactions between groundwater, soil, and materials placed in the soil. Monitors can be placed in the soil and groundwater can be collected from various locations within the lysimeter and at the bottom. A lysimeter can be constructed for laboratory testing similar to a column test or buried in the ground as a field test. Waste materials can be embedded in soil within a lysimeter to study the release of waste components under simulated burial conditions due to reaction with naturally-occurring precipitation, controlled additions of water, or both. A schematic drawing of a typical large-scale lysimeter that was used in field testing (taken from McConnell et al. 1998) is provided in Figure 6.1a. It consisted of a right-circular cylinder 3.12 m high with a 0.91 m inside diameter constructed of 12-gauge Type 316L stainless steel. The bottom 20 volume% was used to collect water that had percolated through the top portion; this was collected for analysis through a stainless steel tube. The top and bottom sections were separated by filters, screens, etc. to keep soil out of the collection volume and promote drainage from the soil. The top 80 volume% of the lysimeter included the waste material test specimens and instruments used to sample, analyze, and monitor pore water, temperature, moisture, etc. The waste materials and probes were backfilled with the soil of interest. The water collected during the test was pumped from the reservoir for analysis. Figure 6.1b shows a cross-section of a lysimeter locating cores that were taken to recover the reacted waste material and sample the surrounding soil for analysis.

Lysimeters used in field tests are usually left uncapped to provide access to meteorological water and allowed to vegetate to simulate evapotranspiration. Evapotranspiration is the release of water vapor from the earth's surface by evaporation from the soil and transpiration from plants. Transpiration is the process in which plants lose water vapor through pores and leaves and replace it with water taken up by the roots. The evapotranspiration rate depends on the temperature and humidity of the air, wind speed, plant type, and the nature of the land surface. To account for the variance in short-term weather patterns, sites are often characterized by the *potential evapotranspiration*, which refers to the greatest amount of water vapor that could be released into the atmosphere if provided an unlimited supply of water.

6.2.1 McConnell and Others

A 10-year project was conducted between about 1985 and 1995 which "(1) studied the degradation effects in EPICOR-II organic ion exchange resins caused by radiation, (b) examined the adequacy of test procedures recommended in the "Technical Position on Waste Form" to meet the requirements of 10 CFR 61 using solidified EPICOR-II resins, (c) obtained performance information on solidified EPICOR-II ion-exchange resins in a disposal environment, and (d) determined the condition of EPICOR-II liners" (McConnell et al. 1998; Rogers et al. 1992). Scientists at INEEL, ANL, ORNL, BNL, and Idaho State University participated in the study,

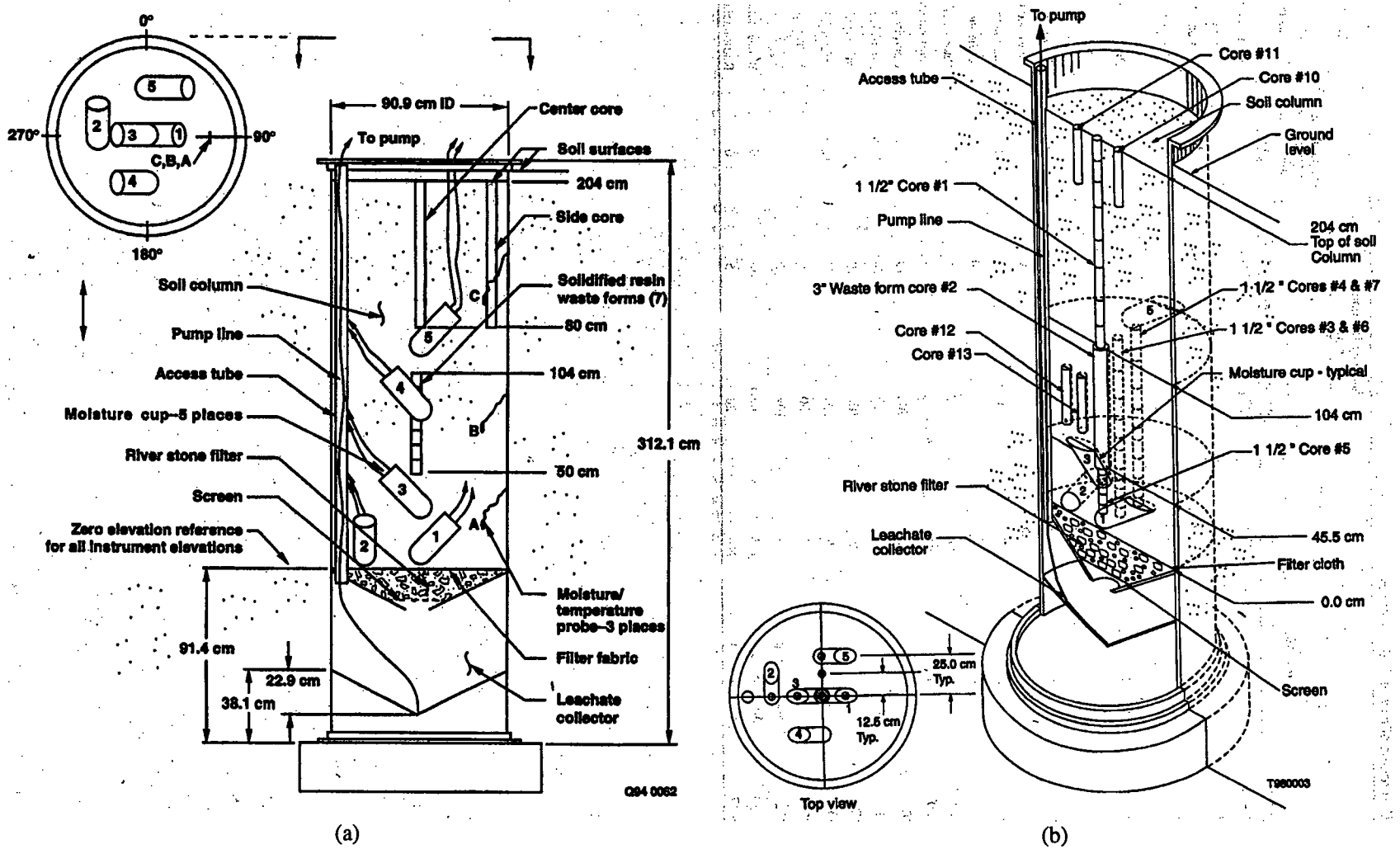

Figure 6.1. Drawings of lysimeter used in field tests by McConnell et al. (1998): (a) Assembled lysimeter and (b) cross-section showing core samplings.

which included resin degradation, resin solidification, and field studies. The results of the field studies are utilized in the discussion of lysimeters. Lysimeters were constructed to measure the releases of ^{60}Co, ^{90}Sr, ^{125}Sb, ^{134}Cs, ^{137}Cs, and trace amounts of other nuclides from ion-exchange resins that were immobilized in either portland type I-II cement or vinyl ester-styrene (VES) and then buried in either soil or sand at the ANL site in Illinois and ORNL site in Tennessee. The lysimeter design is shown in Figure 6.1 and the tests of interest are summarized in Table 6.1. After about 10 years, both of the lysimeters filled with silica oxide sand (obtained from Unimin Corporation) and the one lysimeter at each site that was filled with soil provided enough accumulated ^{90}Sr in the effluent to evaluate the test method and analysis.

Table 6.1. Lysimeter test conditions used by McConnell et al. (1998)

Lysimeter No.	Fill Material	Waste Form	Initial inventory	
			^{90}Sr, mCi	^{137}Cs, mCi
ANL-3	ANL soil	PF-7 resin in VES	27	464
ANL-5	Unimin silica oxide sand	PF-7 resin in portland cement	19	312
ORNL-1	SRNL soil	PF-7 resin in portland cement	19	312
ORNL-5	Unimin silica oxide sand	PF-24 resin in portland cement	3	1432

The results of tests at both sites with the lysimeters filled with sand appear to show similar release behaviors. Figure 6.2a displays the results for lysimeter ANL-5 and Figure 6.2b displays the results for lysimeter ORNL-5. More water passed through each of the lysimeters at the ORNL site than passed through any of the lysimeters at the ANL site: the total accumulated leachate recovered in ORNL-5 was 8864 L, whereas the total recovered in ANL-5 was 6081 L. These are in good agreement with the accumulated precipitation at the ORNL and ANL sites (8683 L and 5957 L, respectively). The cumulative ^{90}Sr activity after 3672 days is 5.98 μCi in ORNL-5, which is 0.20 % of the initial inventory in the waste form. The cumulative ^{90}Sr activity after 3641 days is 4.16 μCi in ANL-5, which is 0.02 % of the initial inventory. About the same amounts of ^{90}Sr were measured to have accumulated in the ANL and ORNL lysimeters, even though the ^{90}Sr inventory in the ORNL waste form was 6-times lower than that in the ANL waste form and the ORNL lysimeter had about 1.5-times the water flow through it. The waste forms were immobilized in the same cement and buried in the same type of sand. The greater release in the ORNL system could be due to the greater release of ^{90}Sr during waste form degradation, more efficient transport of released ^{90}Sr, or both.

The leachate results for tests ANL-5 and ORNL-5 were fitted empirically with the diffusion-limited release (diffusion out of the waste form), uniform release, and solubility-controlled release models to best represent the 10-year results; the model parameters are summarized in Table 6.2. As seen in Figures 6.2a and 6.2b, all three models represent the general release behavior, and the mechanism cannot be discerned from the data set. The solubility-controlled release model (open circles) was most similar to the ANL-5 test results but under-estimated the ORNL-5 results, whereas the uniform release model (triangles) was most similar to the ORNL-5 test results but under-estimated the ANL-5 results (except after 10 years). The waste form

Table 6.2. Model Parameters used by McConnell et al. (1998)

Model	Parameter	ANL-5	ORNL-5
Diffusion-limited	Diffusion coefficient, D_{wf}	1 x 10^{-15} cm^2 s^{-1}	5 x 10^{-14} cm^2 s^{-1}
Uniform dissolution	Fractional release rate, q	1.3 x 10^{-4} yr^{-1}	4.0 x 10^{-4} yr^{-1}
Solubility-limited	Solubility limit	1680 pCi L^{-1}	1260 pCi L^{-1}
Transport-limited	K_d and D_{md}	K_d = 36; D_{md} = 8.0	K_d = 36; D_{md} = 7.5

diffusion control model under-estimated the ANL-5 results but over-estimated the ORNL-5 results. Based on the differences and similarities in the test conditions, diffusive release from the waste from should be slightly faster from the ANL waste form due to the high concentration gradient between ^{90}Sr in the waste form and in the groundwater. The uniform dissolution rates should be the same for the two identical waste form matrices, and the solubility limits should be

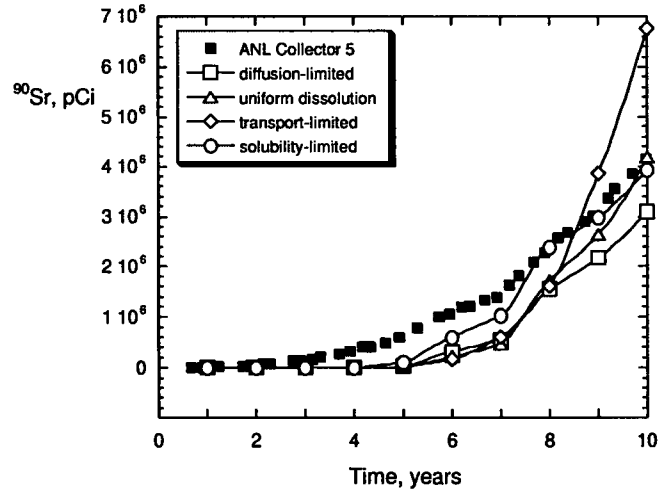

(a)

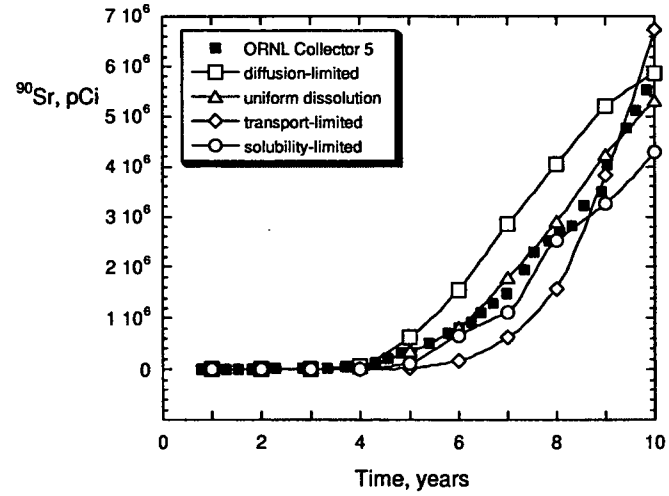

(b)

Figure 6.2. Results from McConnell et al. (1998): Measured and modeled release of ^{90}Sr in lysimeter tests (a) ANL-5 and (b) ORNL-5.

about the same. The parameter values giving the good fits seen in Figures 6.2a and 6.2b are contrary to these expectations. Diffusion is modeled to be 50-times faster from the ORNL waste form, the uniform dissolution of the cement in the ORNL waste form is modeled to be 3-times faster, and the solubility in the ORNL lysimeter is modeled to be 25% lower. All of these unexpected parameter values may reflect the effects of the higher flows of water passing through the ORNL lysimeter. Higher water flow rates are expected to maintain lower Sr concentrations in the solution contacting the waste form (yielding a lower apparent solubility), could increase the effective uniform dissolution rate of the cement, and increase the diffusion of Sr from the cement (yielding a higher apparent diffusion coefficient). The models do not explicitly take into account the difference in water flow rates.

The laboratory-measured values of K_d for Sr were 6.4 mL/g in sand from the ANL site and 6.3 mL/g in sand at the ORNL site using a short-term batch test method (McConnell. et al. 1998;Table 27). Direct regression of the lysimeter results using the 1-dimensional *Disposal Unit Source Term (DUST)* model gave a K_d value of 36 with a dispersion coefficient of 8 cm, and it was concluded that "the laboratory K_d value may not be appropriate for the field application" (McConnell et al. 1998; page 137). Fits to the transport-limited model (diffusion control by the geology) are included in Figures 6.2a and 6.2b. The fact that the laboratory tests provide a saturated system whereas the soil in the lysimeters is about 50% saturated (average) probably has the greatest impact on the K_d model.

Figure 6.3 shows the distribution of ^{90}Sr calculated using the 2-dimensional *Breach, Leach, and Transport (BLT)* model (McConnell et al. 1998; Figure 96). The authors note that "although the general shapes of the contours appear to be consistent with the data, the predicted magnitudes are

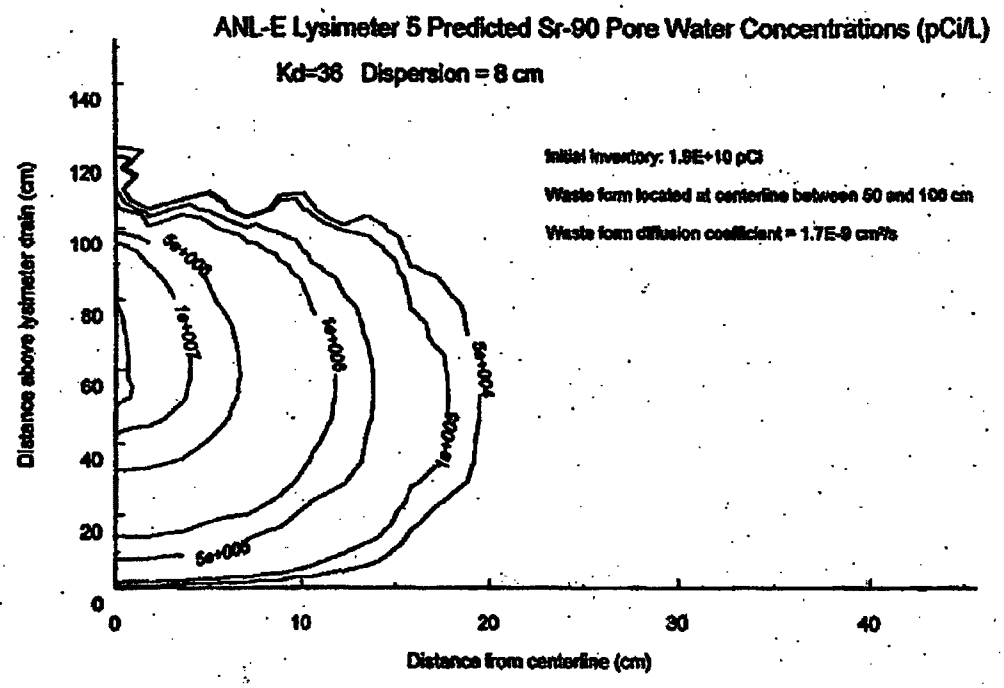

Figure 6.3. Results from McConnell et al. (1998): Predicted plume of ^{90}Sr in lysimeter ORNL-5. The wasteform is located from 50 to 100 cm above the lysimeter drain.

much greater than the observed soil concentrations" and "The model predicts higher concentrations beneath the waste form than observed" and "if the predicted concentrations were normalized to the measured soil concentration alongside the waste forms, reasonable agreement could be obtained between predictions and measurements" (McConnell et al. 1998; page 137). One conclusion from the field study is that "the limiting step in receiving Sr-90 in leachate water is not release of the nuclide from the waste forms..., but rather, the movement is limited by environmental characteristics (including soil and quantity of soil water)" (McConnell et al. 1998; page 145). Colloid-based transport of ^{90}Sr was also found to be significant.

The coupling between chemical reaction (dissolution of the waste form or leaching of the radionuclides) and mass transport involves the same processes as the coupling in laboratory column flow-through tests and can be evaluated using the same theoretical approach and calculations. An important difference between laboratory tests and lysimeter tests is that the latter system has much lower fluid flow rates and requires a much longer time to reach steady state, which is generally not attained in field studies conducted with lysimeters (and is not attained in these tests). This adds uncertainty to the waste form degradation mechanism and kinetics that are determined from the lysimeter results.

The analytical forms of the waste form diffusion, uniform dissolution, and solubility models all represent the time dependence of measured results well, but the Kd model for transport-control does not. Under these test conditions, the process controlling the release of Sr from the waste form dominates the measured behavior, but this test method is not adequate to distinguish between the possible mechanisms controlling ^{90}Sr release or deconvolute the kinetics of ^{90}Sr release from the effects of the groundwater flow rate and dispersion. The appropriate laboratory tests conducted under well-controlled conditions are needed to identify the release mechanism, which can then be coupled with a transport model that takes into account the effects of groundwater flow (advection), as well as sorption and other processes that retard contaminant transport (e.g., through K_d), to calculate long-term migration away from the waste form. Discrepancies between the laboratory and field measurement, such as occurred in this study, indicate that either the laboratory tests were not appropriate or the field conditions were not modeled adequately; the results of lysimeter tests are not sufficient to identify which is the cause.

6.2.2 Jantzen and Others

A lysimeter study was conducted at Savannah River National Laboratory in which a small piece of radioactive glass was buried for a total of 24 years (Jantzen et al. 2008). The lysimeter was open and exposed to meteoric water for 11 years, during which time leachate was collected and analyzed for gross α and gross β/γ. It was then capped and remained undisturbed for 13 years. No samples showed α activity above the background measured in a control test, but ^{137}Cs and β emitters (^{90}Sr, ^{90}Y, and ^{137}Cs) were detected. Analysis of a soil core indicated that Cs and Sr had migrated from the burial location both upwards towards the surface and downwards. The soil was known to have become saturated during several periods of heavy rainfall. The sample (in the shape of a puck about 1.3 cm in diameter and 1.3 cm long) was placed about 22 cm below the surface of the sediment layer, which had a total depth of 51 cm. The diameter of the lysimeter was 33 cm, so the volume of sediment in the lysimeter was about 43,620 cm^3 and the volume of the glass was about 1.73 cm^3. The volumetric water contents of saturated soils range from about 22% for sandy loams to about 36% for clay and clay loams (Baes and Sharp 1983). Using the value for clay soils, it is estimated that the lysimeter contained up to 15.7 L of groundwater at any time in contact with about 8 cm^2 glass surface.

Analytical results indicated that Pu isotopes in the glass were not transported from the glass to the adjacent sediment during the test. The ^{137}Cs and total beta activities measured in a vertical core of the sediment adjacent to the specimen are plotted in Figure 6.4. Both profiles show the distribution expected for diffusion from a point source that is distorted away from the surface only slightly. This behavior is consistent with that predicted for ORNL-5 by the DUST calculations in a similar environment. The long-term transport appears as nearly-spherical diffusion with only a small downward advection component. This probably reflects a tendency of the distributions to be homogenized in the pore water during episodes of saturation. This data set does not provide insights to the glass dissolution behavior (which is well understood from separate laboratory tests), but can inform and help parameterize transport models that are coupled with the release model under the evolving conditions that occurred during the lysimeter study.

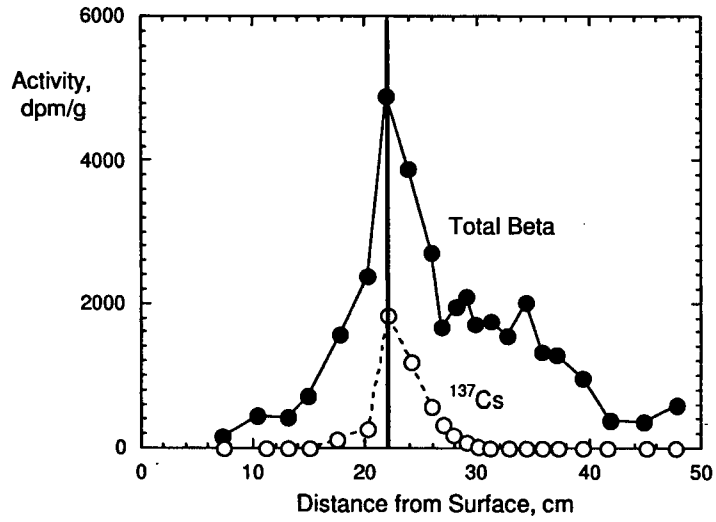

Figure 6.4. Results from Jantzen et al. (2008): Total beta and ^{137}Cs beta activities measured in core of sediment adjacent to specimen in SRNL lysimeter. The vertical line represents the location of the specimen.

6.3 Relevance of Field Tests to Surface Disposal Systems

Field tests and field measurements characterize the system that laboratory tests and models must represent, identify the range of conditions that are of interest, and then confirm the quantitative model. Characterizations of surface disposal systems are required to address both the chemical and the physical nature of the phases containing the contaminants and the effective surface area and pore structure. Iterations and comparisons between laboratory and field data would help identify the key interactions affecting contamination transport and the test conditions that should be used to determine the process controlling the release of contaminants from the waste form and measure the rates for the range of relevant field conditions. Lysimeter tests are not well-suited for determining the process(es) controlling the release from the waste form or for measuring the release rates, although they can be used to confirm the rates measured in laboratory tests. This is because the conditions in the lysimeter cannot be controlled to the precision that are needed to distinguish the controlling process or attain the steady-state conditions required to parameterize the release model. They are suitable for evaluating the transport behavior of released

contaminants and confirming coupled reaction-transport models and parameterizing the transport models. Field measurements over a range of scales can be used to provide the continuum-level values that are needed for model parameters and establish the degree of heterogeneity that must be taken into account by the model; this is discussed further in Section 7.2.

Although lysimeter tests provide a valuable link between laboratory tests (e.g., column tests) and large-scale field studies such as those discussed in Section 5, they present the same orders-of-magnitude discrepancy when directly compared with rates measured in laboratory tests that occurs for those large-scale field studies. This is probably indirect evidence of the important coupling of chemical dissolution and mass transport in both systems. Combined with the insights from laboratory tests discussed in Section 4 and mass balance approaches discussed in Section 5, small-scale lysimeters would provide a more practical means of studying the coupling between reaction rates and transport processes than large field studies, and could be used to better relate laboratory results with observed release and transport behavior. The combined use of laboratory tests to measure release rates, lysimeters to measure transport rates, and the mathematical simplifications of field systems that are used by inverse mass balance calculations may provide an effective approach for modeling surface disposal sites.

7 Discussion

Important features regarding mineral dissolution, laboratory testing, and mass balance modeling have been discussed through the critical evaluations of literature information presented in the preceding sections. This section provides summaries of three issues: (1) the discrepancies between rates measured directly in laboratory experiments and those inferred from field data by mass balance models, which is the primary objective of this report, (2) the reactive transport modeling approach currently used for predicting contamination transport, and (3) the relevance of insights gained from analyzing the discrepancy and potential use of reactive transport modeling by itself and combined with inverse modeling for assessing surface disposal systems.

7.1 Comparison of Laboratory and Field Rates

Ganor et al. (2009) recently discussed why the mineral dissolution rates measured in laboratory tests should not be expected to agree with the rates determined from field analysis. Since the same major issues evaluated in this review are presented in their analysis, the results of the present analysis are discussed by evaluating the assessment by Ganor et al. (2009). The first is that the low dissolution rates for silicate dissolution inferred from the field analyses would be practically impossible to measure using a laboratory experiment. The reason is that the change in solution concentrations from the initial solution to the final would be too small to measure in a static test even after several years. The changes in concentrations would be even smaller in dynamic tests such as a flow-through column test. As an example, Ganor et al. (2009) considered the field dissolution rate of plagioclase in the Panola regolith cited by White and Brantley (2003) as 2.8×10^{-16} mol m^{-2} s^{-1}. These results were also evaluated in Ebert 2010. From the reported composition, the reaction is

$$\underset{\text{oligoclase}}{Na_{0.77}Ca_{0.23}Al_{1.3}Si_{2.77}O_8} + 1.23H^+ + 3.695H_2O \rightleftharpoons \underset{\text{kaolinite}}{0.615Al_2Si_2O_5(OH)_4} + 1.54H_4SiO_4 + 0.77Na^+ + 0.23Ca^{2+}. \quad (7.1)$$

Dissolution of 1 mole of oligoclase generates 1.54 moles of dissolved silica, 0.77 moles Na^+ and 0.23 moles Ca^{2+}. Changes in the dissolved silica concentration would be the most readily detected because the change would be greater than that of other components. For an analytical uncertainty of 2% for each measurement, a difference of at least 2.83% is necessary to distinguish two Si concentrations (the square root of the sum of the squared uncertainties). The dissolution rate in a static test is calculated as

$$rate = \frac{\Delta C\ V}{S\ f(Si)\Delta t} \quad (7.2)$$

where ΔC is the change in concentration of the Si used to measure the rate over the test interval Δt, S is the surface area and V the solution volume, and f(Si) is the stoichiometric coefficient of dissolved Si in the reaction. From Equation 7.1, f(Si) = 1.54. The surface area can be expressed as the product of the plagioclase mass and the specific surface area $\overline{S}$ of the particles. Equation 7.2 can be expressed in terms of ΔC as

$$\Delta C = 1.54 \times rate \times \frac{m \bar{S} \Delta t}{V}. \quad (7.3)$$

For an initial SiO_2 concentration of 189 μmol L^{-1}, a 2.83% change is an additional 5.35 μmol L^{-1}. This is the value of ΔC. Experimental values for the mass and specific surface area of the size fraction of crushed plagioclase and solution volume can be used in Equation 7.2 to calculate Δt, which is the required test duration to achieve that value of ΔC. Equation 7.2 can be rewritten to solve for Δt and, after substituting values and conversion factors, expressed as

$$\Delta t(\mathrm{d}) = \frac{V\,sol.(\mathrm{L})}{1\,\mathrm{g\,plag}} \times \frac{5.35\times10^{-6}\,\mathrm{mole\,Si}}{\mathrm{L}} \times \frac{1\,\mathrm{mole\,plag}}{1.54\,\mathrm{mole\,Si}} \times \frac{\mathrm{m^2\,plag\,sec}}{2.8\times10^{-16}\,\mathrm{mole\,plag}} \times \frac{1\,\mathrm{g\,plag}}{\bar{S}\,\mathrm{m^2\,plag}} \times \frac{1\,\mathrm{day}}{8.64\times10^{4}\,\mathrm{sec}}. \quad (7.4)$$

This gives

$$\Delta t(\mathrm{d}) = 1.44\times10^{5}\,\frac{\mathrm{m^2\,d}}{\mathrm{g\,L}} \times V(\mathrm{L}) \times \frac{1\,\mathrm{g\,plag}}{\bar{S}\,\mathrm{m^2\,plag}}. \quad (7.5)$$

Brantley and Mellott (2000) report the BET specific surface area of 37-44 μm oligoclase to be 7260 cm^2/g. From previous experience, a nearly equal volume of water is needed to wet a volume of finely crushed glass with negligible excess (pooled) water. With a density of about 2.65 g/cc, 1 g of plagioclase would be wetted by about 0.5 g water. If 1 g of this size fraction was reacted with 1.5 mL ground water solution, so that 1 mL water could be recovered for analysis, 298 days would be required to produce a measureable difference in the Si concentration if the plagioclase reacted at the field rate. Additional 298-day test intervals would be needed for each subsequent point, and at least 3 data points would be needed to regress the experimental rate over a total duration of about 2.5 years.

An important assumption used in the above calculations is probably incorrect: dissolution in the laboratory test will almost certainly occur congruently due to the initial absence of kaolinite in the system. The solution must first become supersaturated with respect to kaolinite and then crystallites must nucleate and grow to provide enough surface area to affect the oligoclase dissolution rate (see discussion in Section 4.2). In the absence of kaolinite, the stoichiometric factor for SiO_2 would be 2.77 instead of 1.54. This would decrease the reaction time necessary to produce a quantifiable difference in the Si concentration from 298 days to 166 days.

By using extreme values of particle size fraction, particle mass, and solution volume, it would be possible to measure the low field dissolution rate in the laboratory. However, as pointed out by Ganor et al. (2007), crushing the plagioclase would expose fresh surface that would be more reactive than the weathered surface that is exposed in the field study and a higher rate would probably be measured. The initial rate enhanced by surface roughness is estimated to be higher than the steady-state rate by a factor of ten or less. This is based on the observation of rapidly decreasing initial rates in single-pass flow-through tests with crushed glass. The same phenomenon is seen in the flow-through tests conducted by Taylor et al. (2000b) shown in Figure 4.1. The Si concentration in the initial sampling is about 20 μM and decreases to about 2 μM when near steady-state conditions are reached after about 800 hours (33.3 days) of reaction

at 25°C. Part of the initial high concentration might be attributable to the dissolution of fines that were not removed when the specimen was prepared, but a large part is due to the rapid dissolution of high-energy surface sites. The time required to dissolve away the fracture-induced high-energy surface features could be significant under field conditions, and an aggressive pre-conditioning step would probably be required to modify the surface condition of the material crushed for use in laboratory experiments so that it simulates the surface texture of aged materials in the field. For small particles, removing the fracture surfaces may result in only a small kernel of remaining material. Dissolution of very small particles results in a rapid loss of surface area which may be difficult to accurately take into account in rate calculations. For example, laboratory tests have been conducted with minerals recovered from field sites and treated to remove alteration phases (e.g., Clow 1992). It would be difficult (but not impossible) to amass enough of the 37-44 μm size fraction of these particles for use in a laboratory test. Using larger weathered grains collected in the field in the laboratory tests would reduce the specific surface area from the value used in the preceding calculations and increase the required test durations.

Many of the laboratory test parameters accelerate the dissolution reaction relative to the field rate. Almost all of the laboratory tests discussed were conducted with a dilute solution (usually demineralized water) and with an imposed pH (usually acidic). Actual ground waters contain measurable concentration of dissolved Si, alkali metals, and alkaline earth elements and have near-neutral pH values. The concentrations of dissolved Al in the ground water are difficult to measure, but Al is known to inhibit the dissolution of many minerals (e.g., Oelkers et al 1994). The absence of dissolved Al in laboratory tests probably contributes to the discrepancy with field rates.

Ganor et al. (2007) also discussed the need to extrapolate laboratory-measured dissolution rates to field conditions and the on-going debate regarding the dissolution rate laws for minerals. They concluded that, contrary to the common view, the dissolution rates measured in laboratory tests are actually *lower* than the field rates after the slowing effects of the system approaching equilibrium are taken into account using the rate law derived by Burch et al. (1993), as discussed in Section 4. [This and related rate laws are discussed in Section 2 of Ebert (2010).] The point is that dissolution slows rapidly as the solution and mineral approach equilibrium. The effect of secondary phase precipitation and the relative surface areas of the dissolving plagioclase and precipitating kaolinite are also discussed by Ganor et al. (2007) as contributing factors to the discrepancy in the laboratory and field rates. They concluded that "the lack of data on precipitation rates of secondary minerals put a major constraint on our ability to accurately simulate the dissolution rate of plagioclase in the field" (Ganor et al. 2007, p 609). The results of Alekseyev et al. (1997) and other studies indicate that dissolution rates are not necessarily controlled by precipitation rates and that the coupling between the dissolving phase, the precipitating phase, and the common solution may be not be as simple as is often assumed using linear rate laws. Alekseyev et al. (1997) suggest that the effect may be due to the differences in the chemical potentials of elements in the dissolving and precipitating phases rather than the solubilities of the phases.

The effect probably goes beyond measurement of the precipitation rate because, whereas secondary (product) phases such as kaolinite are present and fully matured in the mineral make-up of field systems, they must nucleate and grow *in-situ* in laboratory tests. As described in Section 4.2, the effect of secondary phase formation can be much more significant when small particles are first formed than in the presence of mature phases. Also, as discussed in Section 4.3, the solid phase composition will lag the solution chemistry and the system will be in disequilibrium to some extent. The extent of disequilibrium will be affected by ground water flow in the field and in dynamic laboratory tests, and will probably be greater than in static tests.

In the field, the reactivity of the mineral solids will evolve based on the integrated time that the solids are contacted by (any) fluid, whereas the chemistry of a particular volume of fluid (and its approach to saturation) will evolve based on the period of time it was in contact with minerals. In any field system, the rock and its component minerals will be much older than the ground water.

7.2 Summary of Reactive Transport Modeling

As described in the preceding chapters, it has long been recognized that chemical principles control the mineral assemblages in rocks and soils and geochemists and earth scientists have historically applied thermodynamic models to systems of interest by assuming the systems are at equilibrium. Ground water hydrologists have at the same time developed transport models with advective and dispersive components that take into account various sorption and precipitation reactions that are usually assumed to be at equilibrium. Reactive transport modeling couples the various processes leading to chemical reactions with the mass transport processes. Differences in local concentrations affect the transport and the fluxes of dissolved species affect the reaction rates. Incorporating the kinetics of the chemical processes is a key challenge for current modeling. Other issues include improving the governing equations for both reaction and transport, assessing the limits for model predictions, and improving the efficiency of computer computations. Reactive transport modeling addresses two aspects of geochemistry for which the equilibrium models are inadequate: "quantify[ing] the spatially observed distributions of the chemical constituents in terms of the causative factors and estimat[ing] the *magnitude of time* involved in the evolution of the hydrogeochemical system" (Narasimhan and Apps 1990). These are both important issues for surface disposal systems.

The conservation of mass expression used to describe mass transport includes a source/sink term for the effect of dissolution and precipitation of solid phases on the solution concentration of the species being tracked. The dependence of the change in concentration of the species of interest C with time on these factors (for one-dimensional flow) is

$$\frac{\partial C}{\partial t} = -v\frac{\partial C}{\partial x} + (D_e + D_{md})\frac{\partial^2 C}{\partial x^2} - \frac{\partial q}{\partial t}. \tag{7.6}$$

The first term on the right hand side represents advective transport and the second term represents dispersive transport. The term in parentheses is the hydrodynamic dispersion coefficient, where D_e is the effective diffusion coefficient *for the geologic medium* and D_{md} is the coefficient of mechanical dispersion; D_{md} is often modeled as the product of the dispersivity, α, and the pore water flow velocity, v. The third term represents the change in concentration within the solid phase due to reaction, which is the dissolution or diffusion rate at which the species C is released from the waste form. Including a dimensionless volumetric moisture content θ to represent the fraction of the total volume that is occupied by water gives

$$\frac{\partial \theta C}{\partial t} = -v\frac{\partial \theta C}{\partial x} + (D_e + D_{md})\frac{\partial^2 \theta C}{\partial x^2} - \frac{\partial q}{\partial t}. \tag{7.7}$$

Note that the chemical reaction term does not depend on the volumetric moisture content, but does depend on the solution composition. Formulations of that dependency were discussed length in Section 4. Coupling the chemical reactions with mass transport involves solving the chemical reaction and mass transport terms simultaneously. Although straightforward, solving the governing equations for chemical reactions and transport simultaneously is computationally

demanding (in terms of computing time and memory requirements) and current approaches ease the computation requirements by decoupling the reaction and transport calculations using operator splitting techniques. In this method, the equations for reaction and transport are solved sequentially (with or without iteration) within each time step (e.g., Steefel and MacQuarrie 1996).

Current modeling approaches utilize the continuum hypothesis to represent heterogeneities present in the modeled system. The discrete details of the system are replaced by idealized representations of the local properties that vary smoothly over space so that spatial changes can be treated using differential calculus. Modeling a porous system as a continuum replaces the discontinuities that occur on the microscopic scale (e.g., the surface of a rock) with functions that are macroscopically continuous. The value of a property at any point in space is taken to be the average of the property values within a selected volume that is large relative to the microscopic scale but small relative to the distance over which changes in the property value are significant. The physical system is represented as sets of connected representative volumes sized appropriately to describe each property macroscopically. A representative volume could be defined as the surface of a rock, but the function describing a property such as the water diffusion constant would vary smoothly over neighboring volumes (i.e., across the surface of the rock). Properties of interest include temperature, porosity, fluid saturation, fluid flow velocities, and mineral concentrations. For most properties, measured values are based on macroscopic scale samples that establish the representative volume. The representative volumes usually differ for different properties, and some properties must be described by more than one volume. For example, the flow of fluid through fractures and through the matrix can be described using a large volume to represent the large distance between fracture structures and a small volume to represent the small distances in the unfractured matrix . Separate functions would be used to describe the flow through each representative volume. Some properties, such as permeability, are themselves continuum values that are not quantified on the molecular scale. The distribution coefficient (K_d) is a familiar example of a continuum value that represents the average of several processes over a selected representative volume, which could be the entire system. Relationships between properties values can be utilized to facilitate modeling, such as the empirical relationships observed between K_d, the overall specific surface area, and the hydraulic conductivity (Tompson and Jackson, 1996).

The dependence of mineral dissolution (and precipitation) rates on the solution chemistry in a static system and the effect of flow on the solution chemistry and dissolution behavior were discussed in Section 4. In the field, the coupling of solute transport and chemical reactions affects both the evolution of the ground water chemistry and the weathering behavior of the stationary solids. The relative rates of mass transport, dissolution, and precipitation will determine whether equilibrium, partial equilibrium, or steady-state will be attained under any particular set of conditions. If chemical reactions occur faster than transport, then local equilibria are expected to prevail over long periods. Local disequilibrium will result (and be maintained) if the chemical reactions are slow relative to transport. What is considered "local" and "long" will depend on the length scale and time scale of interest. The transport of solutes by ground water will be greatly affected by the presence of fractures, and the coupling of transport with chemical reactions will further influence dispersal (e.g., Steefel and Lichtner 1998 and references therein). The availability of reactive surface sites of the various minerals will also affect the system behavior. This will change over time as phases dissolve completely or become overgrown with product phases, and as flow paths change due to the opening and closing of channels due to dissolution or precipitation of phases in the channels, etc. (e.g., Steefel and Van Cappellen 1990).

A major focus of reactive transport modeling is up-scaling models developed for molecular scale reactions to field scales. Figure 7.1 illustrates the typical length and time scales for measured values and models. Up-scaling is usually done in steps by first linking the molecular scale model with mesoscale measurements (such as bench-scale laboratory experiments) to parameterize the models, then linking the mesoscale properties to the continuum-scale based on pilot-scale measurements to determine continuum-level model parameters, and then up-scaling to the macro-scale utilizing measurements that characterize the heterogeneity of the physical and chemical properties over the region of interest. Each up-scaling step represents a decrease in the specificity of the analysis, a smoothing of the modeled processes, and a homogenization of the system being modeled. Many of the techniques that have been discussed and evaluated in this report and approaches used for measuring and modeling in the laboratory and field can be used when up-scaling the molecular scale models for application to macro-scale systems. In essence, the discrepancy addressed in this report between the up-scaling of molecular scale models by using mesoscale laboratory tests and the down-scaling of field tests by using continuum scale homogenations. Additional discussion of these methods will be included in a future report on modeling waste systems.

Recent advances in the understanding and modeling of the physics and chemistry of coupled reactive-transport behavior within a complex geological system are leading to a powerful direct geochemical modeling approach. However, the demanding information needs and computing requirements will likely limit the full application of that approach to systems demanding such detailed analyses, such as a high-level radioactive waste disposal system. Mass-balance and inverse modeling approaches remain an economical alternative for assessing many systems of interest either alone or to inform simplified reactive transport models.

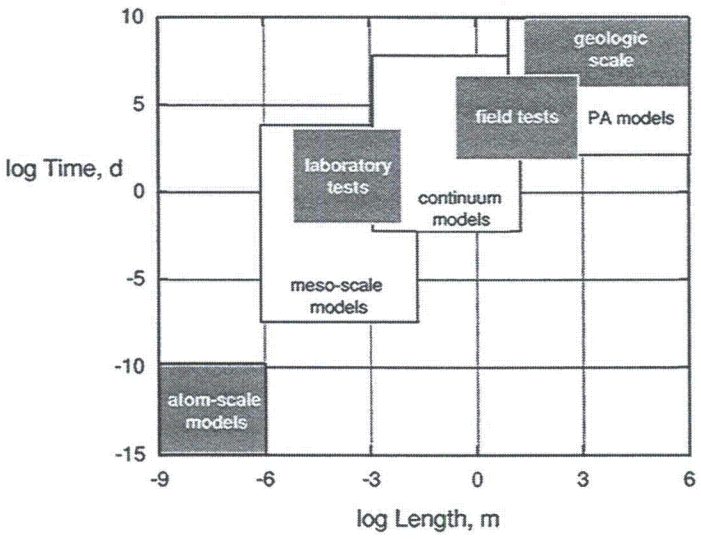

Figure 7.1. Schematic illustration of the time and length scales for atomistic models, laboratory measurements, and field applications.

7.3 Recommendations for Surface Disposal Systems

Many of the insights derived from this study of the discrepancy between the measured laboratory rates and inferred field rates can be applied to surface disposal systems, and recommendations for applying those insights are summarized in this section. These are intended to be ideas for further thought and consideration, and remain to be vetted and assembled into a recommended course of action. An important part of designing the approach includes taking into account important similarities and differences between surface sites and the field sites that have been examined. The fine-scale physical heterogeneities in waste disposal systems are expected to be greater than that in geological systems simply because of the much larger scale of natural formations, but the chemical heterogeneity may be similar. Recent analysis of radioactive slag wastes by Veblen et al. (2004) indicated a wide variety of phases are present in "rock like, porous, altered material that resembled a sandstone" and "glassy slag(s) and dense dark slags that ranged from fine grained to very coarsely crystalline." It may be that only a few phases bear contaminants and are of direct interest, but interactions with other phases could significantly affect the behavior of those phases. The degradation behaviors of these phase assemblages due to weathering are expected to mimic those of naturally-occurring rocks and can be modeled using the approaches developed for geological systems. Probably the biggest difference between surface disposal systems and natural systems may be a greater range of porosities or size distribution in the surface sites. The rocks and soils in the natural systems considered in the studies that were evaluated had size distributions influenced by millennia of weathering, abrasion, erosion, etc., whereas surface disposal systems consist of recently deposited (randomly dumped) materials sized according to the industrial process in which they were generated. This may simply result in different contributions of weathering due to run-off, water in fractures, or pore water than occurs in natural systems, although the same processes are involved.

A near-surface waste site can be modeled as one or more regoliths (a layer of loosely consolidated primary minerals and weathering products) that are composed of aggregated phases, some of which contain radioactive and hazardous contaminants, possibly distributed in a glassy phase or other matrix analogous to a rock. The volume of "rock" can be characterized using sets of representative particle sizes, porosity, and distributions of contaminated phases analogous to the rocks and minerals considered in the field studies. For example, the distributions of phases within the pieces of waste material may be restricted to the near-surface region.

Both inverse modeling methods (e.g., mass-balance) and forward modeling methods (e.g., reactive transport) can be applied to waste systems in the same way they are applied to natural systems. The utilization of each approach will depend on the available data base and the opportunities to collect additional data. As mentioned earlier, inverse modeling methods provide a possible explanation for the change in groundwater chemistry measured over a previous time period and forward models provide a prediction for future evolution. Since it is unlikely that groundwater samples will be available spanning a sufficient duration to estimate weathering kinetics, forward models using input kinetics, such as reactive transport models, and requiring only a current estimate of the groundwater chemistry may be more relevant to the chemical reactions of waste sites than inverse models. However, inverse modeling will probably be more useful for characterizing the hydraulic processes, for example, on the scale of a lysimeter or smaller field sample used in a column experiment. Another contribution of inverse modeling to waste systems is the insight provided regarding the approaches and uncertainties associated with characterizing the field (waste site) environment and the approaches and uncertainties in obtaining laboratory-measured kinetics and using those results to represent behavior in the field (waste site), which was the focus of the present study.

The component phases comprising the waste site can be characterized with respect to composition (mineralogy) and the distribution of the contaminants, and the fractional distribution of exposed surface areas can be estimated by modal analysis, as was discussed for field samples (see Section 5.1.2). Laboratory experiments can be conducted with actual site materials, with the individual phases, and with mechanical mixtures of the component phases to measure contaminant release rates for forward modeling. As is concluded in this report based on comparisons of field rates with laboratory rates, the effects of dissolution and precipitation of neighboring phases on the water composition can have an appreciable effect on the dissolution rate of the phase of interest and should be taken into account in laboratory tests. Likewise, the effects of laboratory test conditions on the measured response (e.g., flow rate in dynamic tests and surface/volume ratios in static tests) should be taken into account to best represent the field conditions. As discussed in detail in a previous report (Ebert 2010), many common test procedures do not provide accurate results if the reaction conditions are not sufficiently controlled or the system is not consistent with the model used to determine the parameter, such as the requirement of steady state or a zero concentration boundary condition. Tests must be conducted to properly control test conditions and interpreted to properly account for testing artifacts, such as the effects of flow rate, the presence of high energy sites generated during crushing, and neglecting chemical affinity effects under near-equilibrium conditions. These and other testing artifacts complicate the use of laboratory-measured values when modeling field conditions.

The degradation of the solid as measured with laboratory experiments can be coupled with governing expressions for transport through the waste site and then the surrounding natural regolith with continuum models. Representative volumes and average values can be selected to model a wide range of porosities, saturation levels, flow rates, etc. throughout the waste system and the underlying regiolith. The same measurement and modeling uncertainties, artifacts, and limitations afflicting the characterization of natural systems are expected to apply to waste sites, although many aspects of waste sites will not be as well-characterized as in natural systems evaluated by field studies. Waste sites are usually contoured to shed rain water rather than to collect it like the catchments and watersheds considered in these field studies. Some waste systems may include an engineered cap, whereas others may simply be large rubble piles. Estimating the water pathways and the effective pore structures and areas contacted by water in such systems may be the most challenging aspect of modeling the site and could dominate the uncertainty in the predicted release of contaminants.

The same factors that lead to the discrepancy between dissolution rates measured with laboratory tests and those inferred from field behavior give rise to an analogous discrepancy between laboratory rates and the behaviors observed in lysimeter studies. These must be taken into account in the design, execution, and analysis of lysimeter tests. Lysimeter studies provide a practical and economical means of calibrating a release model generated by separate (and appropriate) laboratory tests and measurements of contaminant transport. These could include lysimeters placed at locations in and around the disposal system or lysimeters filled with materials representative of (or collected from) the disposal system used in the laboratory. A key difference between these envisioned lysimeter studies and those discussed in Section 6.2 is that a separate lysimeter test would be conducted to measure the transport properties without restricting the source term to release during waste form degradation. That is, the release and transport processes would be studied separately. Tests can be conducted with leachants doped with various concentration of the contaminant elements and with lysimeters (or columns) filled with different size fractions of materials to determine continuum-scale values of transport parameters, which can be determined by inverse modeling of that system. This could provide information needed to characterize particular size ranges of solids and pores. The contaminant release from the waste material that is characterized with a series of laboratory tests (e.g., with column tests) can then be

coupled with the transport properties measured with lysimeter tests and evaluated using inverse modeling methods in a forward model to predict future release under particular conditions. The model can be validated with confirmation tests using the same lysimeter system with an embedded surrogate waste material. The general 4-step process is

1. Conduct lysimeter tests to measure groundwater transport properties and exposure conditions; utilize inverse modeling methods.
2. Conduct laboratory tests to measure dissolution properties of waste material under relevant conditions (e.g., static tests for stagnant conditions, dynamic column test for flowing groundwater).
3. Develop coupled reactive transport model based on the conservation of mass equation.
4. Conduct lysimeter test with embedded waste material to confirm coupling of dissolution and transport processes in model.

The lysimeter and laboratory tests are more easily conducted under saturated conditions, although methods exist for studying reactive transport under unsaturated conditions. Unsaturated conditions simply impose a scaling parameter on several terms in the model (e.g, see Equation 7.7) that could be taken into account in steps 3 and 4. A waste material that can be treated as a point source should be used in the initial tests to confirm the process models that are used in the chemical reaction and contaminant transport parts of the coupled model. Subsequent tests can be conducted with a distribution of several sources in the lysimeter to better represent the large system. Reacted solids can be recovered from various locations in the lysimeter to characterize the extent of degradation.

8 Comments and Conclusions

The objective of the study summarized in this report was to assess the discrepancy between dissolution rates measured in the laboratory and dissolution rates inferred from field studies. This is an important issue in geochemical research because the natural weathering of minerals affects climate, global warming, and cooling; supplies mineral nutrients to plants and animals; controls the compositions of streams, lakes, and ground waters; affects the of soils, such as water retention and drainage. Although many studies point to the discrepancy between laboratory and field rates and propose contributing factors, little has been written evaluating the methods by which the rates are measured and the inherent uncertainties. That has been the approach of this evaluation.

8.1 Comments Addressing Laboratory and Modeling Approaches

The main focus regarding field rates was the mass-balance approach that has been used since the late 1960's to relate the compositions of stream waters and ground waters to the weathering of the minerals they contact as they flow over or percolate through a regolith. The mass-balance method is essentially a bookkeeping exercise that assigns changes in solute concentrations entering and exiting a volume of interest to various process that act as sources and sinks within that volume. Mass balance can be applied to solute concentrations, but is most often applied to solute fluxes. Fluxes must be used to calculate the mineral dissolution rates. The primary interest here is mineralogical sources and sinks, but meteorological, biological, and anthropogenic factors must be taken into account in most field studies. The method provides dissolution or precipitation rates that represent average values over time, space, and reaction conditions within the field system. That is, continuum-type averages over the entire system. Although the models do not provide unique interpretations of the measured changes in the water compositions, they do provide useful insights into the relative importance of particular chemical and physical processes.

The reaction conditions in laboratory experiments are much better constrained than the reactions in the natural system, including the groundwater composition and pH, temperature, and particle size and surface area. Although this results in better precision in the measured rate, it excludes the effects of other reactions on the solution chemistry, the catalytic or inhibitory effects of solutes that are provided by other phases in the field system, and the presence of biota (e.g., microbes) that can affect the dissolution rates in natural systems.

The principle processes involved in mineral weathering include (1) factors that are related to the field environment and physical parameters such as climate, hydraulic conductivity, mineral grain size and exposed surface area, and (2) factors that are related to the mineral, such as kinetics of dissolution and precipitation reactions, solute catalytic and inhibiting effects, and solubility. The range of values affecting the dissolution rate is significantly different in the field, where minerals experience the full range of environmental factors, and in laboratory tests, where a single parameter value may be simulated or the factor may be neglected. Although the full ranges of variables are experienced in the field, an average or representative value must be selected for mass-balance modeling. For most variables that affect the dissolution rate, the rate for an average value may be significantly different than the average of rates for a range of values because the effects are not linear. The nonlinear effect of temperature was discussed in Section 5.6, but the effects of particle size (surface area), solution flow, and product phase precipitation on the mineral dissolution rate are also nonlinear.

Inverse modeling relies on both analysis of the mineral content of the regolith and the ground water compositions and component fluxes. Whereas the extent of alteration of a mineral itself will depend on the integrated time it is contacted by solution, the composition of the solution collected for analysis will depend on the interval of time it is in contact with the mineral, that is, the residence time when passing through a watershed or the laboratory test system. An important component of mass-balance modeling is identifying the mineral phases and their abundance in the volume of interest. The mineral content will have evolved due to weathering reactions over tens of thousands of years, whereas the stream or ground water may have passed through in only months or years. It is very unlikely that the solution will equilibrate with the assemblage of minerals during that time or that the system will reach steady state.

In many comparisons of field and laboratory weathering rates made in the past, laboratory rates were cited with no description of the test method or test conditions used to measure them, as if there was a unique rate characteristic of the material. In contrast, the dissolution rates of most silicate minerals are known to be influenced by the chemistry of the solution contacting it, particularly the dissolved Al and Si concentrations and the pH. The composition of the solution contacting the mineral in a dynamic (flow-through) laboratory test will evolve to a steady-state condition as the mineral dissolves, but the steady-state solution composition that is attained will depend on the test conditions, including the flow rate. This is a critical aspect of dynamic laboratory tests (including column tests) that is often neglected. The initial reaction with crushed material is almost always dominated by high-energy surface features formed during crushing (such as fracture blades, points, excess steps, kinks, and defects). These features dissolve more quickly than the bulk material and must be dissolved before the surface attains "steady-state texture" that dissolves at the rate appropriate for projection to long times. The freshly crushed mineral provides a higher density of reactive sites than does the surface that is maintained as the material continues to dissolve. Laboratory tests are usually considered to attain a steady state conditions when the solution compositions in several sequential analyses are the same within analytical uncertainty. Tests with small particles under aggressive conditions may never reach steady state due to the detectable loss of surface area as the material dissolves. On the other hand, enough material might not dissolve under non-aggressive conditions for the surface to attain a steady-state texture within the duration of a laboratory test. The rate that is measured in this case would be higher than the rate that is appropriate for long-term weathering. In this regard, the greater age of minerals in the field means the surfaces have attained a stable texture and are less reactive than the freshly formed surfaces that are generated by crushing the mineral for use in a laboratory test.

What is often not addressed in flow-through laboratory tests is the fact that that the measured dissolution rate is characteristic of the mineral dissolution rate *at the flow rate used in the test.* This issue was raised in the earlier discussion of laboratory column flow tests in Section 4. The only conditions under which the mineral dissolution rate is independent of the flow rate are (1) when the flow rate is zero and the solution is static and (2) when the flow is fast enough to maintain far-from-equilibrium conditions. Highly dilute far-from-equilibrium conditions are desirable for measuring parameter values for the kinetic factors in the rate law, such as the dependence on pH and temperature, but do not represent field conditions that are at or near equilibrium. Although it has been argued that affinity effects are negligible for values of $\Delta G < -6$ kcal/mol (e.g., Velbel 1989), Figures 4.3, 4.7a and 4.9a show that the slowing effect can occur further from equilibrium, for example, at $\Delta G \approx -10$ kcal/mol, in relatively dilute solutions.

8.2 Comments Addressing Previous Explanations of Discrepancy

All of the effects that have been proposed as contributing to the discrepancy between dissolution rates inferred from field studies and measured in laboratory tests and listed in the introduction are considered to be reasonable, although the relative impacts that they have on the rate vary with the system. A few comments are provided regarding these factors and their typical effects:

Difficulty in quantifying the surface area and wetted surface in natural systems
The accessible mineral surface area in the field system cannot be measured. Estimates are made based on the mineral contents of a limited number of field samples that are analyzed and the assumed size distribution of rocks in the regolith. The chemical and physical heterogeneities of a field system are almost always up-scaled by continuum approximations of the microscopic details (see Section 7.2), and many key parameters (e.g., permeability) are themselves macroscopic representations of microscopic distributions. Chemical heterogeneities are produced by the non-uniform distributions of minerals and affect the overall mobility and mixing of contaminants. Physical heterogeneities are associated with preferential flow paths and contaminant migration pathways for advection and dispersion due to the spatial variability in a geological formation. Model calculations are made using an "equivalent homogeneous medium" to represent an averaged (or smoothed) heterogeneous system, and the degree to which a parameter (or system) is homogenized will affect the predictions that are made. It should be noted that the lack of knowledge regarding the porous nature of a system and the need to use a homogenized representation of the system means that, although reliable average values can be calculated, agreement with a single particular observation—such as the dissolution rate measured in a particular laboratory test—is unlikely.

Limitations on flow and transport into low permeability zones in heterogeneous materials in natural systems
The restricted accessibility of ground water to mineral surfaces exposed in tight cracks, constricted channels, and pores restricts their contributions to the ground water composition to diffusive releases. This contribution may nevertheless be significant in systems with slow ground water flows and serve to recharge water within fractures after infrequent episodes of flushing by storm water. The average values of the groundwater flow and mineral dissolution rates in the mass balance calculations are coupled in the analyses. It was proposed in Section 5.3 that that relationship is evidenced by field results.

Transport control rather than reaction control in natural systems
This addresses the impact of the relative rates of chemical reactions (dissolution and precipitation) and mass transport on the likelihood that the solution will equilibrate with the dissolving solids. In complex field systems, reactions in tight cracks, constricted channels, and pores that may comprise a significant part of the system, releases will likely be controlled by transport limitations of water accessing the region and the egress of dissolved components rather than the degradation reactions.

Inhibition by surface coatings in natural systems
The dissolution rates in the field can decrease due to the reacting minerals becoming encased in alteration products, which generate a diffusion barrier. Laboratory tests to measure dissolution rates do not usually proceed to the point where sufficient alteration phases form to physically affect the dissolution rate. In the field, the alteration phases may affect the rate physically by sorption to block surface reaction sites or chemically by affecting the solution chemistry and reaction affinity.

Greater soil age in natural systems
The effect of aging is interpreted to occur through a smoothing of the surface due to the loss of more reactive surface sites over time. Laboratory experiments clearly show the preferential dissolution of fractured surfaces during the early stages of dissolution. It is reasonable that the mineral surfaces remaining after extensive dissolution will be dominated by the least active surface sites that exist under the prevailing conditions to minimize the surface free energy.

Differences in degree of saturation and reaction affinity attained in laboratory experiments and in natural systems
This is the only effect that can by itself reasonably account for a five orders of magnitude decrease in the dissolution rate as the system approaches equilibrium. Neither field tests nor laboratory tests (not the vast majority) consider how near the system conditions are to equilibrium. It is likely that laboratory experiments are much further from equilibrium than the natural system, but this needs to be better evaluated. Test results discussed in this report point to the fact that the simple linear free energy dependence usually taken to represent the approach to saturation may greatly under-represent the slowing effect of moderate dissolved concentrations. In field measurements, it may not be possible to distinguish the effects of solution saturation from that of secondary phases that cover the mineral and provide transport barriers.

Slow precipitation of secondary minerals
This will affect the dissolution rates in both laboratory experiments and in the field, it is probably more significant in natural systems. This is because secondary phases are usually precipitated *in-situ* during laboratory experiments designed to promote the precipitation of secondary phases, whereas they are already present in the natural system over the duration for which the dissolution rate is being determined. The smaller and more abundant precipitated secondary phases expected to be generated in laboratory tests also have more reactive surfaces compared to the mature phases present in natural systems. The higher specific surface areas and higher solubilities of the smaller precipitates that form initially will enhance their effect on the rates in laboratory tests and they usually precipitate faster than the primary material dissolves. Freshly precipitated phases have more active surfaces that have a greater impact on the dissolution rate than mature phases. The dissolution and precipitation kinetics of the primary and secondary phases are not always coupled. It has been suggested that differences in the chemical potentials of individual components of the primary and secondary determine the effect rather than the solubilities of the phases.

Brief duration of laboratory experiments relative to natural systems
This effect is primarily through the residence time in which the solution volume of interest is in contact with the solids. Part of this effect is the more mature mineral surfaces that are present in natural systems, which have fewer reactive sites, and part is the greater disequilibrium between the solution and solids in the laboratory experiments. That is, the effect of time is due to the effects of other factors.

Temperature differences between laboratory experiments and in natural systems
The large scale of natural systems leads to variations in temperature both spatially and over time. Field studies typically use annual average temperatures, whereas laboratory experiments maintain a constant and uniform temperature. The rate at the average of a range of temperatures will be lower than the average of the rates at those temperatures. However, the sensitivities of the dissolution rates of most minerals to temperature are small for the range of ambient temperatures.

Lower pH values in laboratory experiments than in natural systems
The dissolution rates of many minerals are affected by the solution pH. The effect is usually quantified as an empirical power law expression, with the common logarithm of the rate being proportional to the pH as log $rate = \eta \times pH$, where the value of η is on the order of 0.5 in alkaline solutions and -0.5 in acidic solutions. With these dependencies, the rate changes by a factor of about 3 for every unit change in the pH. As with other variable values, the pH will vary locally in the natural system and change with time. The mass balance calculations assign an average pH to the system, but the dissolution rate does not vary linearly with the pH. The effects of averaging the pH and other environmental variables over the field system are convoluted with the values of the mineral dissolution rates, as are the effects of mass transport.

Grain size effects in laboratory experiments
Neglecting fines with very high surface energies, the effects of grain size itself are primarily how accurately the surface area can be determined and how the surface area changes as the specimen dissolves. It is argued in this report that the initial and final geometric surface areas provide a better measure of the dissolved volume than does the BET surface area. The reacted volume is proportional to the solution concentration, which is used to quantify the dissolution rate in laboratory tests, and the surface area is used to scale the laboratory rate to field systems. The surface areas in the field are used to calculate the field rate in the mass balance calculations.

Disturbed near-surface regions due to comminution (crushing for size reduction) in laboratory experiments
This is a very important effect in laboratory tests. Crushing produces a much greater abundance of reactive sites than occur on weathered mineral surfaces. The dissolution of these high-energy reactive sites occurs faster than the smoothed surfaces that result after they dissolve, and it is the behavior of the smooth surfaces (referred to earlier as having a steady-state texture) that is appropriate for comparisons to field rates and long-term predictions. The effect of disturbed surfaces is usually apparent in laboratory flow-through tests as the concentrations decrease towards constant steady state values. The effect may persist even after the solution attains an apparent steady-state composition but may be too subtle to detect. The initial transient behavior due to preparation artifacts does not affect subsequent measurements. In static tests, the initial dissolution of artifact sites will contribute to the accumulated dissolved mass at all test durations. The relative impact decreases as more material dissolves, but, depending on the test conditions, the solution may become saturated before all the artifact sites have dissolved. This could result in the rate being too high or too low, depending on the surface area that is used in the calculation.

8.3 Conclusions

Added to the above list of discrepancies based on this review is whether direct comparison of rates measured in the laboratory with rates deduced from field measurements is technically justified. This point questions the validity of direct comparison because important field properties present both aleatory (random chance) and epistemic (absence of knowledge) uncertainties. Some field parameters are too difficult to calculate at the scale of interest and representative average (continuum level) values must be used. Parameters that vary throughout the natural system in space and time must often be represented by single values to calculate dissolution rates, such as temperature and pH, even though the response used to represent the rate represents the integrated effects of a range of values. The macroscopic scale over which field system variables are averaged are greater than the scale addressed by the laboratory experiments, i.e., the dissolution of a particular small mineral phase that is distributed throughout the field system. Although the laboratory experiments are on the mesoscale, some important molecular scale values that are important to the process models used to define the dissolution rates in both

laboratory tests and field studies are currently not well defined and may be unknowable, such as the concentration of reactive sites or activated complexes on a mineral surface.

Probably the most important field variable is the groundwater flow rate. This has a several-orders-of-magnitude effect on the dissolution rate in laboratory flow-through tests (both fluidized bed and column test methods) through the solution compositions and probably has a similar impact on field dissolution. However, only the effective flow averaged over long times and very large volumes is known and used in mass balance calculations. Insight from laboratory tests suggests that mineral dissolution rates can vary greatly with the solution composition, which is determined in part by the ground water flow rate. An important aspect of the effect of composition (and flow rate) on the dissolution rate is that the effect is not linear.

An important difference between the dissolution environment in the field and in laboratory tests is the nature of secondary phases and their resulting influence on the dissolution of the primary phase. In the field, the primary minerals are often thickly coated by their weathering products, which are often present in equal or greater abundance than the primary minerals. Both the dissolution of the primary phases and the precipitation of the product phases have likely attained steady state with the ground water, and the incongruent dissolution reactions, such as those given in Table 5.5, proceed at characteristic rates under those conditions. In laboratory tests, secondary phases must nucleate and form in sufficient numbers to provide enough surface area to affect the solution chemistry before the dissolution rate of the primary mineral is influenced. Most laboratory tests are conducted with leachant solutions that do not contain all of the components required to form secondary phases. Even when those components are added to the solutions, nucleation of the secondary phases requires appreciable supersaturation of the solution and available nucleation sites. While this occurs readily in static tests at elevated temperatures, as discussed in Sectios 4.2 and 4.3, it is not observed in the type of flow-through tests used to measure the dissolution rates. The solution concentration generated during mineral dissolution can become much more concentrated in the absence of secondary phase crystallites as the mineral dissolves congruently than when it dissolves incongruently. Species that would otherwise be sequestered in product phases, such as SiO_2, remain in solution and affect the mineral dissolution rate that is measured. In the field, some of the released SiO_2 would be removed from solution due to the formation of various secondary phases and would be excluded from the outflowing Si flux that is used to infer the extent of mineral dissolution by mass balance. Only a small number of reactions (equal to the number of species that is tracked) can be accounted for in mass balance calculations. In the field, most minerals dissolve incongruently as modeled due to the abundance of secondary phases present in near proximity. In most laboratory tests, minerals dissolve congruently due to the absence of secondary phases under the experimental conditions.

Most geochemists normalize the dissolution rates measured in laboratory tests to the BET surface area, although the mass of a mineral that dissolves is proportional to the reacted volume. Of course, normalization to the surface area allows the results to be scaled to other surface areas, including the extensive surface areas relevant to field systems. It is suggested here that laboratory test results would be better normalized to the geometric surface area because it provides a better representation of the reacted volume than does the BET surface area. The mineral surface areas in the field are based on geometric estimates (even though the surface areas of field samples are sometimes measured with BET). The BET surface areas are almost always higher than the geometric surface areas, typically seven-times higher for size fractions commonly used in laboratory tests, so using the BET surface area yields a lower normalized rate. In the case of measuring dissolution rates, much of the surface area is due to specimen preparation artifacts that are either allowed to dissolve away before the rate is measured in dynamic experiments or by

allowing enough material to dissolve that their contribution is negligible in static tests. The geometric approximation provides a better estimate of the remaining surface area.

From this initial evaluation of the discrepancy between dissolution rates measured in the laboratory and those inferred from field measurements and models, several tentative conclusions are drawn. These are referred to as tentative because some are based on expectations and await experimental verification.

- The laboratory and field rates are based on different metrics and represent different scales: The laboratory tests are usually normalized to BET surface areas of uniformly sized particles assembled with a uniform porosity and reacted with a homogenous and dilute solution at a uniform flow rate. The rate is based on reaction of several grams of minerals retained in a small volume of water. The field rates are normalized to estimated geometric surface areas of minerals fixed in randomly sized rocks having a range of fractures and complex pore structures reacted with a non-homogeneous groundwater solution at rates that vary spatially and over time. The rate is based on reacting perhaps hundreds or thousands of kilograms of various minerals that are strewn over many hectares and several meters deep reacting with kiloliters of groundwater with compositions and flow paths that differ locally.

- Laboratory experiments can provide valuable insights into the mineral dissolution mechanism that bear on modeling behavior in field systems: identify solutes that catalyze and inhibit dissolution; quantify affinity effects and the approach to equilibrium; support the development and parameterization of the dissolution and precipitation rate laws; and track changes in the surface texture as minerals dissolve and precipitate.

- Field studies provide valuable measures of the combined effects of many processes and variables on the weathering of materials and distribution of solutes (and contaminants). The contribution of a single process is dependent on the contributions assigned to other processes in the system. The most important other variables are probably the groundwater composition and flow path. The effects of these and most other dependencies on mineral dissolution rates are not linear.

- The laboratory dissolution rate is measured directly for a single well-characterized material. The field rate is inferred based on differences between input and output fluxes of solutes assigned to changes in the amounts of a particular phase. The number of phases is restricted to the number of solutes with measured fluxes in order to solve the mass-balance equations. Forward models, such as reactive-transport models, do not impose a limitation on the number of phases.

- Direct quantitative comparisons of laboratory rates and inferred field rates are not valid *a priori* because the reaction conditions are significantly different and the field response is the net effect of several coupled processes. Other processes that can affect both the dissolution kinetics and contaminant transport in the field are excluded from laboratory tests.

- Important factors that often have not been fully taken into account include: (1) effects of the fluid flow rate, (2) effects of the solution chemical affinity, and (3) effects of other phases, particularly secondary (alteration) phases. These are known to affect the measured laboratory rates and expected to also affect the inferred field rates. The primary effects of the fluid flow and the presence of other phases occur through the

solution chemistry and impact the dissolution rate through the chemical affinity. The fluid flow determines the relative importance of advection and diffusion and thereby the transport of dissolved species away from the dissolving primary mineral. The precipitation of secondary phases provides a sink for some of the components released from the primary mineral that affects the solution chemistry, and the precipitation kinetics may be coupled with the dissolution kinetics.

- The dissolution kinetics of various primary minerals may become coupled with the dissolution and precipitation of other minerals through a common solution chemistry and with the precipitation rates of their product phases, many of which are reaction products of other primary minerals. Field dissolution occurs in the presence of the full assemblage of other primary and secondary phases that may affect the dissolution behavior, whereas most laboratory experiments have measured the dissolution of minerals in isolation (i.e., those laboratory rates that have been compared with field rates). Other laboratory tests (and lysimeter studies) have been conducted with actual samples to provide a representative mixture of minerals and other phases. Distinguishing the dissolution rates of particular minerals in the mixture provides the same challenge as interpreting the field data.

- The coupling of primary mineral dissolution and secondary mineral precipitation is expected to differ significantly in laboratory tests and in the field. This is because product phases in the field have matured over the long weathering time and precipitation rates are expected to be nearly steady-state. In laboratory tests, secondary phases must nucleate from a supersaturated solution and grow. The surface area of secondary phases will change from zero prior to nucleation, then to very high (and highly reactive due to the small size and abundance of reactive sites) soon after nucleation, and then to low as many small particles are replaced by far fewer large particles with lower specific surface areas and less-reactive surfaces. The influence of precipitating secondary phases on the dissolution kinetics of the dissolving primary phase may change as the secondary phases mature and as transport limitations change. The coupling of dissolution and precipitation rates is not well understood and is an area of active research.

- The variations in field conditions that affect dissolution rates may not be properly represented by using average values because the effects of many variables on the rate are not linear. This includes temperature, particle size, and fluid flow. In most cases, the arithmetic average values are expected to under-estimate the accumulated effects of the range of variable values. For example, the extent of reaction after three months at 35°C plus three months at 15°C will be greater than the extent of reaction after six months at 25°C.

- The further development of models to describe the reactive-transport of contaminants through disturbed regoliths (e.g., waste disposal systems) and adjacent natural regoliths requires interfacing the continuum models for transport with the discrete models for release from contaminated materials and waste forms. This is very similar to comparing the inferred field rate (continuum) to the laboratory rate (discrete).

8.4 Final Comments on Relevance to Surface Disposal Systems

The objective of this review and analysis was to assess the discrepancy between the mineral dissolution rates measured in laboratory tests and those inferred from inverse modeling of field data. The reason this effort was undertaken is to provide insights for relating laboratory test

methods to the assessments of surface disposal systems containing radioactively contaminated slags and concretes. Evaluation of the literature followed two major paths: evaluating specific aspects of the laboratory methods that affect measured values and modeling at the molecular scale to determine the dissolution rate, and evaluating aspects of the approaches used to model the large (macroscale and geoscale) field systems that impact the dissolution rate that is inferred. Reviews of laboratory test methods addressed details such as the effects using crushed materials have on determining the surface area, taking the effects of flow rate in dynamic tests into account when modeling and determining the dissolution rate, and the effects of secondary phase precipitation on the continued dissolution of a primary phase. Some of these effects can introduce artifacts to the laboratory measurements and others affect how accurately the test method models the natural system. Reviews of the mass balance calculation methods identify the difficulties of modeling the complex coupling of the dissolution reactions with groundwater transport and interactions with the host geology and the indirect relationship between the measured changes in the composition of the groundwater at various samplings and the inferred dissolution rate of a particular mineral. The dissolution rate of a mineral of interest is coupled in the mass balance with several other processes: the dissolution and precipitation rates of other minerals that are contacted by the same volume of groundwater; groundwater advection; the effects of sorption, diffusion, and other dispersive forces on the dissolved constituents; uptake by biota; and the decay of constituent radioelements. The measured flux of a constituent must then be assigned to the dissolution of particular amounts of potential primary phases having particular surface areas to obtain a dissolution rate.

A major reason for the several orders of magnitude discrepancies noted between mineral dissolution rate measured in the laboratory and inferred from field studies is the difference in the degree of disequilibrium imposed on the mineral. Most field systems calculations are dominated by slowly percolating groundwater with a nearly steady-state composition that is close to equilibrium with a suite of mineral phases. Most laboratory tests are conducted either under far-from-equilibrium conditions or with flow rates that are much higher than in the system they are intended to represent, and the effect of the flow rate on the dissolution rate is not always taken into account.

It is not practical (and may not be possible) to replicate mineral dissolution under natural percolation conditions in a laboratory experiment due to limitations of monitoring the flow rate or the dissolution reaction itself. Instead, we must rely on modeling to link the chemical reaction kinetics that are measured with laboratory tests and expressed in a molecular scale model with the characteristics of groundwater flow that are measured at the continuum-level and confirmed at the field scale for use in the mass balance calculations. The material-specific weathering reactions utilized in the mass balance calculations can be quantified at the molecular scale with laboratory experiments and modeled for use in forward modeling (e.g., affinity-controlled dissolution of minerals and diffusion-controlled release of contaminants from concretes) while the more general hydraulics of the macroscopic waste pile is treated using input from field-scale measurements, including lysimeters. As emphasized by the comparison of laboratory and field rates, it will be important to model the weathering reactions under the same conditions present in the field system. For the catchments discussed in this report, the groundwater was presumed to be nearly equilibrated with the host geology. Systems affected by a significant amount of faster moving water (e.g., run-off) will likely be further from equilibrium. Mineral reaction models can be formulated to reliably represent changes in the dissolution rate as equilibrium is approached, but the effects of secondary phase precipitation on the dissolution kinetics are not yet well quantified. Another factor that must be considered is the transient nature of interactions with phases that may be completely dissolved during the time periods of interest.

The approaches taken to study and model the weathering of subaerial and aquifer minerals in various catchments and regoliths are adaptable to and appropriate for the modeling of near-surface and buried waste sites. Contaminated solids can be characterized using the same techniques and methods used to characterize minerals encapsulated in rock (e.g., Veblen et al. 2004), and the distributions in the waste system can likewise be modeled using the methods developed for field studies. The physical characteristics of a waste system, such as the distributions of particle size (from boulders to fines), effective porosities (the network of voids between particles), ranges of temperature, hydrology and flow in vadose (unsaturated) and saturated zones, etc., can be measured, modeled, and parameterized in the same way as a natural regolith. It is presumed that a surface disposal site can be modeled in the same way (and as precisely) as a natural regolith for performance assessments, although acquisition of the detailed information regarding both chemical reactions and transport that is required for forward modeling will probably be cost-prohibitive for most waste systems. It is expected that modeling groundwater flow and water contact conditions in piles of rubble will provide the greatest challenge, will have the highest uncertainty, and will be a dominant factor affecting contaminant release. A potential approach is to treat the pile as a set of co-located sub-systems having continuum property values that are representative of boulders, coarse gravel, sand, sandstone, and crystalline rock. A fraction of the total inventory can be assigned to each subsystem and subjected to the relevant groundwater flow conditions. Each subsystem could be treated individually or part of a coupled system. The latter approach would be computationally more challenging and may not be justified due to the uncertainties associated with modeling each subsystem.

The application of mass transfer models to waste systems is currently being evaluated for actual waste materials, including continuum contamination distribution models and computer simulations. An important distinction of the surface waste sites is that they are large but of finite dimensions. Coupled reactive-transport models for waste disposal sites usually address essentially point sources or a grouping of point sources (e.g., Bacon et al. 2004; Bacon and McGrail 2005) whereas continuum models generally describe variations without abrupt changes or discontinuities for modeling geologic scale systems. Modeling surface disposal sites presents an intermediate system that blends aspects of atomic, mesoscale, and macroscale phenomena and must utilize tools developed for both forward and inverse modeling approaches. Insights gained from this evaluation of the discrepancies between mineral dissolution rates measured in laboratory experiments and those inferred from field data are being utilized in an on-going study of modeling and testing approaches for assessing the behavior of surface disposal systems.

9 References

Aagaard, P., and Helgeson, H.C. (1982). "Thermodynamic and kinetic constraints on reaction rates among minerals and aqueous solutions I. Theoretical considerations," *American Journal of Science 282,* 237-285.

Acker, J.G. and Bricker, O.P. (1992). "The influence of pH on biotite dissolution and alteration kinetics at low temperature," *Geochimica et Cosmochimica Acta, 56,* 3073-3092.

Adams, P.B. (1984). "Glass corrosion. A record of the past? A predictor of the future?" *Journal of Non-Crystalline Solids, 67,* 193-206.

Alekseyev, V.A., Medvedeva, Prisyagina, N.I., Meshalkin, S.S., and Balabin, A.I. (1997). "Change in the dissolution rates of alkali feldspars as a result of secondary mineral precipitation and approach to equilibrium," *Geochimica et Cosmochimica Acta, 61,* 1125-1142.

Amrhein, C. and Suarez, D.L. (1992). "Some factors affecting the dissolution kinetics of anorthite at 25C," *Geochimica et Cosmochimica Acta, 56,* 1815-1826.

Anbeek, C. (1992a). "Surface roughness of minerals and implications for dissolution studies," *Geochimica et Cosmochimica Acta, 56,* 1461-1469.

Anbeek, C. (1992b). "The dependence of dissolution rates on grain size for some fresh and weathered feldspars," *Geochimica et Cosmochimica Acta, 56,* 3957-3970.

Anbeek, C. (1993). "The effect of natural weathering on dissolution rates," *Geochimica et Cosmochimica Acta, 57,* 4963-4975.

ASTM (2009). "Standard Practice for the long-term behavior of waste package materials including waste forms used in the geologic disposal of high-level nuclear waste," C 1174 in Annual Book of ASTM Standards, Vol. 12.01, West Conshohocken, Pennsylvania: ASTM-International.

Bacon, D.H., White, M.D., and McGrail, B.P. (2004). *Subsurface Transport Over Reactive Multiphases (STORM): A Parallel, Coupled, Nonisothermal Multiphase Flow, Reactive Transport, and Porous Medium Alteration Simulator, Version 3.0. User's Guide.* Pacific Northwest National Laboratory report PNNL-14783.

Bacon, D.H. and McGrail, B.P. (2005). *Waste Form Release Calculations for the 2005 Integrated Disposal Facility Performance.* Pacific Northwest National Laboratory report PNNL-15198.

Baes, C.F. and Sharp, R.D. (1983), "A Proposal for Estimation of Soil Leaching and Leaching Constants for Use in Assessment Codes." *Journal of Environmental Quality,* 12(1), 17-28.

Bajpai, R.K. and Narayan, P.K. (2008). "Sandstone uranium deposits of Meghalaya: natural analogues for radionuclide migration and backfill material in geological repository for high level radioactive waste disposal," *Journal of Applied Geochemistry, 10,* 475-480.

Baxter, E.F. and DePaolo, D.J. (2000). "Field measurement of slow metamorphic reaction rates at temperatures of 500 and 600°C," *Science, 288,* 1411-1414.

Blum, A.E., and Stillings, L.L. (1995). "Feldspar Dissolution Kinetics," in *Chemical Weathering Rates of Silicate Minerals; Reviews in Mineralogy Volume 31,* A.F. White and S.L. Brantley, (eds.): Mineralogical Society of America. 291-351.

Bowser, C.J. and Jones, B.F. (2002). "Mineralogic controls on the composition of natural wasters dominated by silicate hydrolysis," *American Journal of Science 302,* 582-662.

Brady, P.V. and Gíslason, S.R. (1997). "Seafloor weathering controls on atmospheric CO_2 and global climate," *Geochimica et Cosmochimica Acta, 61,* 965-973.

Brantley, S.L. and Stillings, L. (1996). "Feldspar dissolution at 25C and low pH," *American Journal of Science 296,* 101-127.

Brantley, S.L., White, A.F., and Hodson, M.E. (1999). "Surface area of primary silicate minerals," in *Growth, Dissolution, and Pattern Formation in Geosystems, Chapter 14*, pp. 291-326. Kluwer Academic Press.

Brantley, S.L. and Mellott, N.P. (2000). "Surface area and porosity of primary silicate minerals," *American Mineralogist*, 85, 1767-1783.

Bricker, O.P., Jones, B.F., and Bowser, C.J. (2003). "Mass-balance approach to interpreting weathering reactions in watershed systems," in *Surface and Ground Water, Weathering, and Soils, Treatise on Geochemistry, Volume 5*, Drever, J.I. (ed.) Elsevier.

Brunauer, S., Emmett, P.H., and Teller, E. (1938). "Adsorption of gases in multimolecular layers." *Journal of the American Chemical Society 60,* 309-319.

Bullen, T.D., Krabbenhoft, D.P., and Kendall, C. (1997). "Kinetic and mineralogic controls on the evolution of groundwater chemistry and 87Sr/86Sr in a sandy silicate aquifer, northern Wisconsin, USA," *Geochimica et Cosmochimica Acta, 60,* 1807-1821.

Burch, T.E., Nagy, K.L, and Lasaga, A.C. (1993). "Free energy dependence of albite dissolution kinetics at 80°C and pH 8.8," *Chemical Geology, 105*, 137-162.

Busenberg, E. and Clemency, C.V. (1976). "The dissolution kinetics of feldspars at 25°C and 1 atm CO_2 partial pressure," *Geochimica et Cosmochimica Acta, 40,* 41-49.

Buss, H.L., Sak, P.B., Webb, S.M., and Brantley, S.L. (2008). "Weathering of the Rio Blanco quartz diorite, Luquillo Mountains, Puerto Rico: Coupling oxidation, dissolution, and fracturing," *Geochimica et Cosmochimica Acta, 72,* 4488-4507.

Byers, C.D., Ewing, R.C., and Jercinovic, M.J. (1986). "Experimental alteration of basalt glass applied to the alteration of nuclear waste glass. In *Advances in Ceramics, Nuclear Waste Management*, D. E. Clark, W. B. White and A. J. Machiels, eds., 733-744. American Ceramic Society, Columbus, Ohio.

Byers, C.D. Jercinovic, M.J., and Ewing, R.C. (1986). *A Study of natural glass analogues as applied to alteration of nuclear waste glass*, Argonne National Laboratory report ANL-86-46.

Cama, J., Ganor, J., Ayora, C., and Lasaga, A.C. (2000). "Smectite dissolution kinetics at 80°C and pH 8.8," *Geochimica et Cosmochimica Acta, 64,* 2701-2717.

Carroll, S., Mroczek, E., Alai, M., and Ebert, M. (1998). "Amorphous silica precipitation (60 to 120°C): Comparison of laboratory and field rates," *Geochimica et Cosmochimica Acta, 62,* 1379-1396

Carroll, S.A. and Knauss, K.G. (2005). "Dependence of labradorite dissolution kinetics on CO_2(aq), Al(aq), and temperature," *Chemical Geology, 217*, 213-225.

Casey, W.H., Banfield, J.F., Westrich, H.R., and McLaughlin, L. (1993). "What do dissolution experiments tell us about natural weathering?" *Chemical Geology, 105*, 1-15.

Chapman, N.A. and McKinley, I.G. (1984). *The potential of natural analogues in assessing systems for deep disposal of high-level radioactive waste*, SKB Technical report TR 84-16.

Chen, Y. and Bradley, S.L. (1997). "Temperature and pH-dependence of albite dissolution rate at acid pH," *Chemical Geology 135*, 275-290.

Chou, L. and Wollast, R. (1984). "Study of the weathering of albite at room temperature and pressure with a fluidized bed reactor," *Geochimica et Cosmochimica Acta, 48*, 2205-2217.

Clow, D.W. (1992). *Weathering rates from field and laboratory experiments on naturally weathered soils*. Ph.D. Dissertation, University of Wyoming, Laramie, WY (unpublished).

Clow, D.W. and Drever, J.I. (1996). "Weathering as a function of flow through an alpine soil," *Chemical Geology 132,* 131-141.

Côme, B. and Chapman, N.A. (1986). *CEC Nuclear Science and Technology Report*, EUR 10671. Commission of the European Communities, Luxembourg.

Dai, Z., Samper, J., and Ritzi, R. Jr. (2010). "Identifying geochemical processes by inverse modeling of multicomponent reactive transport in the Aquia aquifer," *Geosphere, 2*, 210-219.

DOE (1994). *High-Level waste borosilicate glass: A compendium of corrosion characteristics, Vol. 2,* J.C. Cunnane, ed., DOE-EM-0177.

Drever, J.I. and Clow, D.W. (1995). "Weathering rates in catchments," in *Chemical Weathering Rates in Silicate Minerals, Vol 31*, pp. 463-483. Mineralogical Society of America.

Drever, J.I., Murphy, K.M., and Clow, D.W. (1994). "Field weathering rates versus laboratory dissolution rates: an update," *Mineralogical Magazine, 58A*, 239-240.

Dussossoy, J.L., Dubois, C., Vernaz, E., and Chambaudet, A. (1992). "Effect of Surface Finish on Nuclear Glass Dissolution Rate," in *Scientific Basis for Nuclear Waste Management XV,* C.G. Sombret, ed., pp. 109-115.

Ebert, W.L., Hoburg, R.F., and Bates, J.K. (1991). "The Sorption of Water on Obsidian and a Nuclear Waste Glass." *Physics and Chemistry of Glasses, 32*, 133-137.

Ebert, W.L., Bates, J.K., and Bourcier, W.L. (1991). "The Hydration of Borosilicate Waste Glass in Liquid Water and Steam at 200°C," *Waste Management,11,* 205-221.

Ebert, W.L. (2010). *Radionuclide Release from Slag and Concrete Waste Materials. Part I: Conceptual models of leaching from complex materials and laboratory test methods*, NRC report NUREG/CR-7025.

Eggleston, C.M., Hochella, M.F. Jr., and Parks, G.A. (1989). "Sample preparation and aging effects on the dissolution rate and surface composition of diopsite," *Geochimica et Cosmochimica Acta, 53,* 797-804.

Ewing, R.C. (1979). "Natural glasses: Analogues for radioactive waste forms," in *Scientific Basis for Nuclear Waste Management,* G.J. McCarthy ed., pp. 35-68.

Ewing, R.C. and Jercinovic, M.J. (1987). "Natural analogues: Their application to the prediction of the long-term behavior of nuclear waste forms," in *Scientific Basis for Nuclear Waste Management X,* J.K. Bates and W.B. Seefeld, eds., pp. 67-83.

Ewing, R.C. (1992). "The role of natural analogues in performance assessment: Applications and limitation," in *Proceedings of the Third Annual International Meeting on High-Level Radioactive Waste Management,* J.S. Tulenko, ed. Pp. 1429-1436. Las Vegas, Nevada. American Nuclear Society.

Friedman, I. and Smith, R.L. (1960). "A new dating method using obsidian, Part 1: The development of the method," *American Antiquities, 25*, 476-522.

Fu, Q., Lu, P, Konishi, H., Dilmore, R., Xu, H., Seyfried, W.E. Jr., and Zhu, C. (2009). "Coupled alkali-feldspar dissolution and secondary mineral precipitation in batch systems: 1. New experiments at 200°C and 300 bars," *Chemical Geology 258*, 125-135.

Ganor, J., Lu, P., Zheng, Z., and Zhu, C. (2007). "Bridging the gap between laboratory measurements and field estimations of silicate weathering using simple calculation," *Environmental Geology, 53,* 599-610.

Gauthier, J.-M., Oelkers, E.H., and Shott, J. (1994). "Experimental study of K-feldspar dissolution rate as a function of chemical affinity at 150°C and pH 9," *Geochimica et Cosmochimica Acta, 58,* 4549-4560.

Glass, B.P. (1984). "Tektites," *Journal of Non-Crystalline Solids, 67*, 333-344.

Grambow, B. and Jercinovic, M.J. (1985). "Weathered basalt glass: A natural analogue for the effects of reaction progress on nuclear waste glass alteration," in *Scientific Basis for Nuclear Waste Management IX,* L.O. Werme, ed., pp. 263-272.

Helgesen, H.C., Murphy, W.M., and Aagaard, P. (1984). "Thermodynamic and kinetic constraints on reaction rates among minerals and aqueous solutions II. Rate constants, effective surface area and the hydrolysis of feldspar." *Geochimica et Cosmochimica Acta, 48,* 2405-2432.

Hellmann, R. and Tisserand, D. (2006). "Dissolution kinetics as a function of the Gibbs free energy of reaction: An experimental study based on albite feldspar," *Geochimica et Cosmochimica Acta, 70,* 364-383.

Hereford, A.G, Keating, E.H., Guthrie, G.D., and Zhu, C. (2007). "Reactions and reaction rates in the regional aquifer beneath the Pajarito Plateau, northern New Mexico, USA," *Environmental Geology, 52,* 965-977.

Hodson, M.E., Lee, M.R., and Parsons, I. (1997). "Origins of surface roughness of unweathered alkali feldspar grains," *Geochimica et Cosmochimica Acta, 62,* 3429-3435.

Hodson, M.E. (1999). "Micropore surface area variation with grain size in unweathered alkali feldspars: Implications for surface roughness and dissolution studies," *Geochimica et Cosmochimica Acta, 62,* 3429-3435.

Holdren, G.R. Jr. and Berner, R.A. (1979). "Mechanism of feldspar weathering-I. Experimental studies," *Geochimica et Cosmochimica Acta, 43,* 1161-1171.

Holdren, G.R., and Speyer, P.M. (1985). "Reaction rate-surface area relationships during the early stages of weathering—I. Initial Observations." *Geochimica et Cosmochimica Acta, 49,* 675-681.

Holdren, G.R., and Speyer, P.M. (1987). "Reaction rate-surface area relationships during the early stages of weathering. II. Data on eight additional feldspars." *Geochimica et Cosmochimica Acta, 51,* 2311-2318.

IAEA (1989). *Natural analogues in performance assessments for the disposal of radioactive wastes,* IAEA Technical report 304.

Jantzen, C.M., Kaplan, D.I., Bibler, N.E., Peeler, D.K., and Plodinec, M.J. (2008). "Performance of a Buried Radioactive High Level Waste (HLW) Glass after 24 Years." *Journal of Nuclear Materials 378,* 244-256.

Jarvis, N.V., Andreoli, M.A.G., and Read, D. (1997). "The Steenkampskrall Natural Analogue Study and Nuclear Waste Disposal in South Africa," Seventh EC Natural Analogue Working Group Meeting, EUR 17851 EN, pp. 9-26.

Jercinovic, M.J. and Ewing, R.C. (1987). Basaltic glasses from Iceland and the deep sea: Natural analogues to borosilicate nuclear waste-form glass, Japanese-Swiss-Swedish project technical report JSS-88-01.

Jercinovic, M.J. and Ewing, R.C. (1992). "Corrosion of geological and archaeological glasses, in *Corrosion of Glass, Ceramics, and Ceramic Superconductors,* D.E. Clark and B.K. Zoitos, eds. pp. 330-371. Noyes Publications.

Johnson, N.M., Kikens, G.E., Borman, F.H., and Fisher, D.W., and Pierce, R.S. (1969). "A working model for the variation in stream chemistry at the Hubbard Brook Experimental Forest, New Hampshire," *Water Resources Research,* 5, 1353-1363.

Knauss, K.G., and Wolery, T.J. (1986). "Dependence of albite dissolution kinetics on pH and time at 25°C and 70°C." *Geochimica et Cosmochimica Acta, 50,* 2481-2497.

Köhler, S.J., Bosbach, D., and Oelkers, E.H. (2006). "Do clay mineral dissolution rates reach steady state?" *Geochimica et Cosmochimica Acta, 69,* 1997-2006.

Kump, L.R., Brantley, S.L., and Arthur, M.A. (2000). "Chemical weathering, atmospheric CO_2, and climate," *Annual Review of Earth Planet Science, 28,* 611-667.

Lasaga, A.C. (1981). "Rate Laws of Chemical Reactions," in *Reviews in Mineralogy, Vol. 8: Kinetics of Geochemical Processes,* ed. A.C. Lasaga and R.J. Kirkpatrick, pp. 1-68. Mineralogical Society of America.

Lasaga, A.C. (1984) "Chemical kinetics of water-rock interactions." *Journal of Geophysical Research 89,* 4009-4025.

Lasaga, A.C. (1995). "Approaches to describing dissolution/precipitation rates," in *Reviews in Mineralogy, Volume 31 Chemical Weathering Rates in Silicate Minerals,* ed. A.F. White and S.L. Brantley, pp. 23-86, Mineralogical Society of America.

Lasaga, A.C., Soler, J.M., Ganor, J., Burch, T.E., and Nagy, K.L. (1994). "Chemical weathering rate laws and global geochemical cycles," *Geochimica et Cosmochimica Acta, 58,* 2361-2386.

Last, G.V., Serne, R.J, and LeGore, V.L. (1995). *Field Lysimeter Studies for Performance Evaluation of Grouted Hanford Defense Wastes*. Pacific Northwest National Laboratory report PNL-10166.

Lichtner, P.C. (1993). "Scaling properties of time-space kinetic mass transport equations and the local equilibrium limit," *American Journal of Science, 293*, 257-296.

Lichtner, P.C. and Tartakovsky, D.M. (2003). "Stochastic analysis of effective rate constants for heterogeneous reactions," *Stochastic Environmental Research and Risk Assessment, 17,* 419-429.

Luo, J-S., Abrajano, T.A.. and Ebert, W.L. (1998). *Natural analogues of nuclear waste glass corrosion,* Argonne National Laboratory report ANL-98/22.

Maher, K., DePaolo, D.J, and Lin, J.C.F. (2004). "Rates of silicate dissolution in deep-sea sediment: in situ measurement using U-234/U-238 of pore fluids," *Geochimica et Cosmochimica Acta, 68,* 4629-4648.

Maher, K., Steefel, C.I., DePaolo, D.J., and Viani, B.E. (2006). "The mineral dissolution rate conundrum: Insights from reactive transport modeling of U isotopes and pore fluid chemistry in marine sediments," *Geochimica et Cosmochimica Acta, 70,* 337-363.

Malmström, M.E., Destouni, G., Banwart, S.A., and Strömberg, B.H.E. (2000). "Resolving the scale-dependence of mineral weathering rates," *Environmental Science & Technology, 34,* 1375-1378.

Mast, M.A., and Drever, J.I. (1987). "The effect of oxalate on the dissolution rates of oligoclase and tremolite." *Geochimica et Cosmochimica Acta, 51,* 2559-2568.

Mast, M.A., Drever, J.I., and Baron, J. (1990). "Chemical weathering in the Loch Vale watershed, Rocky Mountain National Park, Colorado," *Water Resources Research, 26,* 2971-2978.

Mazer, J.J., Bates, J.B. (1992). "Obsidians and tektites: Natural analogues for water diffusion in nuclear waste glasses," in *Scientific Basis for Nuclear Waste Management XV,* C.G. Sombret, ed., pp. 513-520.

McConnell, J.W. Jr., Rogers, R.D., Jastrow, J.D., Cline, S.R., Findlay, M.W., Davis, E.C., Wickliff Hicks, D.S., Sanford, W.E., Sullivan, T.M., Neilson, R.M. Jr., Brey, R.R., Fuhrmann, M., Larson, I.L., Rogers, J.W., and Hilton, L.D. (1998). *Low-Level Waste Data Base Development Program,* NUREG/CR-6569, U.S. Nuclear Regulatory Commission.

McKenzie, W.F. (1990). *Natural glass analogues to alteration of nuclear waste glass: A review and recommendations for further study*, Lawrence Livermore National Laboratory report UCID-21871.

Mogollon, J.L., Ganor, J., Soler, J.M., and Lasaga, A.C. (1996). "Column experiments and the full dissolution rate law of gibbsite." *American Journal of Science, 296,* 729-765.

Murphy, W.M. and Pearcy, E.C. (1992). "Source-term constraints for the proposed repository at Yucca Mountain, Nevada, derived for the natural analog at Peña Blanca, Mexico," in *Scientific Basis for Nuclear Waste Management XV,* C.G. Sombret, ed., pp. 521-527.

Nagy, K.L. and Lasaga, A.C. (1992). "Dissolution and precipitation kinetics of gibbsite at 80°C and pH 3: The dependence on the solution saturation state," *Geochimica et Cosmochimica Acta, 56,* 3093-3111.

Narasimhan, T.N., and Apps, J.A. (1990). Reactive Chemical Transport in Ground-Water Hydrology: Challenges to Mathematical Modeling, Lawrence Berkeley Laboratory report LBL-29492.

Newton, R.G. (1985). "Ballidon glass burial experiments," *Glass Technology, 26,* 21-38.

Nugent, M.A., Brantley, S.L., Pantano, C.G., and Maurice, P.A. (1998). "The influence of natural mineral coatings on feldspar weathering," *Nature, 395,* 588-591.

Oblath, S.G. and Grant, M.W. (1985). *Special Wasteform Lysimeters Initial Three-year Monitoring Report.* Savannah River Laboratory report SRL-DP-1712.

Oelkers, E.H., Schott, J., and Devidal, J.-L. (1994). "The effect of aluminum, pH, and chemical affinity on the rates of aluminosilicate dissolution reactions," *Geochimica et Cosmochimica Acta, 58,* 2011-2024.

Oxburgh, R., Drver, J.I., and Sun, Y.-T. (1994). "Mechanism of plagioclase dissolution in acid solution at 25C," *Geochimica et Cosmochimica Acta, 58,* 661-669.

Pačes, T. (1973). "Steady-state kinetics and equilibrium between ground water and granitic rocks." *Geochimica et Cosmochimica Acta, 47,* 1855-1863.

Pačes, T. (1983). "Rate constants of dissolution derived from the measurements of mass balance in hydrological catchments." *Geochimica et Cosmochimica Acta, 47,* 1855-1863.

Pačes, T. (1994). "Modeling the hydrologic and biogeochemical response of a catchment area to anthropogenic inputs," *Chemistry of Aquatic Systems: Local and Global Perspectives*, G. Bidoglio and W. Stumm, eds.

Parkhurst, D.L. and Appelo, C.A.J. (1999). *User's Guide to PHREEQC (version 2)–a computer program for speciation, reaction-path, advective transport and inverse geochemical calculations.* U.S. Geological Survey Water Resources Investigation Report 99-4259. Denver Colorado. http://wwwbrr.cr.usgs.gov/projects/GWC_coupled/phreeqc/html/final.htm

Pearcy, E.C., Prikryl, J.D., and Leslie, B.W. (1995). "Uranium transport through fractured silicic tuff and relative retention in areas with distinct fracture characteristics," *Applied Geochemistry, 10,* 685-704.

Petit, J.C., (1992a). "Reasoning by analogy: Rational foundation of natural analogue studies," *Applied Geochemistry, Supplemental Issue No. 1,* 9-11.

Petit, J.C. (1992b). "Natural analogues for the design and performance assessment of radioactive waste forms: A review," *Journal of Geochemical Exploration, 46,* 1-34.

Petrovich, R. (1981a). "Kinetics of dissolution of mechanically comminuted rock-forming oxides and silicates-I. Deformation and dissolution of quartz under laboratory conditions," *Geochimica et Cosmochimica Acta, 45,* 1665-1674.

Petrovich, R. (1981b). "Kinetics of dissolution of mechanically comminuted rock-forming oxides and silicates-II. Deformation and dissolution of oxides and silicates in the laboratory and at the Earth's surface," *Geochimica et Cosmochimica Acta, 45,* 1675-1686.

Plummer, L.N. and Black, W. (1980). "The mass balance approach: application to interpreting the chemical evolution of hydrologic systems." *American Journal of Science 280,* 130-142.

Rogers, R.D., McConnell, J.W., Jastrow, J.D., and Wickliff, D.S. (1992). "Contributions of Lysimeter Data to the Development of Site Specific Performance Assessment Plans." in *Stabilization and Solidification of Hazardous, Radioactive, and Mixed Wastes, Vol. 2, ASTM STP 1123, Gilliam, T.M, and Wiles, C.C. Eds.* Pp. 448-465. Philadelphia, Pennslyvania: American Society for Testing and Materials.

Rowe, G.L. and Brantley, S.L. (1993). "Estimation of the dissolution rates of andesitic glass, plagioclase and pyroxene in a flank aquifer of Poás Volcano, Costa Rica," *Chemical Geology, 105,* 71-87.

Sigurdsson, H. and D'Hondt, S., Arthur, M.A., Bralower, T.J., Zachos, J.C., Van Fossen, M., and Channel, J.E.T. (1991). "Glass from the Cretaceous/Tertiary boundary in Haiti," *Nature,* 349, 482-487.

Simmons, A.M. (2002). *Natural Analogue Synthesis Report*, Bechtel SAIC Co. LLC report TDR-NBS-GS-000027 REV00 ICN 02.

Steefel, C.I., and Van Cappellen, P. (1990). "A new kinetic approach to modeling water-rock interaction: The role of nucleation, precursors, and Ostwald ripening," *Geochimica et Cosmochimica Acta, 54,* 2657-2677.

Steefel, C.I., and MacQuarrie, K.T.B. (1996). "Approaches to Modeling of Reactive Transport in Porous Media", in Reactive Transport in Porous Media, Reviews in Mineralogy Vol. 34,

Lichtner, P.C., Steefel, C.I., and Oelkers, E.H., eds., Mineralogical Society of America, pp. 83-129.

Steefel, C.I., and Lichtner, P.C. (1998). "Multicomponent reactive transport in discrete fractures: I. Controls on reaction front geometry," Journal of Hydrology 209, 186-199.

Stillings, L.L. and Brantley, S.L. (1995). "Feldspar dissolution at 25°C and pH 3: Reaction stoichiometry and the effect of cations," *Geochimica et Cosmochimica Acta, 59,* 1483-1496.

Stockman, H., Krumhansl, J., Ho, C.K., and McConnell, V. (1994). *The Valles Natural Analogue Project*, NUREG/CR-6221, SAND94-0650.

Strachan, D.M. (2003). *Ancient glass studies: Potential low-activity waste disposal at Hanford*, Pacific Northwest National Laboratory report PNNL-14213.

Swaboda-Colberg, N.G. and Drever, J.I. (1993). "Mineral dissolution rates in plot-scale field and laboratory experiments," *Chemical Geology, 105,* 51-69.

Swank, W.T., and Douglass (1977). Nutrient budgets for undisturbed and manipulated hardwood forest ecosystems in the mountains of North Carolina, in *Watershed Research in Eastern North America*, Correll, D.L. (ed.), Smithsonian Inst. P 343-364.

Taylor, Aa. and Blum, J.D. (1995). "Relation between soil age and silicate weathering rates determined from the chemical evolution of a glacial chronosequence," *Geology, 23,* 979-982.

Taylor, Aa.S., Blum, J.D., Lasage, A.C., and MacInnis, I.N. (2000a). "Kinetics of dissolution and Sr release during biotite and phlogopite weathering." *Geochimica et Cosmochimica Acta, 64,* 1191-1208.

Taylor, Aa.S., Blum, J.D., and Lasage, A.C. (2000b). "The dependence of labradorite dissolution and Sr isotope release rates on solution saturation state." *Geochimica et Cosmochimica Acta, 64,* 2389-2400.

Tompson, A.F.B., and Jackson, K.J. (1996). "Reactive Transport in Heterogeneous Systems", in Reactive Transport in Porous Media, Reviews in Mineralogy Vol. 34, Lichtner, P.C., Steefel, C.I., and Oelkers, E.H., eds., Mineralogical Society of America, pp. 269-310.

Van der Weijden, C.H. and Pacheco, F.A.L. (2004). "ΔG_r dependence of weathering rates under natural conditions," *Geochimica et Cosmochimica Acta, 68,* A444.

Vandiver, P.B. (1992). "Corrosion and conservation of ancient glass and ceramics," in *Corrosion of Glass, Ceramics, and Ceramic Superconductors*, D.E. Clark and B.K. Zoitos, eds. pp. 393-430. Noyes Publications.

Van Iseghem, P., Timmermans, W., and Neerdael. (1990). "In-situ testing of nuclear waste glasses in a clay laboratory-results after two years corrosion," in *Scientific Basis for Nuclear Waste Management XIII,* V.M. Oversby and P.W. Brown, eds., pp. 283-289..

Veblen, L.A., Farthingt, D., O'Donnell, E., and Randall, J.D. (2004). *Characterization of Radioactive Slags.* NUREG-1703, Washington, D.C.: U.S. Nuclear Regulatory Commission.

Velbel, M.A. (1985). "Geochemical mass balances and weathering rates in forested watersheds of the southern Blue Ridge." *American Journal of Science 285*, 904-930.

Velbel, M.A. (1986). The mathematical basis for determining rates of geochemical and geomorphic processes in small forested watersheds by mass balance: examples and implications, in *Rates of Chemical Weathering of Rocks and Minerals*, Coleman, S. and Dethier, D. (eds.). Academic Press, New York, New York.

Velbel, M.A., (1989). "Effect of chemical affinity on feldspar hydrolysis rates in two natural weathering systems," *Chemical Geology, 78,* 245-253.

Velbel, M.A. (1990). "Influence of temperature and mineral surface characteristics on feldspar weathering rates in natural and artificial systems: a first approximation." *Water Resources Research, 26,* 3049-3053.

Velbel, M.A. (1993). "Constancy of silicate-mineral weathering ratios between natural and experimental weathering: Implication for hydrologic control of differences in absolute rates," *Chemical Geology, 105*, 89-99.

Velbel, M.A. (1993). "Weathering and pedogenesis at the watershed scale: Some recent lessons from studies of acid-deposition effects," *Chemical Geology, 107*, 337-339.

Walter, M.B, Serne, R.J., Jones, T.L., McLaurine, S.B. (1986). *Chemical Characterization, Leach, and Desorption Studies of Solidified Low-Level Waste*. Pacific Northwest Laboratory report PNL-6047. Richland, Washington: Pacific Northwest Laboratory.

Walton, F.B. and Johnson, L.H. (1981). "Field test evaluation of glass blocks from the Chalk River National Laboratories," *Tenth Information Meeting of the nuclear Fuel Waste Management Program,* Atomic Energy of Canada, Ltd. pp. 53-60.

Wehrli, B., Wieland, E., and Furrer, G. (1990). Chemical mechanisms in the dissolution kinetics of minerals; the aspect of active sites." *Aquatic Sciences 52*, 3-31.

Werme, L.O., Hench, L.L. and Lodding, A. (1985). "Nuclear waste glass interfaces after 1 year burial in stripa," in *Scientific Basis for Nuclear Waste Management VII,* C.M. Jantzen, J.A. Stone, and R.E. Ewing, eds., pp. 37-44.

White, A.F. (2003). "Natural Weathering Rates of Silicate Minerals," in *Treatise on Geochemistry, Volume 5 Surface and Ground Water, Weathering, and Soils,* J.I. Drever, ed. Elsevier

White, A.G. (1995). "Chemical weathering rates of silicate minerals in soils," in *Chemical Weathering Rates in Silicate Minerals, Vol 31*, pp. 407-461. Mineralogical Society of America.

White, A.F. and Peterson, M.L. (1990). "Role of Reactive-Surface-Area characterization in geochemical kinetic models," in *Chemical Modeling of Aqueous Systems II*: American Chemical Society.

White, A.F. and Blum, A.E. (1995). "Effects of climate on chemical weathering in watersheds," *Geochimica et Cosmochimica Acta, 59,* 1729-1747

White, A.F., Blum, A.E., Schulz, M.S., Bullen, T.D., Harden, J.W., and Peterson, M.L. (1996). "Chemical weathering rates of a soil chronosequence on granitic alluvium: I. Quantification of mineralogical and surface area changes and calculation of primary silicate reaction rates," *Geochimica et Cosmochimica Acta, 60,* 2533-2550.

White, A.F., Blum, A.E., Bullen, T.D, Vivit, D.V., Schula, M, and Fitzpatrick, J. (1999). "The effect of temperature on experimental and natural chemical weathering rates of granitoid rocks," *Geochimica et Cosmochimica Acta, 63,* 3277-3291.

White, A.F., Bullen, T.D., Schulz, M.S., Blum, A.E., Huntington, T.G, and Peters, N.E. (2001). "Differential rates of feldspar weathering in granitic regioliths," *Geochimica et Cosmochimica Acta, 65,* 847-869.

White, A.F. and Brantley, S.L. (2003). "The effect of time on the weathering of silicate minerals: why do weathering rates differ in the laboratory and field?" *Chemical Geology, 202*, 479-506.

Wicks, G.G. (1986). "WIPP/SRL in-situ testing program," *Advances in Ceramics, 20*, 657-667.

Wicks, G.G. (1992). "Nuclear waste glasses: Corrosion behavior and field tests," in *Corrosion of Glass, Ceramics, and Ceramic Superconductors*, D.E. Clark and B.K. Zoitos, eds. pp. 218-268. Noyes Publications.

Wronkiewicz, D.J., Bates, J.K., Gerding, T.J., Veleckis, E., and Tani, B.S. (1992). "Uranium Release and Secondary Phase Formation During Unsaturated Testing of UO_2 at 90°C," *Journal of. Nuclear Materials, 190,* 107-127.

Yang, C., Samper, J., and Montenegro, L. (2008). "A coupled non-isothermal reactive transport model for long-term geochemical evolution of a HLW repository in clay," *Environmental Geology, 53,* 1627-1638.

Zhu, C. (2000). "Estimate of recharge from radiocarbon dating of groundwater ages and numerical flow and transport modeling. *Water Resources Research 36,* 2607-2620.

Zhu, C. (2005). "In situ feldspar dissolution rates in an aquifer," *Geochimica et Cosmochimica Acta, 69,* 1435-1453.

Zhu, C. and Lu, P. (2009). "Alkali feldspar dissolution and secondary mineral precipitation n batch systems: 3. Saturation states of product minerals and reaction paths," *Geochimica et Cosmochimica Acta, 73,* 3171-3200.

NRC FORM 335
(12-2010)
NRCMD 3.7

U.S. NUCLEAR REGULATORY COMMISSION

BIBLIOGRAPHIC DATA SHEET

(See instructions on the reverse)

1. REPORT NUMBER
(Assigned by NRC, Add Vol., Supp., Rev., and Addendum Numbers, if any.)

NUREG/CR-7105

2. TITLE AND SUBTITLE

Radionuclide Release from Slag and Concrete Waste Materials

Part 2: Relationship Between Laboratory Tests and Field Leaching

3. DATE REPORT PUBLISHED

MONTH	YEAR
10	2011

4. FIN OR GRANT NUMBER

N6669

5. AUTHOR(S)

W. L. Ebert

6. TYPE OF REPORT

Technical

7. PERIOD COVERED *(Inclusive Dates)*

2011

8. PERFORMING ORGANIZATION - NAME AND ADDRESS (If NRC, provide Division, Office or Region, U.S. Nuclear Regulatory Commission, and mailing address; if contractor, provide name and mailing address.)

Argonne National Laboratory
9700 South Cass Ave.
Argonne, IL 60439

9. SPONSORING ORGANIZATION - NAME AND ADDRESS (If NRC, type "Same as above", if contractor, provide NRC Division, Office or Region, U.S. Nuclear Regulatory Commission, and mailing address.)

Division of Risk Analysis
Office of Nuclear Regulatory Research
U. S. Nuclear Regulatory Commission
Washington, DC 20555-0001

10. SUPPLEMENTARY NOTES

Mark Fuhrmann, NRC Project Manager

11. ABSTRACT (200 words or less)

Technical literature has been evaluated to assess the several-orders-of-magnitude discrepancy that is commonly reported between the mineral dissolution rates that are inferred from mass-balance calculations for natural systems and those measured in laboratory experiments. This was done to gain insights that may be useful for modeling the weathering behaviors and contaminant releases from waste materials in surface disposal sites. Predicting the concentrations and movement of contaminants in groundwater requires an understanding of (1) groundwater flow, (2) processes affecting contaminant dispersal and groundwater mixing, and (3) physical and chemical reaction processes that affect the concentration of a contaminant in groundwater. Inverse modeling of field measurements to extract mineral dissolution rates is affected by uncertainties in all three of these factors, whereas most laboratory measurements used in direct modeling address only the dissolution of an isolated material in a well-constrained system. Both approaches and the origins of uncertainties in each that are likely to contribute to the differences between the dissolution rates that are determined are evaluated. Information and insights pertinent to assessing the long-term weathering of waste materials under subaerial conditions are provided by each approach, and several aspects are evaluated in detail to support the use of inverse and direct modeling in future applications.

12. KEY WORDS/DESCRIPTORS (List words or phrases that will assist researchers in locating the report.)

Leaching, radionuclide, leach tests, leaching models, contaminant release, leaching mechanisms, radionuclide release, models of leaching, weathering, waste leaching, radioactive waste

13. AVAILABILITY STATEMENT

unlimited

14. SECURITY CLASSIFICATION

(This Page)

unclassified

(This Report)

unclassified

15. NUMBER OF PAGES

16. PRICE

Federal Recycling Program

UNITED STATES
NUCLEAR REGULATORY COMMISSION
WASHINGTON, DC 20555-0001

OFFICIAL BUSINESS